

DISSERTATION

**Photoinduced Electron Transfer Reactions  
between 2,2'-Dipyridyl,  
3,3',4,4'-Benzophenone Tetracarboxylic Acid  
and various DNA-Bases and Amino Acids in  
Aqueous Solution of Different pH**

**Truong Xuan Nguyen**

zur Erlangung des akademischen Grades des Doktors der  
technischen Wissenschaften

Doktoratsstudium der Technischen Wissenschaften im  
Technische Universität Graz „Institut für Physikalische und  
Theoretische Chemie“



**Betreuer:**

**O.Univ.-Prof.Dipl.-Ing.Dr.rer.nat. Günter Grampp**

**Graz, im September 2011**

## EIDESSTATTLICHE ERKLÄRUNG

Ich erkläre an Eides statt, dass ich die vorliegende Arbeit selbständig verfasst, andere als die angegebenen Quellen/Hilfsmittel nicht benutzt, und die den benutzten Quellen wörtlich und inhaltlich entnommenen Stellen als solche kenntlich gemacht habe.

Graz, am .....  
.....  
(Unterschrift)

## STATUTORY DECLARATION

I declare that I have authored this thesis independently, that I have not used other than the declared sources/resources, and that I have explicitly marked all material which has been quotes either literally or by content from the used sources.

.....  
.....  
place, date (signature)

## Abstract

This thesis presents the photoinduced electron transfer reaction in aqueous solution of different pH. Two types of fluorophores, 3,3',4,4'-benzophenone tetracarboxylic acid (BPTC) and 2,2'-dipyridyl (DP), and two classes of quenchers including amino acids and DNA-bases, were used. Chemical kinetics (e.g. rate constant) is investigated by time-resolved laser spectroscopy while a chemical thermodynamic study (e.g. redox potentials) is carried out by cyclic voltammetry. These obtained information allows the proposal of mechanisms for the reactions between fluorophores and quenchers. In most cases electron transfer is found, however the experiment reveals that there is a coupling of the electron transfer and acid-base reaction (i.e. proton transfer) by means of step-wise pathways.

## Zusammenfassung

Diese Dissertation untersucht die Kinetik von photoinduzierten Elektronentransferreaktionen in wässriger Lösung bei verschiedener pH. Zwei Arten von Fluorophoren, 3,3',4,4'-Benzophenon tetracarboxylsäure (BPTC) und 2,2'-Dipyridyl (DP), sowie zwei Klassen von Löscher, Aminosäuren und DNA-Basen, werden verwendet. Die Geschwindigkeitskonstante der Reaktion wurden mit zeitaufgelöster Laserspektroskopie untersucht und die Thermodynamik (z.B. Redox-Potentiale) mit zyklischer Voltammetrie untersucht. Damit konnten die Reaktionsmechanismen der Reaktionen zwischen Fluorophor und Löscher aufgeklärt werden. In den meisten Fällen wird ein Elektronentransfermechanismus beobachtet.

*For my family  
my wife*

# Acknowledgement

I would never have been able to accomplish my dissertation without the support of many people. The following list is still long and this printed page can never fully express my gratitude and appreciation to you.

First, I am greatly indebted to my supervisor, Prof. Dr. Günter Grampp, whose encouragement, excellent guidance, caring and support from the initial to the final level enabled me to develop an understanding of the field, photochemistry.

It is an honor for me to thank Assoc. Prof. Dr. Stefan Landgraf, who has made available his assistance in a number of ways. I have gained invaluable knowledge on modern and fast kinetics from his lectures. Thanks too for supplying of the LED-325nm arrangement.

I would like to thank Dr. Asim Mansha for instructing me on laser apparatus and sharing the laser lab. Special thanks go to Dr. Daniel Kattnig for helping on simulation of the transient absorbance. Many thanks go to Muhammad Tahir Soomro for sharing the electrochemical experiments.

I am heartily thankful to Dr. Kenneth Rasmussen, who was abundantly helpful. He taught me on ESR and scientific working and provided me an excellent atmosphere for doing my research. It was always a great time.

I would also like to thank ESR & Photochemistry group members, Dr. Arnulf Rosspeintner, Dr. Christine Onitsch, Dr. Boryana Mladenova, Dr. Faiza Iftikhar, Dr. Muhammad Zahid, Dr. Noureen Siraj and Sadia. Many thanks go to Freißmuth, Hofmeister, Eisenkölbl and Lang, without those people this study would not have been successful.

I wish to thank my friends and colleagues & friends Kraiwan, Kunal and Pawel for helping me get through the difficult times, and for all the emotional support, entertainment, and caring.

It is a pleasure to thank Österreichische Austauschdienst (ÖAD) for a scholarship and Institut für Physikalische und Theoretische Chemie - Graz for providing laboratory facilities.

I wish to express my deepest gratitude and love to my beloved family, for their patience, understanding and visiting me in Graz, and my wife Thanh Nga with her endless love through the duration of my study.



# Contents

1. <i>Introduction</i> . . . . .	1
2. <i>Theoretical Considerations</i> . . . . .	5
2.1 From electron transfer to photoinduced electron transfer . . . . .	6
2.2 Electron Transfer Theory . . . . .	7
2.2.1 The role of diffusion . . . . .	8
2.2.2 Marcus theory of electron transfer . . . . .	10
2.2.3 Adiabatic and diabatic electron transfer . . . . .	15
2.2.4 The standard reaction Gibbs energy of electron transfer . . . . .	18
2.3 The formation and fate of the electronically excited states . . . . .	20
2.3.1 The rules governing the transition between two energy states . . . . .	20
2.3.2 The formation of photoexcited states . . . . .	21
2.3.3 The reactivity of the excited states . . . . .	22
2.3.4 The fate of photoexcited states . . . . .	25
2.4 Photo-induced proton transfer <sup>[1]</sup> . . . . .	30
2.5 Proton coupled electron transfer . . . . .	33
2.5.1 Basic concepts . . . . .	34
2.5.2 Thermodynamics of the PCET reaction . . . . .	34
2.5.3 pH-dependence of PCET . . . . .	36
2.5.4 Kinetic solvent isotope effects of PCET . . . . .	37
3. <i>Experimental</i> . . . . .	39
3.1 Reagents . . . . .	40
3.1.1 Reactants . . . . .	40
3.1.2 Buffer solutions . . . . .	40
3.2 Steady-state measurements . . . . .	46
3.2.1 Absorption spectroscopy . . . . .	46
3.2.2 Determination of pK <sub>a</sub> s by UV-VIS spectroscopic method. . . . .	48
3.3 Time-resolved laser flash photolysis measurements . . . . .	51

3.3.1	Triplet-triplet (T-T) or transient absorption (TA) spectra . . .	53
3.3.2	Determination of $pK_a^*$ s by means of T-T absorption titration method. . . . .	54
3.3.3	Quenching experiments . . . . .	57
3.3.4	Radical absorption spectra . . . . .	57
3.4	Cyclic voltammetry (CV) . . . . .	57
3.5	Data evaluation . . . . .	59
3.5.1	Stern-Volmer relation . . . . .	59
3.5.2	pH-dependence of the observed quenching rate constant $k_q^{obs}$ .	65
4.	<i>Results and Discussion</i> . . . . .	67
4.1	Determination of $pK_a$ s of BPTC . . . . .	68
4.2	Determination of $pK_a^*$ s of triplet BPTC . . . . .	71
4.3	Quenching results of triplet DP . . . . .	73
4.3.1	Results of quenching by Thymine . . . . .	74
4.3.2	Results of quenching by Thymidine . . . . .	79
4.3.3	CV results of DP . . . . .	80
4.3.4	CV results of Thymine . . . . .	81
4.4	Quenching results of triplet BPTC . . . . .	83
4.4.1	T-T absorption spectra . . . . .	83
4.4.2	Results of quenching by Alanine . . . . .	85
4.4.3	Results of quenching by Histidine . . . . .	89
4.4.4	Results of quenching by Methionine . . . . .	91
4.4.5	Results of quenching by Adenine . . . . .	93
4.4.6	Results of quenching by Adenosine . . . . .	95
4.4.7	Results of quenching by Thymine . . . . .	95
4.4.8	Results of quenching by Thymidine . . . . .	100
4.4.9	CV results of BPTC . . . . .	102
5.	<i>Conclusions and Outlook</i> . . . . .	105
5.1	Conclusions . . . . .	106
5.2	Outlook . . . . .	107
	<i>Appendix</i> . . . . .	109

# List of Abbreviations

Ade	Adenine
Ala	DL-Alanine
BPTC	3,3',4,4'-benzophenone tetracarboxylic acid
CPET	Concerted proton and electron transfer
CV	Cyclic voltammetry
dAde	Adenosine
DP	2,2'-dipyridyl
dThy	Thymidine
ET	Electron Transfer
ETPT	Electron transfer followed by proton transfer
His	DL-Histidine
Met	DL-Methionine
PCET	Proton coupled electron transfer
PET	Photoinduced Electron Transfer
PTET	Proton transfer followed by electron transfer
T-T	Triplet-Triplet
TA	Transient absorption
Thy	Thymine



# List of Figures

2.1	Molecular orbital description of a redox reaction . . . . .	7
2.2	Molecular orbital description of a photoinduced electron transfer process . . . . .	7
2.3	Illustration of five-step electron transfer . . . . .	8
2.4	Description of the Smoluchovski's model . . . . .	9
2.5	Schematic one-dimensional free energy of the precursor complex ( $D...A$ ) and the successor complex ( $D^+...A^-$ ) with nuclear coordinates. $q$ is the nuclear displacement corresponding to the changing geometries of the system. The activation energy $\Delta G^*$ , total reorganization energy, $\lambda$ , and the standard reaction Gibbs energy of the electron transfer reaction, $\Delta G^0$ , are discussed later. . . . .	11
2.6	Marcus parabola (electron transfer rate constant as a function of driving force) and the diffusion limit. . . . .	15
2.7	Different regions in the Marcus theory of electron transfer . . . . .	16
2.8	Diabatic and adiabatic electron transfer . . . . .	16
2.9	Enthalpy changes ( $\Delta H$ s) for formation of $D^+$ or $A^-$ . . . . .	19
2.10	Franck-Condon excitation . . . . .	22
2.11	Förster's acid-base equilibria and energy cycle . . . . .	24
2.12	Jablonski diagram that includes electron transfer as one of the deactivation pathways. . . . .	27
3.1	Structures of all compounds used. . . . .	42
3.2	Absorption spectra of fluorophores, DNA bases and their mixtures. . . . .	47
3.3	Absorption spectra of BPTC, amino acids and their mixtures. . . . .	48
3.4	Absorption spectra of BPTC at pH=2.1 and pH=13.0 . . . . .	49
3.5	Absorption diagram of BPTC (pH-range: 2.1-13.0). <b>1</b> : First segment where Eq. 3.8a can be applied. <b>2</b> : Second segment where Eq. 3.8b can be employed. . . . .	50
3.6	Illustration of four-state energetics of XeCl-excimer laser and the excimer, $XeCl^*$ , which is generated by a series of reactions. . . . .	51

3.7	The 150W Xe-lamp intensity response profile, monitored at 800V input for R928-PMT, of the cuvette that contained only water. . . . .	52
3.8	The PMT synchronized an oscilloscope-probe arrangement. R = offset-control; S = switch; T = FET-probe tip. . . . .	53
3.9	Decay profiles of BPTC ( $1 \times 10^{-4}$ M) in water at pH=12.0, $\lambda_{obs} = 550nm$ . Upper curves: monitored without probe at 500 $\Omega$ PMT-resistor. Dot-line: experimental; Solid line: exponential fit. Lower curves: monitored with probe at 5k $\Omega$ PMT-resistor; 1M $\Omega$ oscilloscope inputs and 1M $\Omega$ probe. Dot-line: experimental; Solid line: exponential fit. . . . .	54
3.10	The laser flash photolysis apparatus. M = mirror; P = Pinhole; L = Lens; LG = Light guide ( $260nm < \lambda \leq 720nm$ ); C = Cable. . . . .	55
3.11	Transient absorption spectra of BPTC ( $1 \times 10^{-4}$ M) at pH=2.0 and pH=12.0, monitored by transient absorbances at 590nm and at 550nm between 360 and 690nm, obtained right after the laser flash. . . . .	55
3.12	T-T absorption monitored by the transient absorbances at 590nm and 550nm, obtained right after the laser flash; and absorption ratio titration, $A_{590nm}/A_{550nm}$ . . . . .	56
3.13	Cyclic voltammogram of $K_3Fe(CN)_6$ (5mM) in $KNO_3$ (0.1M) vs. Ag/AgCl. Scan initiated in negative direction at 100 mV/s. Glassy carbon electrode, area = 0.03cm <sup>2</sup> . . . . .	58
3.14	Cyclic voltammograms of dipyriddy and thymine as functions of pH . . . . .	59
3.15	Photodiode response to laser pulses and TA signal profile . . . . .	60
3.16	Typical transient absorption obtained by the laser-flash photolysis. . . . .	61
3.17	Demonstration of experimental data (solid line) resulting from the addition of transient absorbance due to <sup>3</sup> F (dotted line) and the free radical anion R (dotted line) . . . . .	63
3.18	Demonstration of the experimental data from BPTC ( $1 \times 10^{-4}$ M) + Thy ( $4.5 \times 10^{-4}$ M) system ( $\lambda_{obs} = 590nm$ ) at pH=2.0 (dashed line) and simulation (solid line) resulting from the fourth kinetic case considered. . . . .	65
4.1	Absorbance values at 257.5nm and 287.5nm as functions of pH. . . . .	68
4.2	Absorption spectra of BPTC ( $4 \times 10^{-5}$ M) at pH=3.01–6.10 and A-diagram. . . . .	69
4.3	Determination of the $pK_{aI}$ of BPTC in water. Graphic representation of Eq. 4.2 at 257.5nm and 287.5nm. . . . .	71

4.4	Determination of the $pK_{aII}$ of BPTC in water. Graphic representation of Eq. 4.3 at 257.5nm and 287.5nm. . . . .	72
4.5	Determination of $pK_a^*$ s of triplet BPTC . . . . .	74
4.6	Decays ( $\lambda_{obs}=325\text{nm}$ ) of triplet DP ( $2 \times 10^{-3}\text{M}$ ) + Thy (concentration increasing from top to bottom: $0 - 4.9 \times 10^{-4}\text{M}$ ) in water at pH=12.0. Insert: Stern-Volmer plot from Eqs. 3.14 and 3.15b. . . . .	75
4.7	Molar fractions of triplet DP, DP and thymine in water. . . . .	76
4.8	pH-dependence of the observed quenching rate constants $k_q^{obs}$ for the reaction between triplet DP and Thy. The dashed line is the simulation according to Eq. 3.29 with $pK_{a,DPH^+}^T = 5.8$ . While the solid line is that with $pK_{a,DPH^+}^T = 5.0$ . See Tab. 4.3 for parameters. . . . .	77
4.9	Transient absorption spectrum obtained at $2\mu\text{s}$ after irradiation of DP ( $7.0 \times 10^{-5}\text{M}$ )+Thy ( $7.5 \times 10^{-3}\text{M}$ ) at pH=2.0. Insert: Decay profiles observed at $\lambda_{obs}=325\text{nm}$ and $370\text{nm}$ . . . . .	78
4.10	Decays ( $\lambda_{obs}=325\text{nm}$ ) for DP+dThy system in water at pH=2.0. Concentration of dThy increases from top to bottom: $0 - 1.5 \times 10^{-2}\text{M}$ . Insert: Stern-Volmer plot from Eqs. 3.14 and 3.15b. . . . .	80
4.11	pH-dependence of the observed quenching rate constant $k_q^{obs}$ for the reaction of triplet DP with dThy. The dashed line is the simulation according to Eq. 4.8 with $pK_{a,DPH^+}^T = 5.8$ . While the solid line is that with $pK_{a,DPH^+}^T = 5.0$ . See Tab. 4.3 for parameters. . . . .	81
4.12	Variation of the apparent standard reduction potential (vs. Ag/AgCl) of DP (1mM) with pH. . . . .	82
4.13	The apparent standard oxidation potential (vs. Ag/AgCl) of thymine (1mM) as a function of pH. Solid line: linear fit, slope = $-55.2 \pm 2.7$ mV/pH. Dashed line (pH<2): extrapolated from fitting. . . . .	83
4.14	The variation of the driving force with pH for ${}^3\text{DPH}^+ + \text{ThyH}$ reaction. Calculated with the triplet energy $E_T=282 \text{ kJmol}^{-1}$ , $E_{\text{DPH}^+}^0 = -1.22\text{V}$ . . . . .	84
4.15	Molar fractions of triplet BPTC and BPTC in water. . . . .	85
4.16	Decay profiles ( $\lambda_{obs}=550\text{nm}$ ) for BPTC+Ala system in water pH=11.9. Concentration of Ala increases from top to bottom: $0 - 1 \times 10^{-3}\text{M}$ . Insert: Stern-Volmer plot from Eqs. 3.25 and 3.15b. . . . .	86
4.17	TA spectra ( $\lambda_{obs}=630\text{nm}$ ) for BPTC ( $1 \times 10^{-4}\text{M}$ ) + Ala ( $5 \times 10^{-2}\text{M}$ ) systems in water at pH=2.0 and 11.9, monitored right after the laser-flash. . . . .	87

4.18	pH-dependence of the observed quenching rate constant $k_q^{obs}$ for the reaction of triplet BPTC with Ala. Solid line is the simulation from Eq. 4.11. . . . .	88
4.19	Decay profiles ( $\lambda_{obs}=590\text{nm}$ ) for BPTC+His system in water at pH=6.2. Concentration of His increases from top to bottom: $0 - 1.5 \times 10^{-4}\text{M}$ . Insert: Stern-Volmer plot from Eqs. 3.25 and 3.15b. . . . .	90
4.20	pH-dependence of the observed quenching rate constant $k_q^{obs}$ for the reaction of triplet BPTC with His. Solid line is the simulation from Eq. 4.13. . . . .	91
4.21	Decay profiles ( $\lambda_{obs}=590\text{nm}$ ) for BPTC+Met system in water at pH=3.4. Concentration of Met increases from top to bottom: $0 - 6 \times 10^{-5}\text{M}$ . Insert: Stern-Volmer plot from Eqs. 3.25 and 3.15b. . . . .	92
4.22	pH-dependence of the observed quenching rate constant $k_q^{obs}$ for the reaction of BPTC triplet with Met. Solid line is the simulation from Eq. 4.11. . . . .	93
4.23	Decay profiles ( $\lambda_{obs}=590\text{nm}$ ) for BPTC+Ade system in water at pH=4.0. Concentration of Ade increases from top to bottom: $0 - 9 \times 10^{-5}\text{M}$ . Insert: Stern-Volmer plot from Eqs. 3.25 and 3.15b. . . . .	94
4.24	pH-dependence of the observed quenching rate constant $k_q^{obs}$ for the reaction of triplet BPTC with Ade. The solid line is the simulation from Eq. 4.11. . . . .	95
4.25	Decay profiles ( $\lambda_{obs}=590\text{nm}$ ) for BPTC+dAde system in water at pH=4.0. Concentration of dAde increases from top to bottom: $0 - 1.2 \times 10^{-4}\text{M}$ . Insert: Stern-Volmer plot from Eqs. 3.25 and 3.15b. . . . .	96
4.26	pH-dependence of the observed quenching rate constant $k_q^{obs}$ for the reaction of triplet BPTC with dAde. Solid line is the simulation from Eq. 4.11. . . . .	96
4.27	Decays ( $\lambda_{obs}=550\text{nm}$ ) of triplet BPTC ( $1 \times 10^{-4}\text{molL}^{-1}$ ) + thymine (concentration increase from top to bottom: $0 - 1.5 \times 10^{-4}\text{M}$ ) in water at pH=8.0. Experimental: dashed lines; simulation with Eq. 3.26: solid lines. . . . .	97
4.28	$k_1$ vs. [Thy] plot for the BPTC+Thy system in water at pH=8.0. . . . .	97
4.29	BPTC ketyl radical anion spectrum in the presence of thymine ( $1.5 \times 10^{-2}\text{molL}^{-1}$ ) at pH=2.0. Insert: Decay profile ( $\lambda_{obs}=630\text{nm}$ ) of BPTC $^{\cdot-}$ , which form the pinacol after the fast protonation of BPTC $^{\cdot-}$ to BPTCH. . . . .	98

4.30	pH-dependence of the observed quenching rate constants $k_q^{obs}$ for the reaction of triplet BPTC with thymine. The solid line is the simulation according to Equation 4.17. . . . .	99
4.31	Decay profile ( $\lambda_{obs}=550\text{nm}$ ) for BPTC+dThy system in water pH=8.0. Concentration of dThy increases from top to bottom: $0 - 1.5 \times 10^{-3}\text{M}$ . Insert: Stern-Volmer plot from Eqs. 3.25 and 3.15b. . . . .	101
4.32	pH-dependence of the observed quenching rate constant $k_q^{obs}$ for the reaction of triplet BPTC with dThy. Solid line is the simulation from Eq. 4.18. . . . .	102
4.33	The apparent standard reduction potential (vs. Ag/AgCl) of BPTC (1mM) as a function of pH. Solid line: linear fit, slope = $-27.8 \pm 2.4$ mV/pH. . . . .	103



# List of Tables

2.1	The formation and fate of an excited state. <sup>a</sup> . . . . .	28
3.1	List of compounds . . . . .	41
3.2	Preparation of buffer stock solutions at room temperature. <sup>[2,3]</sup> . . . . .	43
3.3	Preparation of buffer solutions for individual pH used in steady-state measurements at room temperature. <sup>a</sup> . . . . .	44
3.4	Preparation of buffer solutions used in time-resolved measurements at room temperature. <sup>a</sup> . . . . .	46
4.1	Experimental ionization constant of BPTC determined by UV-VIS spectrometry. . . . .	70
4.2	Results of $pK_a^*$ -values. . . . .	73
4.3	Quenching rate constants of triplet DP by quenchers ( $k_{qi}$ ) . . . . .	78
4.4	Quenching rate constants of triplet BPTC by quenchers ( $k_{qi}$ ) . . . . .	89



# 1

## Introduction

A part of the research described in this thesis has been submitted in:

---

T.X. Nguyen, Dr.D. Kattnig, Dr.A. Mansha, Dr.A.V. Yurkovskaya, Prof.N. Lukzen and Prof.G. Grampp. *Kinetics of Photoinduced Electron Transfer between DNA bases and Triplet 3,3',4,4'-Benzophenone tetracarboxylic Acid in Aqueous Solution of Different pH. Proton Coupled Electron Transfer?* ChemPhysChem 2011.

Electron transfer is among the simplest natural phenomena, yet certainly one of the most critical. Gaining knowledge of electron transfer is a key to having insights into important biological activities in the living cell such as: migration of electrons over the long-range of protein and DNA; enzymatic redox reactions; protein biosynthesis and DNA damage/repair; photosynthetic energy conversion in green plants; nitrogen fixation; and respiration.

The electron transfer process inducing charge separation plays a leading role in chemical, electrochemical and biochemical reactions. Unsurprisingly, it has been given great attention by scientists in a variety of fields. Their extensive efforts have provided an understanding of the fundamental principles of the process, how it is influenced by the surrounding environment, and how it can be applied. The ultimate goal is to control the process.

Photoinduced electron transfer has been widely used to study such biochemical processes directly. Two types of sensitizers, aromatic carbonyl compounds ( $n-\pi^*$  triplet state, e.g. benzophenone-4-carboxylic acid) and aza-aromatic compounds ( $\pi-\pi^*$  triplet state, e.g. 2,2'-dipyridyl) have attracted considerable interest. The interaction of excited triplet states of benzophenone-4-carboxylic acid with amino acid residues provides the information of charge migration on peptide chains and proteins.<sup>[4-8]</sup> Reactions of photoexcited dipyrindyl and amino acids, dipeptides and macromolecules have been applied to the investigations of the spatial structure of protein, as reported in a huge number of articles.<sup>[6,9-16]</sup>

Biological systems are water-based systems. In fact water in intracellular fluids constitutes approximately 60% of the total body mass. Therefore, pH of the solution is an essential parameter which should be considered. For example, redox centers (cofactors) can only function within a certain range of pH. In other words, their sensitivity and selectivity varies with pH of the solution. Some crucial chemical physical aspects, if not most, arise when studying biological systems such as electron transfer, proton transfer (acid-base reactions) and proton coupled electron transfer (coupling between electron transfer and acid-base reactions).

It is important to know: (1) How the system determines which reaction-channels are feasible (i.e., reduction/oxidation potentials). (2) How fast the reaction occurs (i.e. rate constants). (3) How the reactant system and reaction rate depend on pH of the medium.

The research presented in this thesis brings the reader into (i) the interaction of triplet excited state dipyrindyl with the nucleobase, thymine and its nucleoside, thymidine; (ii) acid-base properties of benzophenone tetracarboxylic acid (BPTC) in the ground and triplet excited states; (iii) reactions between triplet excited BPTC

---

and DNA bases, adenine, adenosine, thymine and thymidine, and amino acids, alanine, histidine and methionine. All work was investigated in water over a wide range of pH (2 -12) by means of both laser-flash photolysis and cyclic voltammetry, assisted by UV-VIS spectrometry.

In chapter 2, Marcus's theory of electron transfer relevant to this thesis research is reviewed. Applying the electron transfer theory as a starting point, then subsequently, the photoinduced electron transfer, photoinduced proton transfer and coupling of proton and electron transfer are discussed.

Chapter 3 gives the necessary experimental information of the used reagents, measurement procedures and data evaluations. In the first section, physical and chemical properties that considered of all compounds are presented. Moreover, buffer solutions employed and the calculation of those prepared for certain purposes are also mentioned in detail. Afterwards, steady-state measurements emphasizing on UV-VIS spectroscopic method to determine  $pK_a$ -values of the fluorophore, 3,3',4,4'-benzophenone tetracarboxylic acid (BPTC), are given. Additionally, a common technique namely triplet-triplet absorption titration by which  $pK_a^*$ -values of BPTC in the excited state are estimated is brought forward. The next part will focus on quenching experiments of the fluorophores by various quenchers including sample preparation and time-resolved measurement routines. Furthermore, a brief description of cyclic voltammetry which used in this work is demonstrated. The final part will discuss data treatments dedicated to some of the most faced kinetic problems in the laser flash photolysis and to pH-dependence of the observed quenching rate constants (i.e. a pH-dependent function).

The next chapter presents and interprets experimental data. Finally, a short summary and outlook to possible future work are presented.



**2**

## **Theoretical Considerations**

In this chapter a general description of electron transfer (ET) reactions in solution originated from Marcus's theory is presented. As a result the photoinduced electron transfer (PET), photo-induced proton transfer and proton coupled electron transfer (PCET) reactions are also mentioned. At the beginning the relation between ET and PET is discussed. In the following part Marcus's theory of electron transfer with the highlighted parameters including verification of experimental results is briefly reviewed. The next section considers the formation, reactivity and fate of the electronically excited states together with the kinetic expressions for these processes. Then the photo-induced proton transfer with water molecules as proton-donors or acceptors is discussed. PCET and the focus on its thermodynamics close this chapter.

## 2.1 From electron transfer to photoinduced electron transfer

The electron transfer is the process by which an electron moves from one chemical specie (donor) to another (acceptor). The oxidation states of both chemical species change. This is known as a redox process. The illustration by molecular orbital description is shown in Fig. 2.1. At the beginning of the 1950's it was possible to determine the rate of a large number of electron transfers between inorganic ions. The early experiments in the electron transfer field were isotopic exchange electron transfer reactions.<sup>[17]</sup> The rates of several self-exchange ET reactions between metal complexes turned out to be very slow.<sup>1</sup> Moreover, it was suggested with the organic donor and acceptor that, because of the large HOMO-LUMO gap, electron transfer would be a largely endothermic process. An idea had been given to turn electron transfer reaction between organic molecules or of complexes into an energetically more favorable process which was involved in the absorption of light. This is known as a photoinduced electron transfer process. Indeed, it was recognized quite early by Eugene Rabinowitch that,

„An electronically excited molecule has an increased tendency to give away an electron, as well as the capacity to replace the one which was removed from its normal level.”<sup>[20]</sup>

When absorbing light, electronic excitation either exploits the large HOMO-LUMO gap prior to electron transfer or creates vacancies in low-lying bonding orbitals,

---

<sup>1</sup> Self-exchange rate constants:  
 $\text{Fe}(\text{H}_2\text{O})_6^{3+}/\text{Fe}(\text{H}_2\text{O})_6^{2+} \quad k = 4\text{M}^{-1}\text{s}^{-1}$ <sup>[18]</sup>  
 $\text{Co}(\text{en})_3^{3+}/\text{Co}(\text{en})_3^{2+} \quad k = 8 \times 10^{-5}\text{M}^{-1}\text{s}^{-1}$  (en=ethylenediamine)<sup>[19]</sup>

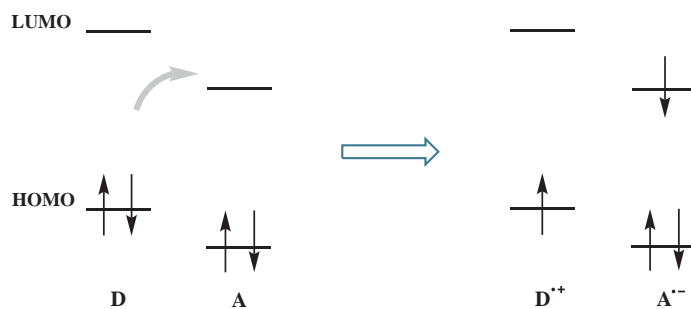


Fig. 2.1: Molecular orbital description of a redox reaction

which serve as much better electron acceptors than unoccupied orbitals of higher energy. The illustration by molecular orbital description is shown in Fig. 2.2. PET, being of great interest since many years, is one of the special cases of electron transfer.

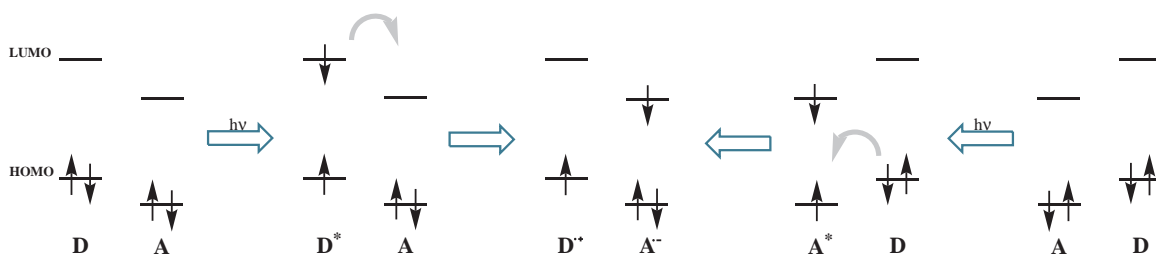


Fig. 2.2: Molecular orbital description of a photoinduced electron transfer process

## 2.2 Electron Transfer Theory

The theory of electron transfer has been developed independently by RA. Marcus, N.S. Hush, V.G. Levich, and RR Dogonadze since 1956. Electron transfer between free ions or molecules in solution can be divided into five steps. The description of these steps is shown in Fig. 2.3.

(1) In the first step, reactants diffuse together out of their solvent shells to form a precursor complex (P).

(2) In a second step, reactants rearrange their bond lengths along with reorganization of solvent molecules to form the activated complex (at the transition state).

(3) In a third step, electron transfer occurs.

(4) In the next step, the oxidized donor and reduced acceptor reorganize their bond lengths along with relaxation of solvent molecules to form the successor complex (S).

(5) In the final step, products diffuse apart to form free ions.

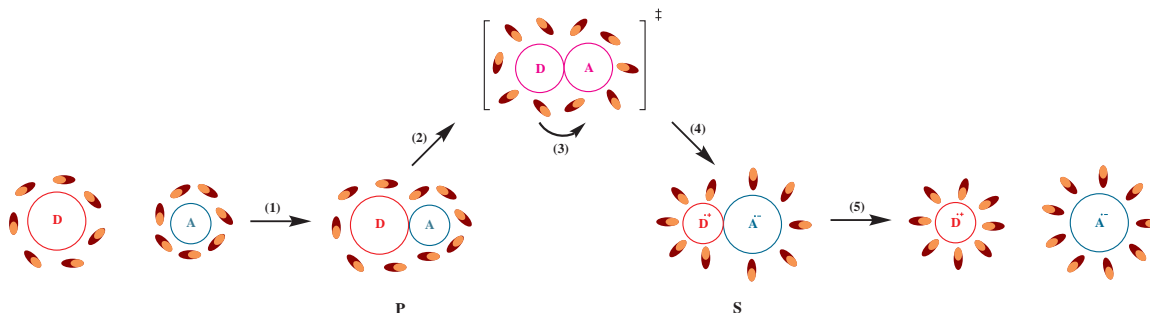


Fig. 2.3: Illustration of five-step electron transfer

### 2.2.1 The role of diffusion

This section mainly presents the Smoluchowski's model for the expression of the diffusion rate constant. The model follows some starting assumptions:<sup>[21]</sup>

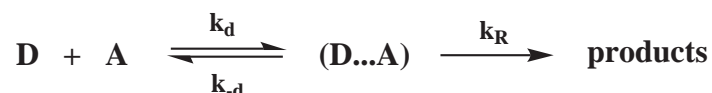
- Donor, D, and acceptor, A, are big (compared to the solvent molecules) and spherical particles (Fig. 2.4). A is great excess.

- All particles A that arrive to the surface of the „black sink”, D, react irreversibly (losing their identities), Scheme 2.1. Meaning that diffusion rate constant  $k_d \gg k_{-d}$ .

- D has a radius that is the sum of radius of D and A,  $\sigma = r_D + r_A$  (the so-called contact model).

- Diffusion is the elementary process that determines the reaction rate between D and A ( $k_R \gg k_d$ ).

Consider A undergoes diffusive motion relative to a stationary D characterized by diffusion coefficient  $D^{diff} = D_A^{diff} + D_D^{diff}$ . In general, the density distribution



Schema 2.1: Diffusional process of the free molecules A and D in solution

of a reacting specie A,  $\rho(r, t)$ , is a time ( $t$ ) and distance ( $r$ ) function or in other

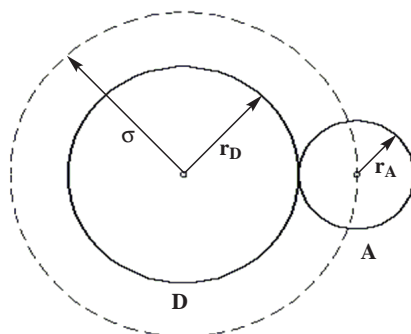


Fig. 2.4: Description of the Smoluchowski's model

words  $\rho(r, t)$  must obey the diffusion equation:<sup>[22]</sup>

$$\frac{\delta\rho(r, t)}{\delta t} = D^{diff}\nabla^2\rho(r, t) + \nabla J_A(r, t) \quad (2.1)$$

where  $\nabla$  is the del operator;  $J_A(r, t)$  is the current density distribution of particles A (flux of particles A falling to the sink D). The flux of particles A is proportional to its density distribution:

$$J_A(r, t) = -w(r, t)\rho(r, t) \quad (2.2)$$

where the factor  $w(r, t)$  is the so-called remote reaction rate.

Now Eq. 2.1 becomes:<sup>[23,24]</sup>

$$\frac{\delta\rho(r, t)}{\delta t} = D^{diff}\nabla^2\rho(r, t) - w(r, t)\rho(r, t) \quad (2.3)$$

with following boundary conditions:

$$\begin{cases} \rho(r, 0) = 1 & \text{initial condition} \\ \rho(\sigma, t) = 0 & \text{inner boundary condition} \\ \rho(\infty, t) = 1 & \text{outer boundary condition} \end{cases} \quad (2.4)$$

One can also write a kinetic law for the reaction in scheme 2.1:

$$\frac{d[\text{D}]}{dt} = -k(t)[\text{D}][\text{A}]_0 \quad (2.5)$$

with the reaction rate constant,  $k(t)$

$$k(t) = 4\pi \int_{\sigma}^{\infty} w(r, t) \rho(r, t) r^2 dr \quad (2.6)$$

Finally from the solution of Eq. 2.3, the Smoluchovski rate constant of diffusion is given:

$$k(t) = 4\pi\sigma D^{diff} \left( 1 + \frac{\sigma}{\sqrt{\pi D^{diff} t}} \right) \quad (2.7)$$

or in its reduced form

$$k_d = k(\infty) = 4\pi\sigma D^{diff} \quad (2.8)$$

According to Stokes-Einstein relation:

$$D_i^{diff} = \frac{k_B T}{6\pi\eta r_i} \quad (2.9)$$

one gets the well known Einstein and Smoluchowski equation for rate constant of diffusion,

$$k_d = \frac{2}{3} \frac{k_B T}{\eta} \left( \frac{1}{r_D} + \frac{1}{r_A} \right) (r_A + r_D) \quad (2.10)$$

where  $\eta$  is viscosity of the solvent.

On the other hand, Collins and Kimball (CK) afterward developed a model for diffusion-influenced the reaction rate constant by introducing an effective radius ( $R_{eff}$ ) of the reaction instead of  $\sigma$  (the so-called generalized CK model)

$$R_{eff} = \sigma \frac{k_0}{k_0 + 4\pi D^{diff}}, \quad (2.11)$$

where  $k_0$  is the kinetic rate constant at  $\sigma$ . Nevertheless, the contact model and generalized CK are still rough to describe the distance-dependent rate constant. Nowadays, encounter theory has been developed which deals with reaction that is governed by a distance-dependent rate. Usually it is under diffusion control and occurs very fast such as reaction of fluorescence quenching or recombination of products, etc. However, a review on diffusion theories is out of the scope of this thesis.

## 2.2.2 Marcus theory of electron transfer

**Rate expression of electron transfer.** The electron being a relative light particle<sup>2</sup>, the Franck-Condon principle can be applied for the electron transfer reaction.

---

<sup>2</sup> The ratio of electronic to nuclear mass  $\frac{m_e}{M_p} \approx 5 \times 10^{-4}$

That means the nuclei do not change their positions and momenta in the molecular entity and its environment during the electron motion. Therefore, electron transfer can occur only after thermal fluctuations bring the geometry of the precursor complex ( $D\dots A$ ) to  $q^*$  (the transition state-TS) in Fig. 2.5,<sup>[25]</sup> at which its and successor complex's potential-energy surfaces cross. According to the classical transition state theory, the rate constant for electron transfer is given by Eq. 2.12.

$$k_{et} = \nu_n \kappa_{el} e^{\frac{-\Delta G^*}{k_B T}} \quad (2.12)$$

Here  $\nu_n$  and  $\kappa_{el}$  are the nuclear frequency and electronic transmission factors at the TS;  $\Delta G^*$  is the activation energy of the electron transfer reaction.  $k_B$  is the Boltzmann constant and T is the absolute temperature.

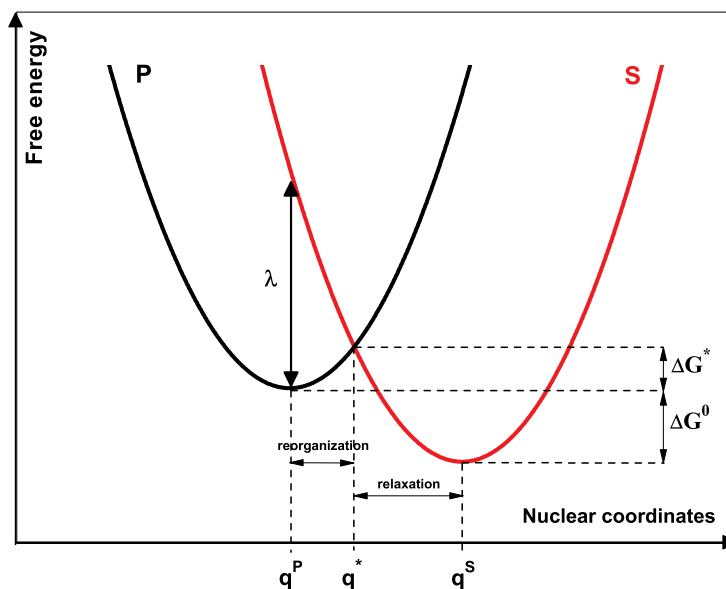


Fig. 2.5: Schematic one-dimensional free energy of the precursor complex ( $D\dots A$ ) and the successor complex ( $D^+\dots A^-$ ) with nuclear coordinates.  $q$  is the nuclear displacement corresponding to the changing geometries of the system. The activation energy  $\Delta G^*$ , total reorganization energy,  $\lambda$ , and the standard reaction Gibbs energy of the electron transfer reaction,  $\Delta G^0$ , are discussed later.

Consider electron transfer from a donor D to an acceptor A in solution, scheme 2.2, the kinetic law reads as

$$v = k_q[D][A] = k_{sep}[(D^+\dots A^-)]$$



From Eq. 2.17,  $k_{et}$  can be calculated from  $k_d$ ,  $K_A$  and the experimental value  $k_q$ .  $k_d$  is expressed by Einstein and Smoluchowski, Eq. 2.10.

In addition, the equilibrium constant for the formation of the precursor complex,  $K_A$  can be expressed by Norman Sutin:<sup>[26]</sup>

$$K_A = 4\pi N_A d^2 \delta d \exp\left(\frac{-w_r}{RT}\right) \quad (2.18)$$

with the coulombic work term given by

$$w_r = \frac{e_0^2 z_D z_A N_A}{4\pi \epsilon_0 \epsilon_S d (1 + \beta d \sqrt{I})} \quad \text{with } \beta = \sqrt{\frac{2N_A e_0^2}{\epsilon_0 \epsilon_S k_B T}}$$

where  $N_A$  is the Avogadro constant;  $R$  is the universal gas constant,  $R = k_B N_A$ .  $r_D$  and  $r_A$  are the mean molecular radii of donor and acceptor, respectively;  $d = r_D + r_A$  is the contact radius of the donor and acceptor molecules; and  $\delta d$  is a reaction zone thickness of roughly  $0.8\text{\AA}$ .  $e_0$  is the elementary charge and  $I$  is the ionic strength of the solution.  $z_D$  and  $z_A$ , respectively, are the charges of the donor and acceptor molecules.  $\epsilon_0$  is the vacuum permittivity (or electric constant); and  $\epsilon_s$  is the static dielectric constant of the solvent.

According to Eq. 2.17, when  $k_{et} \gg k_{-d}$ , one sees that  $k_q \approx k_d$ , and the rate of product formation is controlled by diffusion of D and A in solution. When  $k_{et} \ll k_{-d}$ , one finds that

$$\frac{1}{k_q} = \frac{1}{K_A k_{et}}$$

and the process is controlled by the activation energy of electron transfer in the (D...A) complex.

**Activation and reorganization energy.** The precursor complex (D...A) and the solvent molecules surrounding it undergo structural rearrangements prior to electron transfer. The energy associated with these rearrangements and the standard reaction Gibbs energy determine the activation energy. This relation is expressed by the classical Marcus equation:<sup>[17]</sup>

$$\Delta G^* = \frac{(\Delta G^0 + \lambda)^2}{4\lambda} \quad (2.19)$$

with,

$$\lambda = \lambda_i + \lambda_o \quad (2.20)$$

where  $\lambda_i$  is the inner reorganization energy implying the energy change of bond lengths and  $\lambda_s$  the outer reorganization energy refers the energy change of solvent molecules.

$$\lambda_i = \sum_i \frac{f_i^R \cdot f_i^P}{f_i^R + f_i^P} \Delta q_i^2 \quad (2.21)$$

Where  $f_i^R$  is the  $i^{\text{th}}$  force constant for reactants and  $f_i^P$  being that for products;  $\Delta q_i$  is the difference in the equilibrium bond distance between the reactant and product state corresponding to an  $i^{\text{th}}$  vibration.

In a two-sphere model,  $\lambda_o$  can be expressed:

$$\lambda_o = \frac{\Delta e_0^2}{4\pi\epsilon_0} \left( \frac{1}{2r_D} + \frac{1}{2r_A} - \frac{1}{d} \right) \underbrace{\left( \frac{1}{\epsilon_\infty} - \frac{1}{\epsilon_s} \right)}_{\gamma} \quad (2.22)$$

where  $\Delta e_0$  is the charge transferred from one reactant to the other;  $\epsilon_\infty$  is optical dielectric constant and  $\gamma$  is the Pekar factor, with

$$\gamma = \frac{1}{\epsilon_\infty} - \frac{1}{\epsilon_s} \approx \frac{1}{n_D^2} - \frac{1}{\epsilon_s} \quad (2.23)$$

Here  $\epsilon_\infty$  is substituted by  $n_D^2$  with  $n_D$  being the refractive index of the solvent. Now the substitution  $\Delta G^0$  of the Eq. 2.19 into the Eq. 2.12 leads to:

$$k_{et} = \nu_n \kappa_{el} e^{-\frac{(\Delta G^0 + \lambda)^2}{4\lambda k_B T}} \quad (2.24)$$

**Inverted region.** The standard reaction Gibbs energy,  $\Delta G^0$ , of an electron transfer reaction corresponds to vertical displacement of the free energy surface of the successor state relative to that of the precursor state (see Figs. 2.5). It is generally approximated to the driving force which is the difference in redox potentials of the donor and acceptor. The dependence of  $k_{et}$  on  $\Delta G^0$  can be investigated, only if, in systems where the distance from donor to acceptor<sup>3</sup>, the reorganization energy, and  $\kappa_{el}\nu_n$  are constant for a series of reactions. Under these conditions, taking the natural logarithm of Eq. 2.24, one obtains:

$$\ln k_{et} = -\frac{1}{4\lambda k_B T} (\Delta G^0)^2 - \frac{1}{2k_B T} \Delta G^0 + \text{constant} \quad (2.25)$$

---

<sup>3</sup> It is difficult to measure the distance dependence of  $k_{et}$  if the reactants are free ions or molecules diffuse in solution.

According to Eq. 2.25, a plot of  $\ln k_{et}$  against  $\Delta G^0$  is predicted to be shaped like a downward parabola, Fig. 2.6.

If  $-\Delta G^0 = \lambda$  (Figs. 2.6 and 2.7(b)), the exponential factor in Eq. 2.24 vanishes, i.e. the rate constant of the electron transfer is maximum. The optimal region is reached.

If  $-\Delta G^0 < \lambda$  (Figs. 2.6 and 2.7(a)), the electron transfer rate increases with larger driving force. This is known as Marcus normal region.

However, If  $-\Delta G^0 > \lambda$  (Figs. 2.6 and 2.7(c)), the electron transfer rate **decreases** with larger driving force. This is called Marcus inverted region. This region was verified experimentally by J.R. Miller and G.L. Closs,<sup>[27]</sup> where the electron donor and acceptor were linked covalently to a molecular spacer of known and fixed size for all compounds in the series.

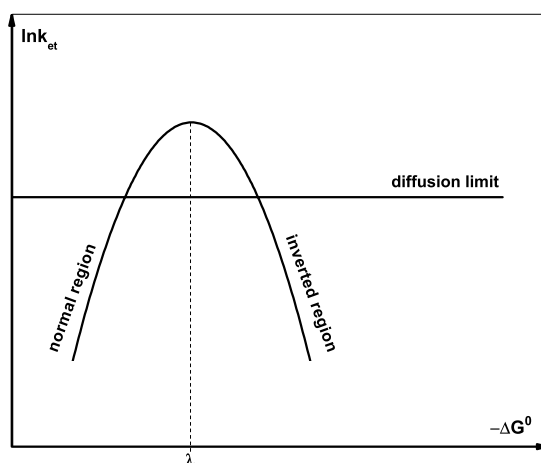


Fig. 2.6: Marcus parabola (electron transfer rate constant as a function of driving force) and the diffusion limit.

### 2.2.3 Adiabatic and diabatic electron transfer

The electronic transmission factor defines two different types of electron transfer reactions, adiabatic and diabatic, Fig. 2.8.

If the electronic coupling between the reactants in the activated complex is so weak that  $\kappa_{el} \ll 1$ , the reaction is diabatic, Fig. 2.8(a). The reactant state stays on the reactant surface energy on most transitions and occasionally crosses to product state. The expression of the rate constant for diabatic electron transfer was given by Levich and Dogonadze:<sup>[28]</sup>

$$k_{NA} = \frac{2\pi V_{RP}^2}{\hbar\sqrt{4\pi k_B T \lambda}} \exp\left(\frac{-\Delta G^*}{k_B T}\right) \quad (2.26)$$

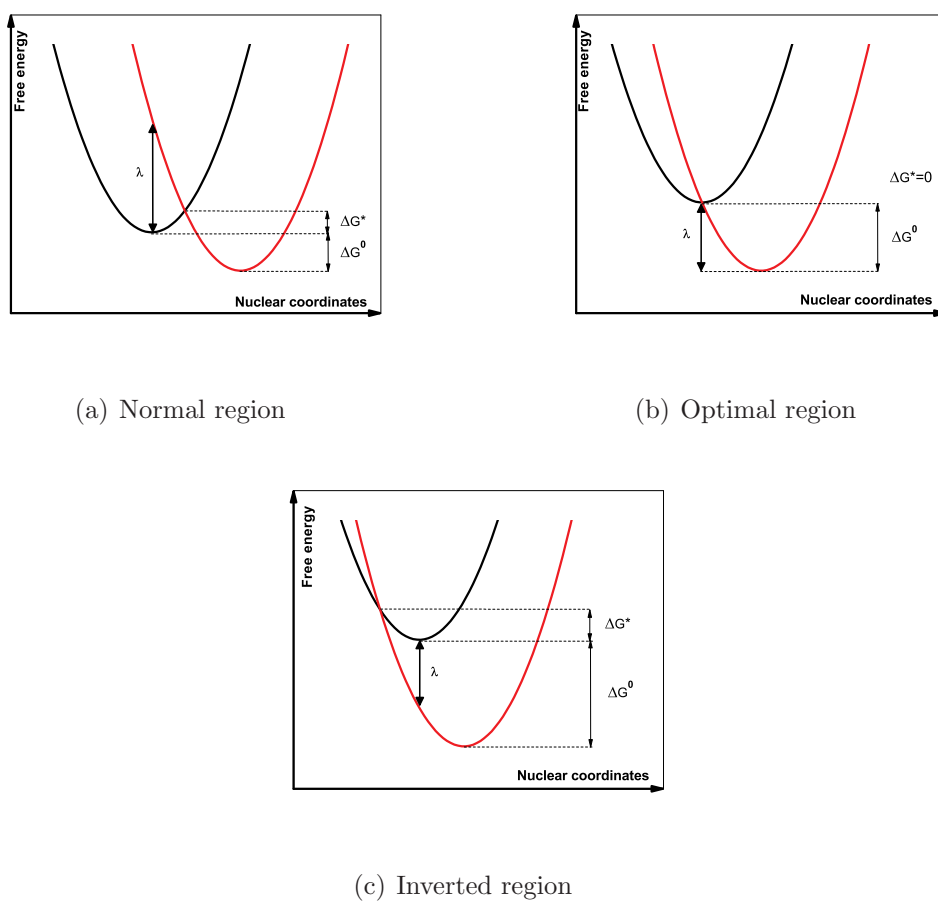


Fig. 2.7: Different regions in the Marcus theory of electron transfer

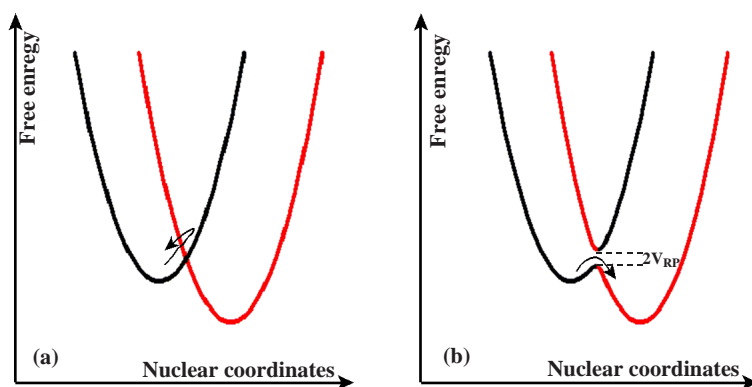


Fig. 2.8: Diabatic and adiabatic electron transfer

where  $\hbar$  is the reduced Planck constant;  $V_{RP}$  is the electronic coupling matrix element between the reactants.

If the electronic coupling between the reactants in the activated complex is suffi-

ciently large that  $\kappa_{el} \approx 1$ , the reaction is adiabatic (weakly adiabatic electron transfer), Fig. 2.8(b). The reactant state always transfers to product state with lower energy surface. The rate constant for the adiabatic electron transfer is expressed by Eq. 2.27<sup>[29]</sup>

$$k_{et} = \frac{k_{NA}}{1 + H_A} \quad (2.27)$$

with  $H_A$  is called the adiabatic parameter. And

$$H_A = \frac{4\pi V_{RP}^2 \tau_L}{\hbar \lambda} \quad (2.28)$$

here the longitudinal relaxation time,

$$\tau_L = \tau_D \frac{\epsilon_\infty}{\epsilon_s} \approx \tau_D \frac{n_D^2}{\epsilon_s}$$

where  $\tau_D$  is the dielectric (Debye) relaxation time of the solvent.

If  $H_A \gg 1$ , from Eqs. 2.27 and 2.28, one can expect that  $k_{et}$  is inversely proportional to  $\tau_L$ . This was verified experimentally for intramolecular electron transfer in aliphatic alcohols.<sup>[30]</sup> For self-exchange electron transfer reaction,  $\Delta G^0 = 0$  and the approximate activation energy is given by

$$\Delta G^* = \frac{\lambda}{4} - V_{RP} = \frac{1}{4}(\lambda_o + \lambda_i) - V_{RP} \quad (2.29)$$

Combining Eqs. 2.27, 2.28, 2.29 and taking into account of the diffusional step of the reactants, the solvent dependence on the electron transfer rate is expected:

$$k_{ET} = K_A \tau_L^{-1} (\lambda_o(\gamma)/16\pi k_B T)^{1/2} \exp\left[-\frac{(\lambda_i/4 + \lambda_o(\gamma)/4 - V_{RP})}{k_B T}\right] \quad (2.30)$$

From Eq. 2.24,  $(\kappa_{el}\nu_n)_{obs}$  can be expressed by

$$(\kappa_{el}\nu_n)_{obs} = \frac{k_{et}}{K_A \exp[-(\lambda_i/4 + \lambda_o(\gamma)/4 - V_{RP})/k_B T]} \quad (2.31)$$

Thus, a plot of  $\log(\kappa_{el}\nu_n)_{obs}$  vs.  $-\log\tau_L\gamma^{-1/2}$  should give a straight line with slope of 1 and it indicates an adiabatic electron transfer reaction. The experimental confirmation was done by Grampp and Rasmussen where  $0.37 < \gamma < 0.53$ .<sup>[31]</sup>

### 2.2.4 The standard reaction Gibbs energy of electron transfer

In general an electron transfer reaction is simply a redox process where an electron donor is oxidized by the electron acceptor.



where  $E_D^0$ ,  $E_A^0$  are, respectively, the redox standard potential of the donor and acceptor;  $E^0$  is the standard potential for the overall reaction. Thus, the standard reaction Gibbs energy (the Gibbs free energy or driving force) of electron transfer reaction can be written

$$\Delta G^0 = -nFE^0 = -nF(E_A^0 - E_D^0) \quad (2.32)$$

When the reactants and/or the products are charged, the coulombic interaction between the donor and acceptor has to be taken into account. The electrostatic work term required to bring the reactants together ( $w_R$ ) and that required to bring the products together ( $w_P$ ) are introduced:

$$\Delta G^0 = -nFE^0 = -nF(E_A^0 - E_D^0) + w_R - w_P \quad (2.33)$$

with,

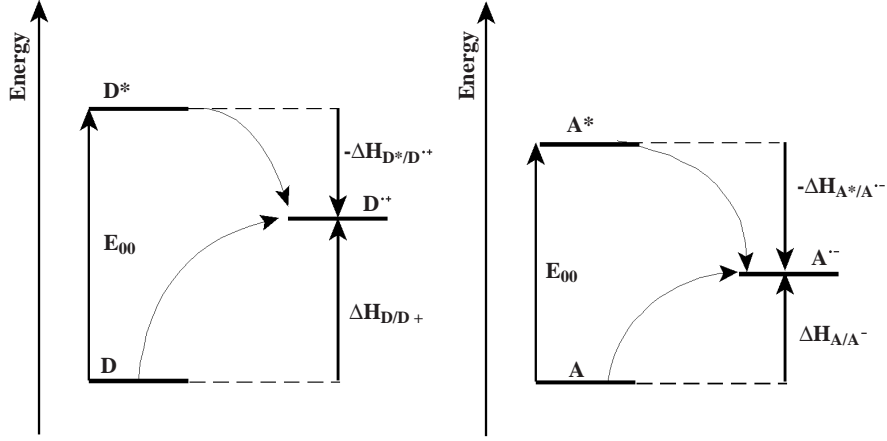
$$w_R = \frac{e_0^2 z_D^R z_A^R}{4\pi\epsilon_0\epsilon_s d} \quad (2.34)$$

$$w_P = \frac{e_0^2 z_D^P z_A^P}{4\pi\epsilon_0\epsilon_s d} \quad (2.35)$$

and  $z_X^R$ ,  $z_X^P$  are the charges of the reactant and the product species X, respectively.

**Special case of PET.** In photoinduced electron transfer, the initial step is the excitation of donor or acceptor. This excitation is called Franck-Condon excitation and is a vertical transition (see more in section 2.3.2). That means an electronic transition takes place much faster than the nuclei can respond (without a change of the nuclear coordinates). The excitation promotes an electron to a higher energy orbital<sup>4</sup> as described in Fig. 2.9. With the assumption the structures of D, D\* and

<sup>4</sup> The electron gains an extra energy and rapidly relaxes (before it has time to react) to the lowest vibrational excited state (Kasha's rule).


 Fig. 2.9: Enthalpy changes ( $\Delta H$ s) for formation of  $D^{\bullet+}$  or  $A^{\bullet-}$ 

$D^{\bullet+}$  ( $A$ ,  $A^*$  and  $A^{\bullet-}$ ) are the same, meaning that  $\Delta G = \Delta H$ , we can write

$$\Delta G_{D^*/D^{\bullet+}} = \Delta G_{D/D^{\bullet+}} - E_{00} \quad (2.36)$$

$$\Delta G_{A^*/A^{\bullet-}} = \Delta G_{A/A^{\bullet-}} - E_{00} \quad (2.37)$$

From the definition of  $E_{redox}^0$  or electromotive force of the half-reaction,  $\Delta G^0 = -nFE_{redox}^0$ , Eqs. 2.36 and 2.37 end up:

$$nFE_{D^{\bullet+}/D^*}^0 = nFE_{D^{\bullet+}/D}^0 - E_{00} \implies E_{D^{\bullet+}/D^*}^0 = E_{D^{\bullet+}/D}^0 - \frac{E_{00}}{nF} \quad (2.38)$$

$$-nFE_{A^*/A^{\bullet-}}^0 = -nFE_{A/A^{\bullet-}}^0 - E_{00} \implies E_{A^*/A^{\bullet-}}^0 = E_{A/A^{\bullet-}}^0 + \frac{E_{00}}{nF} \quad (2.39)$$

If the photoinduced electron transfer between neutral molecules results in the formation of free ions (FIS)

$$\Delta G^0 = -nF(E_A^0 - E_D^0) - E_{00} \quad (2.40)$$

If the photoinduced electron transfer between neutral molecules results in the formation of the solvent-separated ion pair (SSIP)

$$\Delta G^0 = -nF(E_A^0 - E_D^0) - \frac{e_0^2}{4\pi\epsilon_0\epsilon_s d} - E_{00} \quad (2.41)$$

where the second term is the coulombic stabilization for two charged species in close proximity. Eq. 2.41 is well known as the Rehm-Weller relation, which provides a useful expression for calculating the free energy change associated with PET reactions.<sup>[32]</sup>

## 2.3 The formation and fate of the electronically excited states

### 2.3.1 The rules governing the transition between two energy states

**The basic of selection rules.** Regardless of vibrational relaxation, in quantum chemistry, the transition between two given energy states is possible if and only if a transition moment is created. In other words, the value of the transition moment integral,  $\int_{-\infty}^{+\infty} \psi_2^* \mu \psi_1 d\tau$ , determines the allowedness or forbiddenness of an electronic transition, with the overall wavefunctions of the two states  $\psi_1$  and  $\psi_2$ , the transition moment operator  $\mu$ . If the value of this integral is non-zero the transition is allowed, otherwise the transition is forbidden. In practice, it is sufficient to check the symmetry<sup>5</sup> of transition moment function,  $\psi_2^* \mu \psi_1$ , without necessity of calculating the integral. The transition moment integral is non-zero if the transition moment function,  $\psi_2^* \mu \psi_1$ , is symmetric in at least one variable.

According to the Born-Oppenheimer approximation, the representation of the overall wavefunctions is the product of the individual  $\psi_v$  vibrational and  $\psi_e$  electronic space and  $\psi_s$  spin wavefunctions:  $\psi = \psi_e \psi_v \psi_s$ .  $\mu = \mu_e + \mu_N$ , electron-dipole operator  $\mu_e$  and nucleus-dipole operator  $\mu_N$ . The probability amplitude  $P$  for the transition between these two energy states is given by:<sup>[33]</sup>

$$P_{1 \rightarrow 2} = \int_{-\infty}^{+\infty} \psi_2^* \mu \psi_1 d\tau = \int_{-\infty}^{+\infty} \psi_{2v}^* \psi_{1v} d\tau_n \int_{-\infty}^{+\infty} \psi_{2e}^* \mu_e \psi_{1e} d\tau_e \int_{-\infty}^{+\infty} \psi_{2s}^* \psi_{1s} d\tau_s + \int_{-\infty}^{+\infty} \psi_{2e}^* \psi_{1e} d\tau_e \int_{-\infty}^{+\infty} \psi_{2v}^* \mu_N \psi_{1v} d\tau_n \int_{-\infty}^{+\infty} \psi_{2s}^* \psi_{1s} d\tau_s$$

The first integral after the plus sign in this equation is equal to zero because electronic wavefunctions of different states are orthogonal. Thus

$$P_{1 \rightarrow 2} = \int_{-\infty}^{+\infty} \psi_{2v}^* \psi_{1v} d\tau_n \int_{-\infty}^{+\infty} \psi_{2e}^* \mu_e \psi_{1e} d\tau_e \int_{-\infty}^{+\infty} \psi_{2s}^* \psi_{1s} d\tau_s \quad (2.42)$$

This is an expression for the probability amplitude in terms of separate electronic space, spin and vibrational contributions. The first integral in Eq. 2.42 is the quantum chemical description of the Franck-Condon principle. The second integral in

---

<sup>5</sup> Function  $f(x)$  is symmetric if  $f(-x) = f(x)$  and thus  $\int_{-\infty}^{+\infty} f(x) \neq 0$   
While function  $f(x)$  is anti-symmetric if  $f(-x) = -f(x)$  and thus  $\int_{-\infty}^{+\infty} f(x) = 0$

Eq. 2.42 is referred to the orbital selection rule. The last term in Eq. 2.42 indicates the spin selection rule.<sup>6</sup> The spin selection rule is the largest contributor, followed by orbital selection rules. The Franck-Condon factor only weakly affects the intensity of the transition.

**Selection rules for molecular transition.**<sup>[34]</sup> For molecules, the rules governing the transition between two given energy states are:

(i) Allowing the changes in the component of the total orbital angular momentum in the direction of the molecular axis that is characterized by orbital quantum number  $\Delta\Lambda = 0; \pm 1$ .

(ii) Total spin angular momentum must be conserved (the spin conservation rule)  $\Delta S = 0$

(iii) Molecular-symmetry properties of the energy states must be conserved.

**Modification of selection rules.**<sup>[34]</sup>

(i) *Spin-orbital interaction.* The spin selection rule can be modified by spin-orbit coupling interactions. The transition between states of unlike multiplicities can occur under the influence of intramolecular and intermolecular perturbations. These perturbations are functions of the magnetic field near the nucleus and are therefore a function of atomic mass (heavy atoms effect).

(ii) *Vibronic interactions.* The symmetry forbidden transition can be made partially allowed by vibronic interactions (the molecular vibration can change the molecular symmetry).

### 2.3.2 The formation of photoexcited states

When electromagnetic radiation acts on an atom or a molecule, the electric field of the radiation tends to disturb the charge cloud around atom or molecule. Then the disturbed molecule becomes a source of electromagnetic radiation which leads to one of the consequential phenomena such as scattering, reflection and absorption. The origin of these phenomena depends on the frequency of the incident radiation,  $\nu_i$ , and natural frequency of the molecule at its energy state,  $\nu_n$ . When  $\nu_i \approx \nu_n$  (an atom or a molecule absorbs light), an electron on the outermost shell of the molecule is promoted to a higher energy level.

---

<sup>6</sup> The product of the second and third integrals is sometimes called the electronic transition moment.

The absorption of light by materials follows Lambert-Beer's law:

$$A = \log \frac{I_0}{I} = l\epsilon C \quad (2.43)$$

where  $A$  is the absorbance at a certain frequency;  $I_0$  and  $I$  are the incident intensity and transmitted intensity respectively.  $\epsilon$  is the molar absorption coefficient;  $l$  is the optical pathlength and the concentration of the absorbing species  $C$ .

In addition to Franck-Condon excitation mentioned earlier, with the quantum chemical description of the Franck-Condon principle, the wavefunction of the lowest vibrational level of the ground state would be projected onto one vibrational wavefunction of the higher electronic state, Fig. 2.10. The overlap matrix element

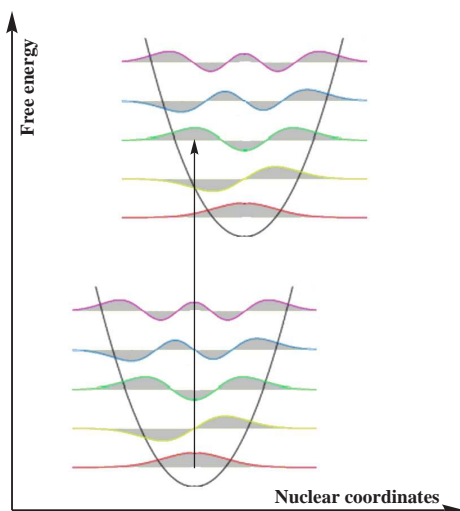


Fig. 2.10: Franck-Condon excitation

between these vibrational nuclear states is defined as the Franck-Condon factor. The molecule undergoes a transition to the upper vibrational state (excited state) that most closely resembles (with the highest probability) the vibrational wavefunction of the lower electronic state (ground state).<sup>[25]</sup> The intensity of the transition (the absorption or emission intensity) is proportional to the modulus squared probability amplitude,  $|P_{1 \rightarrow 2}|^2$  or  $|P_{2 \rightarrow 1}|^2$ , - probability of the transition (proportional to the Einstein coefficient of absorption or emission as well).

### 2.3.3 The reactivity of the excited states

As a result of excitation, molecules in an electronically excited state have chemical and physical properties that differ from those of ground-state molecules. These differences such as dipole moment, redox potential, acidity and basicity lead to alter the

reactivity of excited state molecules. Changes in dipole moment and polarizability are often observed by the effect of solvent on the absorption and emission spectra. The energy difference between absorption and emission is expressed in frequency terms as the following equation:

$$\Delta\nu = \nu_a - \nu_f = \frac{2(\mu_e - \mu_g)^2}{\hbar a^3} \Delta f \quad (2.44)$$

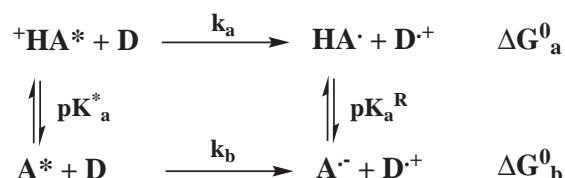
with the Onsager factor  $\Delta f$ ,

$$\Delta f = \left\{ \frac{\epsilon_s - 1}{2\epsilon_s + 1} - \frac{n_D^2 - 1}{2n_D^2 + 1} \right\} \quad (2.45)$$

Here  $\mu_g$  and  $\mu_e$  denote the ground state and excited state dipole moments. The plot of the quantity  $\Delta\nu$  vs.  $\Delta f$  gives the information about the difference between ground state and excited state dipole moments.

As described earlier,  $E_{D^+/D}^0 < E_{D^+/D}^*$  means that the excited state is a better electron donor than the ground state. While  $E_{A^*/A^-}^0 > E_{A^*/A^-}^*$  implies that the excited state is a better electron acceptor than its ground state.

**Excited state acidity and basicity.**<sup>[35]</sup> Both protonated and deprotonated forms of excited molecules may participate in electron transfer reactions, Scheme 2.3. Corresponding driving forces of the reaction in Scheme 2.3 can be expressed:



Schema 2.3: Reaction scheme of the protonated and deprotonated excited molecules

$$\Delta G_a^0 = nF[E_{D^+/D}^0 - E_{+HA/HA\cdot}^0] - E_{00}^a \quad (2.46)$$

$$\Delta G_b^0 = nF[E_{D^+/D}^0 - E_{A^*/A^-}^0] - E_{00}^b \quad (2.47)$$

The difference in driving forces between involved excited states is given,

$$\Delta\Delta G^0 = \Delta G_b^0 - \Delta G_a^0 = [nF(E_{+HA/HA\cdot}^0 - E_{A^*/A^-}^0) + (E_{00}^a - E_{00}^b)] \quad (2.48)$$

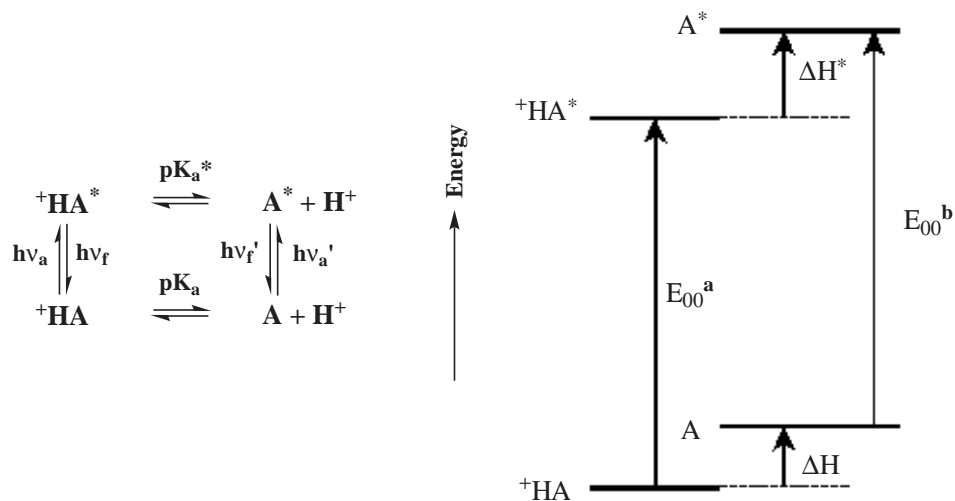
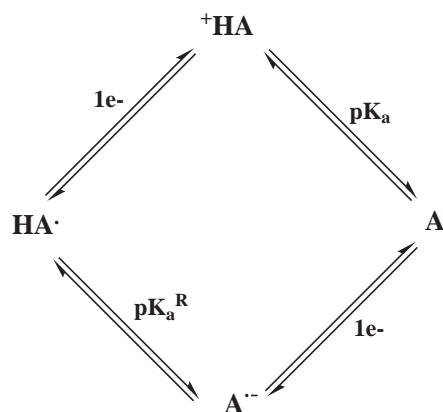


Fig. 2.11: Förster's acid-base equilibria and energy cycle

On the other hand, from Förster's cycle with the assumption that the entropic change from acid to conjugate base in the ground state equals to that in the excited state, one gets:

$$\begin{aligned}
 E_{00}^a - E_{00}^b &= \Delta H - \Delta H^* = \Delta G_{+HA}^0 - \Delta G_{+HA^*}^0 \\
 &= -RT \ln K_a + RT \ln K_a^* = 2.303RT(pK_a - pK_a^*) \quad (2.49)
 \end{aligned}$$

Here  $\Delta H$  (and  $\Delta G_{+HA}^0$ ) and  $\Delta H^*$  (and  $\Delta G_{+HA^*}^0$ ) are enthalpies (and free energy) of proton dissociation in the ground and the excited states, respectively.



Scheme 2.4: Acid-base equilibrium involving its radicals for  $+HA$

Furthermore, when one considers the acid-base equilibrium involving its radicals, Scheme 2.4, it can be read as follows. The energy changes by whichever pathway

starting from  ${}^+HA$  to  $A^-$  must be conserved.

$$-nFE_{+HA/HA}^0 + RT\ln K_a^R = -RT\ln K_a - nFE_{A/A^-}^0 \quad (2.50)$$

And we have:

$$nF(E_{+HA/HA}^0 - E_{A/A^-}^0) = 2.303RT(pK_a^R - pK_a) \quad (2.51)$$

From Eqs. 2.48, 2.49 and 2.51, resulting equation has a form:

$$\Delta\Delta G^0 = 2.303RT(pK_a^R - pK_a^*) \quad (2.52)$$

In the case of endothermic electron transfer reactions, e.g.  $\Delta G_a^0, \Delta G_b^0 \gg 0$ , one may write:

$$\ln \frac{k_a}{k_b} = \frac{\Delta G_b^* - \Delta G_a^*}{RT} \propto \frac{\Delta\Delta G^0}{RT} = 2.303(pK_a^R - pK_a^*) \quad (2.53)$$

The outcome of Eq. 2.53 is significant for predicting the reactivity of  ${}^+HA^*$  and  $A^*$  based on the knowing of  $pK_a^R$  and  $pK_a^*$  values. If  $pK_a^R > pK_a^*$  then  $k_a > k_b$  and vice versa.

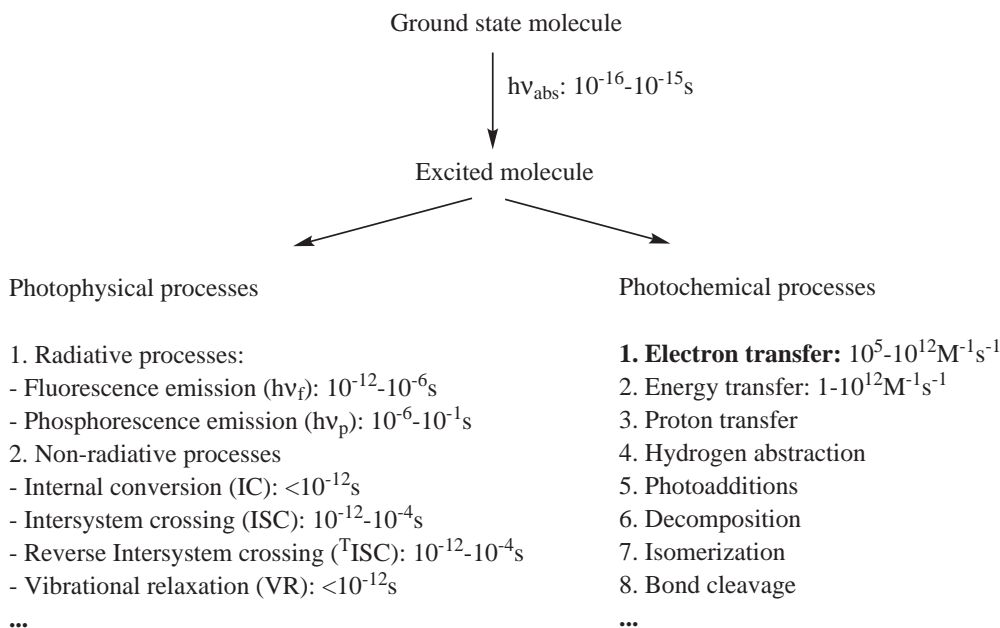
### 2.3.4 The fate of photoexcited states

Since the quantum yield is one of the most important notions to photochemists, it should be mentioned for the sake of completeness. The primary quantum yield,  $\phi$ , is defined as the number of photophysical or photochemical events that lead to primary products divided by the number of photons absorbed by the molecule in the same interval.

$$\phi = \frac{\text{number of events}}{\text{number of photons absorbed}} = \frac{\text{rate of process}}{\text{intensity of light absorbed}}$$

A molecule excited to a higher energy state must eventually return to the ground state by photophysical processes (radiative and/or non-radiative processes), unless it involves a photochemical reaction and loses its identity, Scheme 2.5. The sum of primary quantum yields  $\phi_i$  for all photophysical and photochemical events  $i$  must be equal to 1. For instance, if an excited singlet state decays to the ground state only via the photophysical processes, then:

$$\phi_f + \phi_{IC} + \phi_{ISC} + \phi_p = 1$$



*Schema 2.5:* The formation and fate of the excited molecule including the time-scale and the bimolecular rate constants

where  $\phi_f$ ,  $\phi_{IC}$ ,  $\phi_{ISC}$  and  $\phi_p$  are the quantum yields of fluorescence, internal conversion, intersystem crossing, and phosphorescence, respectively. If the excited singlet state also participates in a primary photochemical reaction with quantum yield  $\phi_R$ , then:

$$\phi_f + \phi_{IC} + \phi_{ISC} + \phi_p + \phi_R = 1$$

### Decay of excited singlet state.

Considering the formation and fate of a singlet excited state in the absence of a photochemical reaction (cf. Fig. 2.12 and Tab. 2.1), the steady-state approximation can be applied:

$$\frac{d[S^*]}{dt} = P[S] - k_f[S^*] - k_{IC}[S^*] - k_{ISC}[S^*] = 0$$

The fluorescent quantum yield is

$$\phi_{f,0} = \frac{k_f[S^*]}{P[S]} = \frac{k_f}{k_f + k_{IC} + k_{ISC}} \quad (2.54)$$

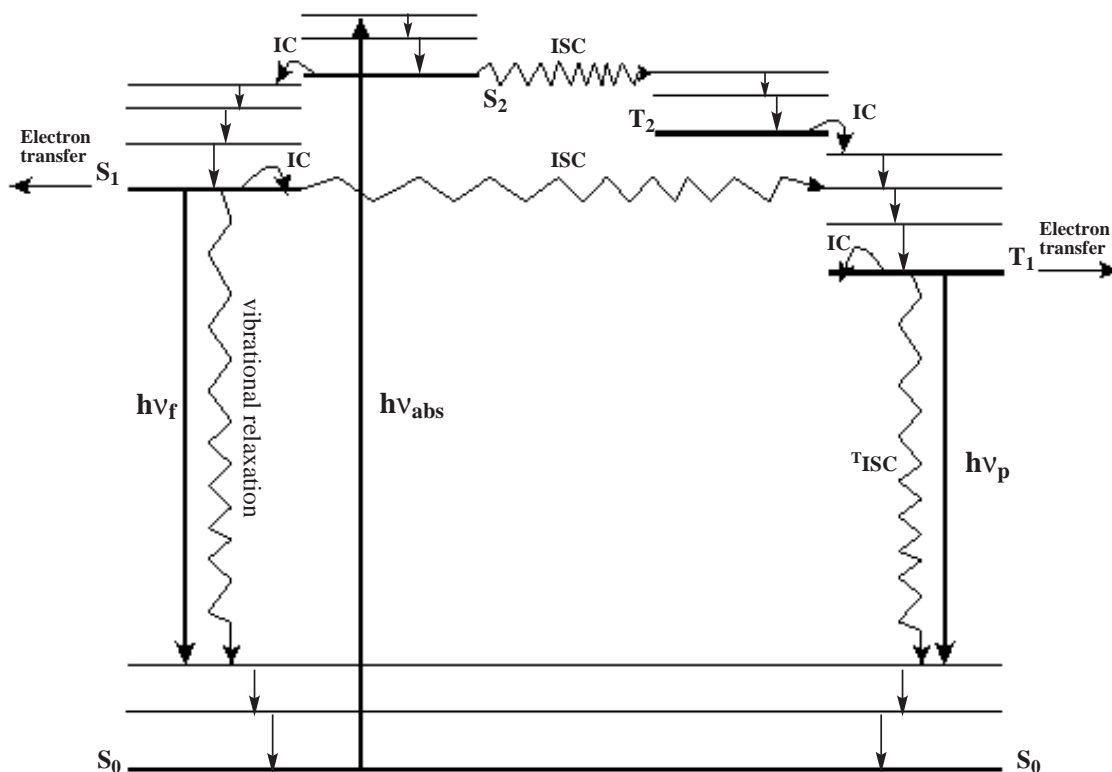


Fig. 2.12: Jablonski diagram that includes electron transfer as one of the deactivation pathways.

The fluorescence lifetime,  $\tau_{f,0}$ , is defined as:

$$\tau_{f,0} = \frac{1}{k_f + k_{IC} + k_{ISC}} \quad (2.55)$$

The addition of a quencher,  $Q$ , opens an additional channel for deactivation of  $S^*$ . Using the steady-state approximation, we have:

$$\frac{d[S^*]}{dt} = P[S] - k_f[S^*] - k_{IC}[S^*] - k_{ISC}[S^*] - k_q[S^*][Q] = 0$$

and actual fluorescence quantum yield

$$\phi_f = \frac{k_f[S^*]}{P[S]} = \frac{k_f}{k_f + k_{IC} + k_{ISC} + k_q[Q]} \quad (2.56)$$

Tab. 2.1: The formation and fate of an excited state.<sup>a</sup>

Step		Rate
Absorption	$S + h\nu_i \rightarrow S^*$	$P[S]$
Fluorescence	$S^* \rightarrow S + h\nu_f$	$k_f[S^*]$
Internal conversion	$S^* \rightarrow S$	$k_{IC}[S^*]$
Intersystem crossing	$S^* \rightarrow T^*$	$k_{ISC}[S^*]$
Phosphorescence	$T^* \rightarrow S + h\nu_p$	$k_p[T^*]$
Singlet quenching	$S^* + Q \rightarrow E + F$	${}^1k_q[S^*][Q]$
Triplet quenching	$T^* + Q \rightarrow E + F$	${}^3k_q[T^*][Q]$
Reverse intersystem crossing	$T^* \rightarrow S$	$k_{ISC}^T[S^*]$

<sup>a</sup> Only important reaction steps in deactivating the excited molecule back to the ground state are mentioned;  $S$  is an absorbing species,  $P$  pumping term,  $S^*$  an excited singlet state,  $T^*$  an excited triplet state and  $Q$  a quencher;  $h\nu_i$ ,  $h\nu_f$  and  $h\nu_p$  are the energies of the incident, fluorescent, and phosphorescent photons, respectively.

The actual fluorescence lifetime,  $\tau_f$ , is defined as:

$$\tau_f = \frac{1}{k_f + k_{IC} + k_{ISC} + {}^1k_q[Q]} \quad (2.57)$$

From Eqs. 2.54 and 2.56 one gets:

$$\frac{\phi_{f,0}}{\phi_f} = 1 + \tau_{f,0} \times {}^1k_q[Q] = 1 + K_{SV}[Q] \quad (2.58)$$

The relationship of fluorescence quantum yields and the quencher concentration  $[Q]$  in Eq. 2.58 is called the Stern-Volmer (SV) equation with  $K_{SV}$  being the SV-constant. This equation is usually used to measure the quenching rate constant by the steady-state measurements with  $\tau_{f,0}$  known.

Note that

$$\frac{\phi_f}{\phi_{f,0}} = \frac{I_f}{I_{f,0}} = \Gamma = (1 + K_{SV}[Q])^{-1} \quad (2.59)$$

is referred to the fractional fluorescence that is unquenched,  $\Gamma$ .

On the other hand, From Eqs. 2.55 and 2.57 one also gets:

$$\frac{\tau_{f,0}}{\tau_f} = 1 + \tau_{f,0} \times {}^1k_q[Q] = 1 + K_{SV}[Q] \quad (2.60)$$

The SV-equation now is generally applied for measuring the quenching rate constant by the lifetime measurements (time-resolved measurements).

### Decay of excited triplet state.

(i) Consider the formation and fate of a triplet excited state in the absence of a photochemical reaction (cf. Fig. 2.12 and Tab. 2.1).

The steady-state approximation applies for this case:

$$\frac{d[T^*]}{dt} = k_{ISC}[S^*] - k_{ISC}^T[T^*] - k_p[T^*] = 0$$

And one easily has an expression for the phosphorescent quantum yield:

$$\phi_P = \frac{d[T^*]}{P[S]} = \frac{k_{ISC}}{(k_f + k_{IC} + k_{ISC})} \frac{k_p}{(k_{ISC}^T + k_p)} \quad (2.61)$$

The triplet quantum yield,  $\phi_T$ , is defined as:

$$\phi_T = \frac{k_{ISC}}{k_f + k_{IC} + k_{ISC}} \quad (2.62)$$

(ii) Assume a triplet excited state is generated without emission from the excited singlet ( $\phi_T \approx 1$ ) and triplet state ( $\phi_P \approx 0$ ) but presence of a photochemical reaction (cf. Fig. 2.12 and Tab. 2.1).

This assumption is, actually, often observed practically with flash photolysis at room temperature. Obviously the Stern-Volmer equation is readily deduced

$$\frac{{}^3\tau_0}{{}^3\tau} = 1 + {}^3\tau_0 \times k_q[Q] = 1 + K_{SV}[Q] \quad (2.63)$$

Here  ${}^3\tau_0$  and  ${}^3\tau$  denote triplet life time of the excited molecule in the absence and presence of quencher, respectively.

### Deviations from the Stern-Volmer equation.<sup>[36]</sup>

(i) Deviation from Stern-Volmer relation may arise if ground state quenching is present.

$K_0$  is the molar equilibrium constant for the formation of the complex (nonfluorescent complex), (SQ) in the ground state then,

$$K_0 = \frac{[(SQ)]}{[S][Q]} = \frac{[S]_0 - [S]}{[S][Q]} = \frac{[S]_0}{[S][Q]} - \frac{1}{[Q]} \quad (2.64)$$

From this equation we have the fractional fluorescence that is not complexed,  $f$

$$f = \frac{[S]}{[S]_0} = \frac{1}{1 + K_0[Q]} \quad (2.65)$$

In this case the fractional fluorescent intensity remaining is given by the product of the noncomplexed fraction,  $f$ , and unquenched fraction,  $\Gamma$  (Eq. 2.59):

$$\frac{I_f}{I_{f,0}} = f \times \Gamma = (1 + K_0[Q])^{-1}(1 + K_{SV}[Q])^{-1} \quad (2.66)$$

Now a rearrangement of Eq. 2.66 yields:

$$\frac{I_{f,0}}{I_f} = 1 + (K_0 + K_{SV})[Q] + K_0K_{SV}[Q]^2 \quad (2.67)$$

Hence, in consequence of combining ground state and dynamic excited state quenching the Stern-Volmer plot is no longer linear.

(ii) In the absence of ground state quenching, a deviation from Stern-Volmer relation may arise due to the quenching „sphere of action”.

The term *sphere of action* means existing a sphere of volume  $V$  within which the probability of quenching is unity<sup>7</sup>. Usually it occurs as the quencher concentration is high, the fluorophore nearby quencher. Thus, only fluorophores not nearby quenchers are fluorescent. The Stern-Volmer equation which describes this situation is

$$\frac{I_{f,0}}{I_f} = (1 + K_{SV}[Q])\exp\left(\frac{[Q]VN_A}{1000}\right) \quad (2.68)$$

where  $V$  is volume of the sphere;  $\exp\left(\frac{-[Q]VN_A}{1000}\right)$  is the probability that no quenchers are nearby observable fluorophores. Hence, one sees a positive deviation from the Stern-Volmer plot.

## 2.4 Photo-induced proton transfer<sup>[1]</sup>

This section focuses on kinetics of proton transfer reactions where water molecules act as proton donors and acceptors.

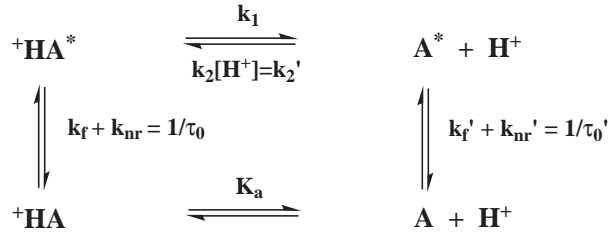
**Proton transfer of singlet excited molecules.** According to Scheme 2.6, one can apply the general rate law for time-evolution of the involved species.

$$\frac{d[{}^+HA^*]}{dt} + (k_1 + k_f + k_{nr})[{}^+HA^*] = k_2'[A^*] \quad (2.69)$$

$$\frac{d[A^*]}{dt} + (k_2' + k_f' + k_{nr}')[A^*] = k_1[{}^+HA^*] \quad (2.70)$$

---

<sup>7</sup> Let's call the quenching sphere of action as the apparent static quenching that occurs before molecules diffuse.



Schema 2.6: Acid-base equilibrium of singlet excited molecules

Assume that at a certain pH value only  ${}^+\text{HA}$  or  $\text{A}$  is excited so that  $[\text{A}^*]_0 = 0$  or  $[{}^+\text{HA}^*]_0 = 0$  at  $t = 0$  is set as initial conditions. These differential equations, then can be passed and their solutions are:

$$[{}^+\text{AH}^*] = [{}^+\text{AH}^*]_0 e^{-t/\tau} \quad (2.71)$$

$$[\text{A}^*] = \frac{k_1 [{}^+\text{AH}^*]_0}{(k_1 + k_f + k_{nr}) - (k_2' + k_f' + k_{nr}')} (e^{-t/\tau_0'} - e^{-t/\tau}) \quad (2.72)$$

here

$$\tau = \frac{1}{k_1 + k_f + k_{nr}} \quad (2.73)$$

From the lifetime measurement we would be able to know the value of  $\tau$  (Eq. 2.71) and thus, determine  $k_1$ . But it is not easy to get  $k_2$  unless the time-evolution curve is fitted properly with Eq. 2.72. Therefore, this method is experimentally impractical.

In 1952 Weller<sup>[37]</sup> reported that the pH-dependences of the fluorescences of aromatic acids and bases are quantitatively related to the kinetics of proton transfer. He was successful to measure the forward and backward proton transfer rate using steady-state approach. He introduced the term probability,  $\rho$  that a molecule will still be in the excited state at time  $t$  after excitation.

$$\frac{d\rho}{dt} + (k_f + k_{nr} + k_1)\rho = k_2'\rho' \quad (2.74)$$

$$\frac{d\rho'}{dt} + (k_f' + k_{nr}' + k_2')\rho' = k_1\rho \quad (2.75)$$

Solutions that come out from these equations lead to the following expressions:

$$\frac{\phi_f}{\phi_{f,0}} = \frac{\rho_0 + k_2'\tau_0'(\rho_0 + \rho_0')}{1 + k_1\tau_0 + k_2'\tau_0'} \quad (2.76)$$

$$\frac{\phi'_f}{\phi'_{f,0}} = \frac{\rho'_0 + k_1\tau_0(\rho_0 + \rho'_0)}{1 + k_1\tau_0 + k'_2\tau'_0} \quad (2.77)$$

In some cases Eqs. 2.76 and 2.77 could be simplified.

If the compound is in the  $^+HA$  form in the ground state and this is only form excited, then  $\rho_0 = 1$ ,  $\rho'_0 = 0$ . And assume the pH increases ( $pH < pK_a$ ) so that  $k'_2$  is small, Eqs. 2.76 and 2.77 simplify to:

$$\frac{\phi_f}{\phi_{f,0}} = \frac{1}{1 + k_1\tau_0} \quad (2.78)$$

$$\frac{\phi'_f}{\phi'_{f,0}} = \frac{k_1\tau_0}{1 + k_1\tau_0} \quad (2.79)$$

From these equations  $k_1\tau_0$  can be determine and therefore, the value of  $k_1$  value. If the pH increases further ( $pH \approx pK_a$ ) so that  $k'_2\tau'_0 \approx k_1\tau_0$ , then the pH-dependence of the quantum yields relative to  $\phi_0$  is given:

$$\frac{\phi_f/\phi_{f,0}}{\phi'_f/\phi'_{f,0}} = \frac{1}{k_1\tau_0} + \frac{k_2\tau'_0}{k_1\tau_0}[H^+] \quad (2.80)$$

Finally  $k_2\tau'_0$  is easily accessible and thus, determines  $k_2$  value. This method mentioned here is a useful experimental method for measuring the forward and backward proton transfer reaction rate. In other words,  $K_a^*$  of the singlet excited state may be measured (or sometimes called as fluorescent titration method). Recall another famous method for determining  $pK_a^*$  derived by Förster, Eq. 2.49 (see section 2.3.3).

$$E_{00}^a - E_{00}^b = 2.303RT(pK_a - pK_a^*)$$

where the 0-0 transition energy ( $E_{00}^a$  or  $E_{00}^b$ ) can be calculated in term of frequencies from corresponding maxima of absorption,  $\nu_a$  and emission,  $\nu_f$ , bands

$$\nu_{00} = \frac{1}{2}(\nu_a + \nu_f)$$

However, since Förster's method gives no information about relevant rates of the involved species, it does not indicate whether or not proton transfer.

If the compound is in the A form in the ground state and this is the only form excited, meaning that  $\rho_0 = 0$ ,  $\rho'_0 = 1$ . In this case  $k_2\tau'_0$  and  $k_1\tau_0$  cannot be separated.

The equation of pH-dependence of the quantum yields relative to  $\phi_0$  has a form:

$$\frac{\phi_f/\phi_{f,0}}{\phi'_f/\phi'_{f,0}} = \frac{k_2\tau_0'}{1 + k_1\tau_0} [H^+] \quad (2.81)$$

and only

$$\frac{k_2\tau_0'}{1 + k_1\tau_0}$$

can be determined.

**Proton transfer of triplet excited molecules.** A similar reaction scheme as Scheme 2.6 is used to describe the proton transfer reaction of triplet excited molecules, only one note now using  $k_p$  (the phosphorescent rate constant) instead of  $k_f$ . Moreover, the general rate law for time-evolution of the involved species is written in the same way. The most important parameter comes out is the triplet lifetime  $\tau$ ,

$$\frac{1}{\tau} = \frac{k_2'}{k_1 + k_2'}(k_p + k_{nr}) + \frac{k_1}{k_1 + k_2'}(k'_p + k_{nr}') \quad (2.82)$$

From Eq. 2.82 it can be seen that at low pH when  $k_2'$  is large

$$\frac{1}{\tau} \approx k_p + k_{nr} \quad (2.83)$$

while at high pH if  $k_1$  is large

$$\frac{1}{\tau} \approx k'_p + k_{nr}' \quad (2.84)$$

Over the intermediate range of pH, an arrangement of Eq. 2.82 leads to

$$\frac{1}{\tau} = \frac{k_1}{k_2} \left[ \frac{1}{[H^+]} \left( \frac{1}{\tau} - (k'_p + k_{nr}') \right) \right] + k_p + k_{nr} \quad (2.85)$$

This equation is significant important in the sense of showing pH-dependent triplet lifetime. A plot  $1/\tau$  vs.  $1/\tau[H^+]$  gives a  $k_1/k_2$  or  $K_a^*$  value in addition to triplet-triplet absorbance titration method using to determine a  $K_a^*$  value.

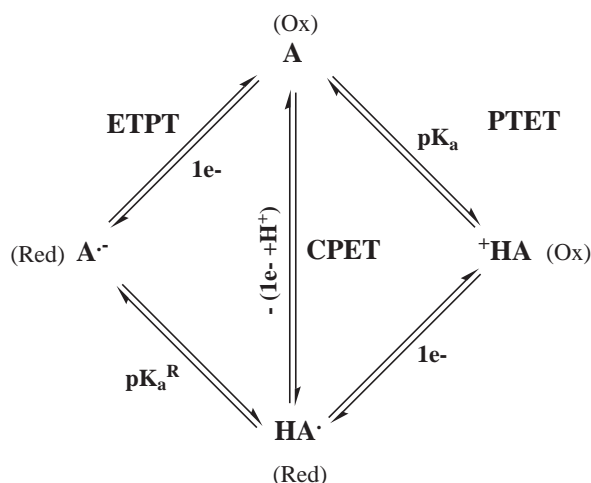
## 2.5 Proton coupled electron transfer

This section represents a general understanding of proton coupled electron transfer. It also helps to answer the question: What factors distinguish a step-wise electron transfer followed by proton transfer or vice versa from a concerted transfer of a proton and an electron.

### 2.5.1 Basic concepts

„Proton coupled electron transfer” (PCET) refers to a process in which proton(s) and electron(s) are transferred in one or more steps. Processes which involve: multiple electrons and protons transfer, hydride transfer (number of electrons and protons are not equal), and protons regulate ET even they do not transfer, are out of scope of this thesis. Here deals only with one proton coupled one electron transfer case. There are many equivalent terms that indicate to this process. Using the below abbreviation and description make the reaction mechanism clearly in author’s point of view. Proton coupled electron transfer may proceed via concerted or stepwise pathways.<sup>[38]</sup> In the former proton and electron transfer are concerted (CPET), eg. the diagonal reaction as illustrated in Scheme 2.7. The latter may include electron transfer followed by proton transfer (ETPT) or proton transfer followed by electron transfer (PTET), eg. square reactions in Scheme 2.7. It is noteworthy in the chemical view that PCET and hydrogen atom transfer are identical. The activation energy barriers required for each, however, are not equal. Photo-induced PCET is one special case of PCET.

### 2.5.2 Thermodynamics of the PCET reaction



Scheme 2.7: Pathways for PCET

Free energy changes for the given three possible pathways as described in Scheme 2.7 can be determined from the redox potentials of the relevant couples. For simplicity here assuming that the redox potential of donor is independent on hydrogen ion (1+) concentration. Whatever the reaction mechanism, maybe, the global Nernst

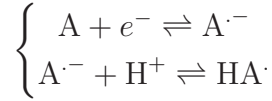
equation can be applied for the thermodynamics of the redox reaction:<sup>[39]</sup>

$$E = E_{ap}^{0,ox/red} + \frac{RT}{nF} \ln \frac{\sum[ox]}{\sum[red]} \quad (2.86)$$

where E is electrode potential;  $E_{ap}^{0,ox/red}$  is the apparent standard potential of the corresponding redox couple.  $\sum[ox]$  and  $\sum[red]$  are the total concentration of oxidized and reduced species in solution, respectively.

With reactions demonstrated in Scheme 2.7, it is assumed that  $\sum[ox] \approx [A]$  and  $\sum[red] \approx [HA]$ .

**ETPT pathway**, consider an electrochemical half-reaction and followed by a protonation:



The equilibrium redox potential reads as

$$E = E_{A/A^-}^0 + \frac{RT}{F} \ln \frac{[A]}{[A^-]} \approx E_{A/A^-}^0 + \frac{RT}{F} \ln \frac{\sum[ox]}{\sum[red] \cdot \frac{K_a^R}{[H^+]}} \quad (2.87)$$

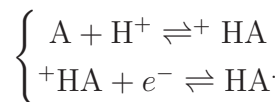
Hence the apparent standard redox potential is

$$E_{ap}^0 = E_{ETPT}^0 + \frac{RT}{F} \ln \frac{[H^+]}{K_a^R} \approx E_{ETPT}^0 - 0.059(pH - pK_a^R) \quad (2.88)$$

The standard free energy change of the PET pathway is given by

$$\Delta G_{ETPT}^0 = -nF[E_{ETPT}^0 - E_{D^+/D}^0] \quad (2.89)$$

**PTET pathway**, a protonation followed by reduction:



For the redox potential one can write

$$E = E_{^+HA/HA}^0 + \frac{RT}{F} \ln \frac{[^+HA]}{[HA]} \approx E_{^+HA/HA}^0 + \frac{RT}{F} \ln \frac{\sum[ox] \cdot \frac{[H^+]}{K_a}}{\sum[red]} \quad (2.90)$$

and,

$$E_{ap}^0 = E_{PTET}^0 + \frac{RT}{F} \ln \frac{[H^+]}{K_a} \approx E_{PTET}^0 - 0.059(pH - pK_a) \quad (2.91)$$

In this case the standard free energy change is found as

$$\Delta G_{PTET}^0 = -nF[E_{PTET}^0 - E_{D^{+}/D}^0] \quad (2.92)$$

**CPET pathway**, consider now a concerted proton and electron transfer:



Applying the global Nernst equation,

$$E = E_{A+H^+/HA^\cdot}^0 + \frac{RT}{F} \ln \frac{[H^+][A]}{[HA^\cdot]} \approx E_{A+H^+/HA^\cdot}^0 + \frac{RT}{F} \ln \frac{\sum[ox]}{\sum[red]} [H^+] \quad (2.93)$$

we have

$$E_{ap}^0 = E_{CPET}^0 + \frac{RT}{F} \ln [H^+] \approx E_{CPET}^0 - 0.059pH \quad (2.94)$$

Finally leading to the expression of the standard free energy change:

$$\Delta G_{CPET}^0 = -nF[E_{CPET}^0 - E_{D^{+}/D}^0] \quad (2.95)$$

### 2.5.3 pH-dependence of PCET

pH-dependence of the driving force playing a crucial role so that it can be used as an experimental tool to discriminate the PCET reaction mechanism.

According to Eq. 2.88, an investigation of  $E_{ap}^0$  with pH should give the information about  $E_{PET}^0$  at which  $pH = pK_a^R$ . From that Eq. 2.89 can be used to calculate the driving force for the proposed EPT reaction.

If a reaction is attributed to the PET reaction, a plot of  $E_{ap}^0$  vs. pH (Eq. 2.91) should give a straight line with a slope of  $-59mV/pH$ . Whence  $E_{PET}^0 = E_{ap}^0$  at  $pH = pK_a$ . From Eq. 2.92 one can calculate the driving force for the PET reaction.

On the other hand, an extrapolation at  $pH = 0$  from the plot of  $E_{ap}^0$  against pH (Eq. 2.94) leads to the  $E_{CPET}^0$  value. Then the driving force of the CPET reaction is given.

Now by a simple comparison we can postulate that which reaction pathway is more favorable in term of thermodynamics, see more in Ref.<sup>[38]</sup>.

#### 2.5.4 Kinetic solvent isotope effects of PCET

Kinetic (solvent) isotope effects (KIEs) refers an isotopic exchange effect on reaction rates by an exchanged solvent. Principally it is referred to the ratio  $k_H/k_D$  if the solvent  $H_2O$  is replaced for  $D_2O$ . Three main factors that cause KIEs are:

- Solvent molecules participate in the reaction as reactants.
- By interaction with reactants, solvent molecules play a role on the stabilization of the activated complex, particularly if this reaction step determines the rate of the reaction.
- In acidic media, an H/D exchange between solvent molecules and reactants may take place.

The range of  $k_H/k_D$  for PCET varies from small ( $\approx 2$ ) to large (larger than the limit of 7.9).

A small value is often observed with solvent exchangeable protons in which H-bonds are formed within precursor complex. For example, KIEs was observed in the intramolecular PCET oxidation reaction of tyrosine residue by trisbipyridine-Ru (III) complex.<sup>[40]</sup> It is shown that  $k_H/k_D = 2$  for EPT at low pH and  $k_H/k_D > 10$  for CPET at pH=10 (the switching mechanism point).

A large KIEs are known for the reaction involving H or D transfer. Huynh and Meyer<sup>[41]</sup> observed a colossal KIEs in the reduction of benzoquinone to hydroquinone by Os(IV)-complexes in 1:1 (vol/vol)  $CH_3CN-H_2O/D_2O$  mixtures. The  $k_H/k_D$  value varies from  $178 \pm 5$  to  $196 \pm 6$  to  $455 \pm 8$  for the complexes of Os (IV) containing sulfur, phosphorus and nitrogen proton-donor, respectively.



**3**

**Experimental**

This chapter describes the reactants, buffer solutions, apparatuses and techniques, measurements procedures, and data handling used in this work.

## 3.1 Reagents

### 3.1.1 Reactants

**Fluorophores** used in this work are 2,2'-dipyridyl and 3,3',4,4'-benzophenone tetracarboxylic acid. BPTC is a generous gift from Dr.Y. Lin, Chinese Academy of Science, Chemistry Department, Beijing.

**Quenchers** include amino acids, DL-alanine, DL-histidine and DL-methionine, and DNA bases, adenine, adenosine, thymine and thymidine.

In Fig. 3.1 structures of all compounds are given. The abbreviation and some important properties of the reactants can be found in Table 3.1.

### 3.1.2 Buffer solutions

All experiments were carried out at room temperature in buffered solutions except for strong acid ( $\text{pH} \leq 2.0$ ) and alkaline ( $\text{pH} \geq 12.0$ ) cases. Water was redistilled from alkaline permanganate.

Since the pH-value is one of the most important parameters in this work, it is necessary to mention some its crucial aspects. Firstly, the pH-value is defined in terms of the activity of hydrogen (1+) ions in solution:

$$\text{pH} = -\log a_{H^+} \quad (3.1)$$

where  $a_{H^+}$  is the activity of hydrogen (1+) ion in aqueous solution. pH would be measured by a pH-meter for a solution with the given compositions at a given temperature. Practical pH measurements generally use the glass electrode, whose response potential usually changes linearly with the inverse of the logarithm of *the activity of hydrated  $H^+$  ions, not the concentration of  $H^+$* .

A buffer solution is defined as an aqueous solution which is resistant to changes in pH with addition of certain amounts of acids/bases or with dilution. pH of a buffer solution that usually containing either a weak acid and its salt or a weak base and its salt is given by well-known Henderson-Hasselbalch equation.<sup>[47]</sup>

$$\text{pH} = \text{p}K_a - \log \frac{C_a}{C_b} \quad (3.2)$$

Tab. 3.1: List of compounds

Compound	Abbreviation		Solubility in water at 25°C <sup>[42]</sup>	$pK_a$	Potentials <sup>h</sup>
3,3',4,4'- benzophenone- tetracarboxylic acid	BPTC	A gift, used as received	—	3.20; 5.12; 2.1 <sup>a</sup> ; 4.7 <sup>a</sup>	—
2,2'-dipyridyl	DP	Sigma-Aldrich $\geq 99\%$ , recrystallized from cyclohexane	—	4.3 <sup>b</sup> ; 5.8 <sup>c</sup>	-1.22 (pH=2.0); -1.42 (pH=6.1)
Thymine	Thy	Alfa-Aesar 97%, used as received	—	9.9 <sup>d</sup>	+1.27 (pH=3.2); +1.45 (pH=0)
Thymidine	dThy	Alfa-Aesar 99%, used as received	—	9.8; 12.9 <sup>d</sup>	—
Adenine	Ade	Alfa-Aesar 99%, used as received	—	4.2; 9.9 <sup>e</sup>	—
Adenosine	dAde	Alfa-Aesar 99%, used as received <sup>g</sup>	—	3.5; 12.5 <sup>e</sup>	—
DL-Alanine	Ala	Alfa-Aesar 99%, used as received	166.9g/kg	2.3; 9.7 <sup>f</sup>	—
DL-Histidine	His	Fluka $\geq 99.0\%$ , used as received	43.5g/kg	1.8; 6.0; 9.2 <sup>f</sup>	—
DL-Methionine	Met	Fluka $\geq 99.0\%$ , used as received	56g/kg	2.3; 9.2 <sup>f</sup>	—

<sup>a</sup> For the triplet state.

<sup>b</sup> Ref. [43]

<sup>c</sup> For the triplet state. Ref. [11]

<sup>d</sup> Ref. [44]

<sup>e</sup> Ref. [45]

<sup>f</sup> Ref. [46]

<sup>g</sup> Need to be stored in the refrigerator at 4°C.

<sup>h</sup> In volts vs. Ag/AgCl

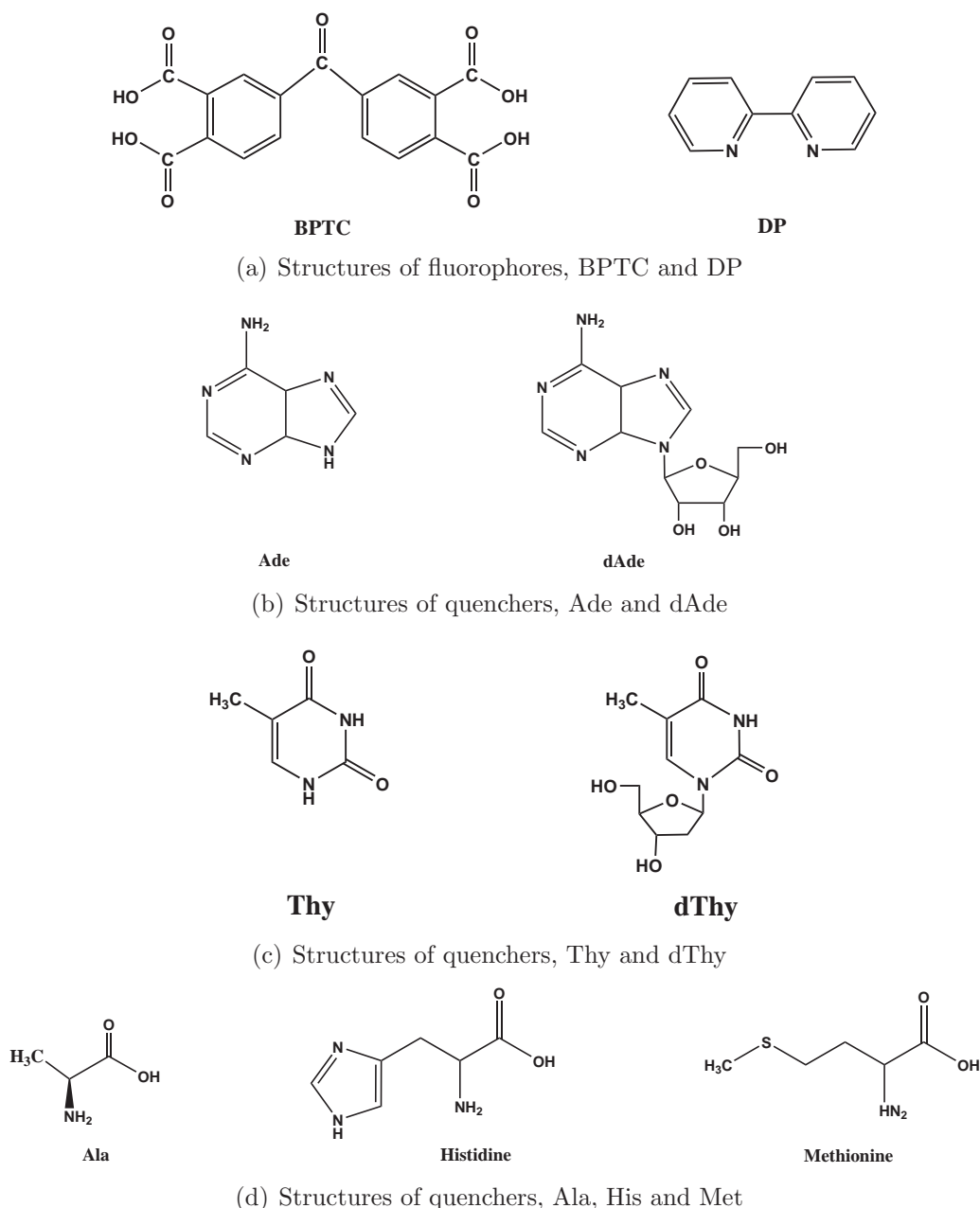


Fig. 3.1: Structures of all compounds used.

where  $K_a$  is the equilibrium constant of the acid-base conjugate couple.  $C_a$  and  $C_b$  are the concentrations of the acid and base conjugate, respectively, in equilibrium.

The buffer capacity (BC or  $\beta$ ) or buffer index can be understood as the concentration of strong acid or sodium hydroxide added to the solution would shift the pH by one unit (in other words, addition of a strong acid or base in a  $\beta$  concentration,

aiming a  $\Delta pH$  of 1). It can be calculated by Eq. 3.3.<sup>[48]</sup>

$$\beta = 2.303 \left( \frac{K_w}{[H^+]} + [H^+] + \frac{C_{buf} K_a [H^+]}{(K_a + [H^+])^2} \right) \quad (3.3)$$

here  $K_w$  is the ion-product constant for water ( $K_w = 1.008 \times 10^{-14}$ ) at 25 °C.

In order to check the pH value achieved, a WTW-522 pH-meter was used. It was calibrated by two-point calibration using pH=4.0, pH=7.0 or pH=9.2 buffer tablets provided from Fluka.

**Buffer composition used in steady state measurements.** Buffer solutions covering a pH-range from 2.61–11.16 were prepared as Tabs. 3.2 and 3.3.

Tab. 3.2: Preparation of buffer stock solutions at room temperature.<sup>[2,3]</sup>

No.	Composition	Supplier <sup>a</sup>
Solution 1	0.01M Citric acid monohydrate	Merck, $\geq 99.5\%$
Solution 2	0.02M $\text{Na}_2\text{HPO}_4 \cdot 2\text{H}_2\text{O}$	Sigma-Aldrich, $\geq 99.5\%$
Solution 3	0.025M $\text{Na}_2\text{B}_4\text{O}_7$ (borax)	Sigma-Aldrich, dry, $\geq 98\%$
Solution 4	0.01M HCl	Roth, 37% in p.a
Solution 5	0.01M NaOH	Sigma-Aldrich, $\geq 99\%$
<b>Notice</b>	All buffer stock solutions was added 0.1M KCl (Fluka $\geq 99.0\%$ ) to keep the ionic strength in constant.	

<sup>a</sup> All substances were used as received.

**Buffer composition used in time-resolved measurements.** Time-resolved measurements require a buffer solution of low concentration to minimize the interaction of the triplet state of the fluorophores with inorganic ions, which might generate the corresponding radicals. Because of this requirement, the buffer solutions were prepared in low concentrations (0.01M) with as few components as possible. The purity and supplier of the buffer-components can be found in Table 3.2 ( $\text{KH}_2\text{PO}_4$  - Fluka  $\geq 99.0\%$ ). Buffer-compositions designed are tubulated in Table 3.4.

- Buffer solutions (0.01M) covering a range of pH from 3.0 to 5.0 were prepared with two components: HCl,  $C_a$  and the main component  $\text{KH}_2\text{PO}_4$ ,  $C_b$ . They were calculated by the following equation named the conservation of hydrogen (1+) ion concentration (cf. Tab. 3.4).

$$[H^+] = [OH^-] + C_a - [H_3PO_4] \quad \text{or} \quad (3.4a)$$

$$[H^+] \approx C_a - [H_3PO_4] = C_a - \frac{[H^+]C_b}{[H^+] + K_{a1}} \quad (3.4b)$$

### 3. Experimental

Tab. 3.3: Preparation of buffer solutions for individual pH used in steady-state measurements at room temperature.<sup>a</sup>

x ml Sol. 1 (10-x) ml Sol. 2		6.0 ml Sol. 3 x ml Sol. 4		6.0 ml Sol. 3 x ml Sol. 5		5.0 ml Sol. 2 x ml Sol. 5	
x	pH <sub>m</sub>	x	pH <sub>m</sub>	x	pH <sub>m</sub>	x	pH <sub>m</sub>
9.9	2.61	2.0	7.76	0.1	8.90	1.0	10.35
9.4	2.71	1.9	7.89	0.4	8.98	2.0	10.68
9.0	2.80	1.8	7.99	0.6	9.24	3.0	10.77
8.5	2.93	1.6	8.16	1.0	9.36	4.0	11.09
8.0	3.10	1.4	8.24	1.4	9.50	5.0	11.16
7.6	3.22	1.2	8.40	1.7	9.57		
7.2	3.35	0.8	8.56	2.0	9.67		
6.8	3.60	0.5	8.67	2.3	9.79		
6.5	3.75	0.2	8.78	3.0	10.10		
6.2	3.93						
5.9	4.14						
5.6	4.35						
5.3	4.57						
5.1	4.79						
4.9	4.93						
4.7	5.13						
4.4	5.37						
4.2	5.65						
4.0	5.82						
3.7	5.91						
3.4	6.18						
3.1	6.37						
2.8	6.50						
2.3	6.73						
1.9	6.86						
1.4	7.16						
0.9	7.44						
0.7	7.52						
0.5	7.67						

<sup>a</sup> Dilute the mixture to 10ml by water except for the mixture already has a volume of 10ml.  
pH<sub>m</sub>: measured after preparation from stock solutions.

here  $K_{a1} = 10^{-2.15}$  is the first dissociation constant of  $\text{H}_3\text{PO}_4$ .

- Buffer solutions (0.01M) employed in a range of pH from 5.0 to 9.0 using two components:  $\text{KH}_2\text{PO}_4$ ,  $C_a$  and  $\text{Na}_2\text{HPO}_4$ ,  $C_b$ . The Henderson-Hasselbalch equation were applied to calculate the buffer compositions (cf. Tab. 3.4).

$$pH = pK_{a2} - \log \frac{C_a}{C_b} \quad (3.5)$$

here  $C_a + C_b = 0.01\text{M}$  and  $K_{a2} = 10^{-7.20}$  is the second dissociation constant of  $\text{H}_3\text{PO}_4$ .

- Buffer solutions (0.01M) performed in a range of pH from 9.5 to 11.0 containing two components: the main component  $\text{Na}_2\text{HPO}_4$ ,  $C_a$  and  $\text{NaOH}$ ,  $C_b$ . The below equation, the conservation of hydroxide-ion concentration, can be used to compute their compositions (cf. Tab. 3.4).

$$[\text{OH}^-] = [\text{H}^+] + C_b - [\text{PO}_4^{3-}] \quad \text{or} \quad (3.6a)$$

$$[\text{OH}^-] \approx C_b - [\text{PO}_4^{3-}] = C_b - \frac{C_a K_{a3}}{[\text{H}^+] + K_{a3}} \quad (3.6b)$$

here  $K_{a3} = 10^{-12.35}$  is the third dissociation constant of  $\text{H}_3\text{PO}_4$ .

- Solutions of  $\text{pH} \leq 2$  and  $\text{pH} > 11$  are adjusted by adding  $\text{HCl}$  and  $\text{NaOH}$ , respectively.

### 3. Experimental

Tab. 3.4: Preparation of buffer solutions used in time-resolved measurements at room temperature.<sup>a</sup>

pH <sub>c</sub>	HCl 0.1M (ml)	KH <sub>2</sub> PO <sub>4</sub> 0.1M (ml)	Na <sub>2</sub> HPO <sub>4</sub> 0.1M (ml)	NaOH 0.1M (ml)	pH <sub>m</sub>	10 <sup>4</sup> ·β (M.pH <sup>-1</sup> )
3.0	22.4	100.0			2.9	49
3.5	7.4	100.0			3.4	17
4.0	2.4	100.0			4.0	5.9
4.5	0.8	100.0			4.4	2.8
5.0		99.4	0.6		5.2	2.5
5.5		98.0	2.0		5.6	5.0
6.0		94.0	6.0		6.0-6.2 <sup>b</sup>	13
7.0		61.2	38.8		7.0	55
8.0		13.8	86.2		7.9-8.1 <sup>b</sup>	27
9.0		2.0	98.0		8.7-9.0 <sup>b</sup>	5.0
9.5			100.0	0.5	9.5	2.4
10.0			100.0	1.5	10.0	4.0
10.5			100.0	4.6	10.6	11
11.0			100.0	14.5	11.0	32

<sup>a</sup> pH<sub>c</sub>: calculated; pH<sub>m</sub>: measured after preparation; Dilute the mixture to 1L by water.

<sup>b</sup>The values varied time to time when a fresh buffer solution was prepared

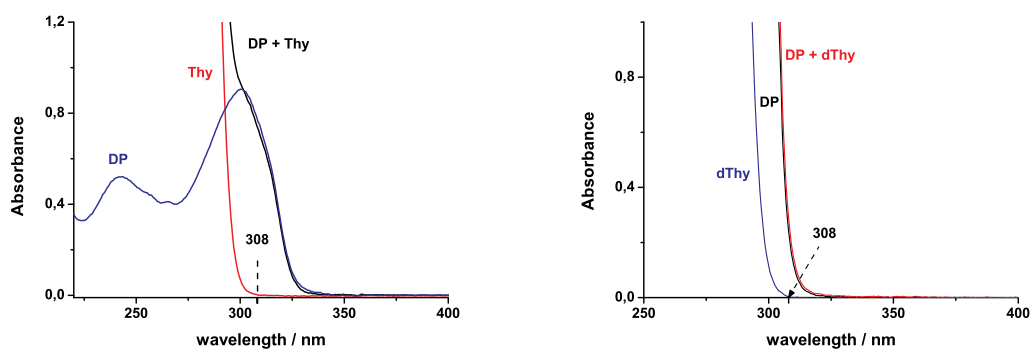
## 3.2 Steady-state measurements

### 3.2.1 Absorption spectroscopy

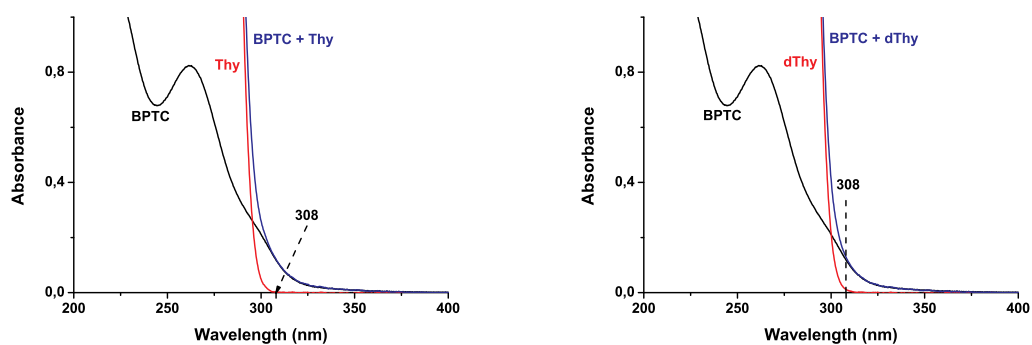
Steady-state absorption spectra were recorded with a Shimadzu UV-3101-PC double beam scanning spectrometer, setting up with: scan speed, medium; slit width, 2.0nm; and sampling interval, auto mode. The doubly distilled water was used as a blank sample.

In Figures 3.2 and 3.3 absorption spectra of fluorophores, all quenchers and their mixtures are presented.

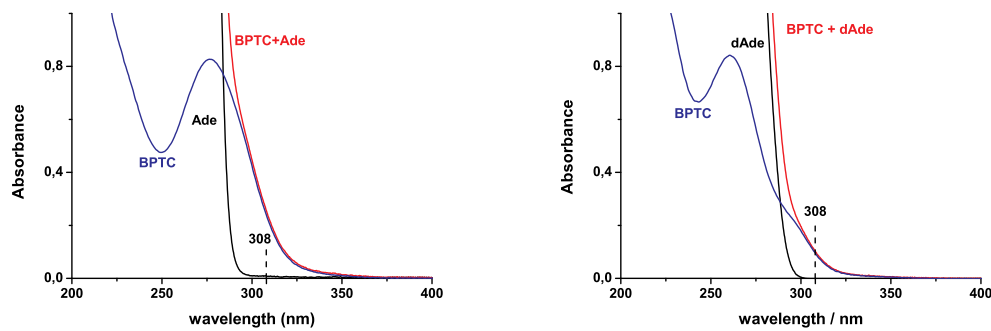
It can be concluded that there is no absorption of quenchers at the excitation wavelength, 308nm, which guarantees that only the fluorophore (DP or BPTC) is excited by the laser beam. The absorption spectrum of a mixture of the fluorophore and quencher shows simple addition of their separate spectra, proving that there is no association between the compounds in the ground state.



(a) Absorption spectra of DP, thymine and (b) Absorption spectra of DP, dThy and DP+Thy mixture in water at pH=2.0 DP+dThy mixture in water at pH=12.0

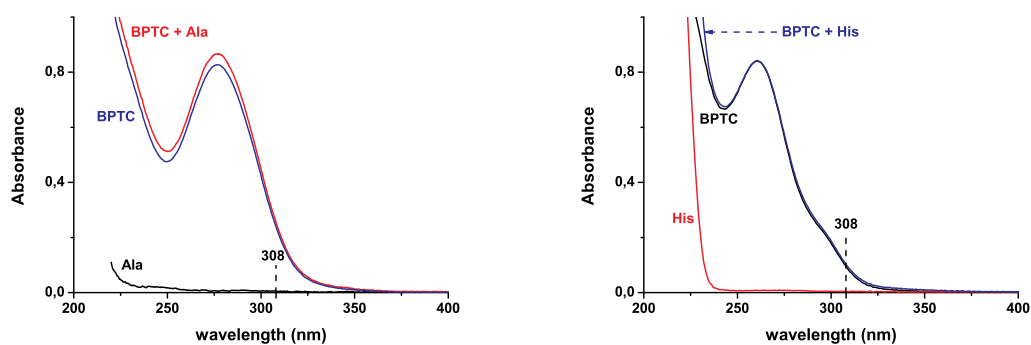


(c) Absorption spectra of BPTC, thymine and (d) Absorption spectra of BPTC, dThy and BPTC+Thy mixture in water at pH=2.0 BPTC+dThy mixture in water at pH=2.0

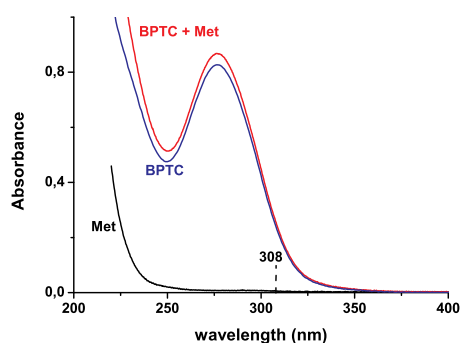


(e) Absorption spectra of BPTC, Ade and (f) Absorption spectra of BPTC, dAde and BPTC+Ade mixture in water at pH=12.0 BPTC+dAde mixture in water at pH=2.0

Fig. 3.2: Absorption spectra of fluorophores, DNA bases and their mixtures.



(a) Absorption spectra of BPTC, Ala and (b) Absorption spectra of BPTC, His and BPTC+Ala mixture in water at pH=12.0 BPTC+His mixture in water at pH=2.0



(c) Absorption spectra of BPTC, Met and BPTC+Met mixture in water at pH=12.0

Fig. 3.3: Absorption spectra of BPTC, amino acids and their mixtures.

### 3.2.2 Determination of $pK_a$ s by UV-VIS spectroscopic method.

By changing the pH of the solution it is possible to control the reactant species present in the solution. Accordingly, it is necessary to know the  $pK_a$ -values. Absorption spectra were obtained by means of a Perkin-Elmer Lambda-12/PECSS double beam scanning spectrometer, setting up 0.5 nm interval data and 60 nm/min scan speed.

A stock solution of BPTC ( $8 \times 10^{-3}$ M) was prepared in doubly distilled water. Standard solutions were prepared by adding 50  $\mu$ L of stock solution to 10 mL of appropriate buffer solutions. The appropriate buffer solutions were used as blank samples.

From the structure compared to phthalic acid which shows two close  $pK_a$  values, BPTC seems to have „two” overlapping  $pK_a$ -values. The UV-Vis spectroscopic

method is mentioned here to determine  $pK_a$ -values of BPTC using an absorbance diagram (A-diagram). A-diagram is a plot of the absorbance measured at different pHs at one wavelength against that at another wavelength. If the compound shows only one deprotonation step, A-diagram will be linear. If the compound involves in two or multi-deprotonation steps, A-diagram will change direction whenever a new equilibrium dominates in the system.

Choosing two appropriate wavelengths for A-diagram is also an important task. For instance, Fig. 3.4 shows the absorption spectra of BPTC at two limiting cases of pH=2.1 and pH=13.0. The neutral and anionic forms of BPTC absorb maxima

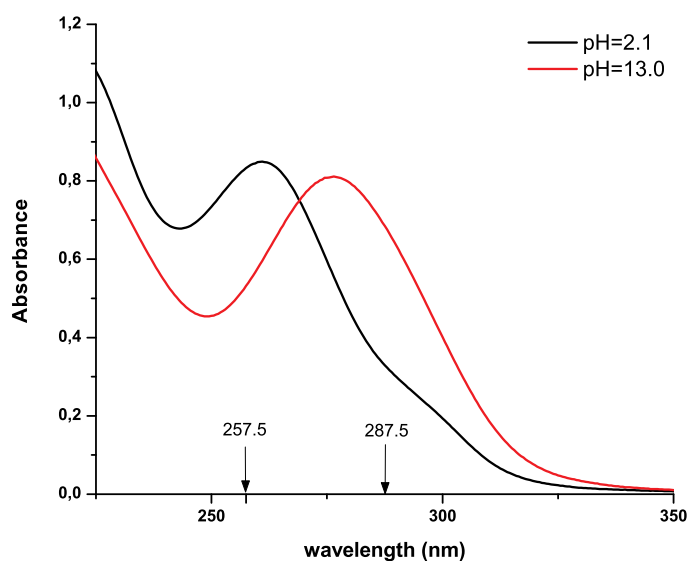


Fig. 3.4: Absorption spectra of BPTC at pH=2.1 and pH=13.0

at 261 nm and 276.5 nm, respectively. It can be seen that at the first selected wavelength (257.5 nm) the absorption of the anionic species tends to a minimum value. While at the second wavelength (287.5 nm) the neutral species absorb much more weakly than the anionic one. Therefore, 257.5 nm and 287.5 nm were chosen as wavelengths for further analysis. Fig. 3.5 shows two linear segments clearly, indicating that two dissociation steps exist. Thus, the protolytic reactions that are supposed to occur can be written down:



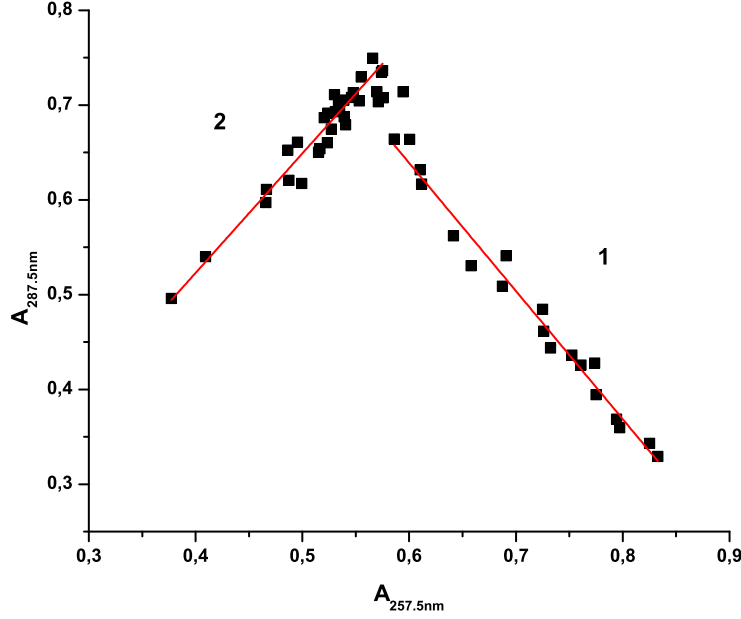


Fig. 3.5: Absorption diagram of BPTC (pH-range: 2.1-13.0). **1**: First segment where Eq. 3.8a can be applied. **2**: Second segment where Eq. 3.8b can be employed.

where  $H_2R$ ,  $HR^-$  and  $R^{2-}$  denote, respectively, the neutral, mono-anionic, and di-anionic forms of BPTC.

If  $K_{aI}$  and  $K_{aII}$  are the dissociation equilibria constants, they can be determined by following equations,<sup>[49,50]</sup>

$$(A_\lambda - A_{\lambda H_2R}) \times 10^{-pH} = -K_{aI} \times A_\lambda + K_{aI} A_{\lambda HR^-} \quad (3.8a)$$

$$(A_\lambda - A_{\lambda HR^-}) \times 10^{-pH} = -K_{aII} \times A_\lambda + K_{aII} A_{\lambda R^{2-}} \quad (3.8b)$$

where  $A_\lambda$  is the absorbance measured at wavelength  $\lambda$ .  $A_{\lambda H_2R}$  and  $A_{\lambda R^{2-}}$  are the absorbances of only specie  $H_2R$  (assuming measured at low pH) and of only specie  $R^{2-}$  (assuming measured at high pH). While  $A_{\lambda HR^-}$  is absorbance due to  $HR^-$  specie. In order to obtain  $K_{aI}$  and  $A_{\lambda HR^-}$  Eq. 3.8a is applied to the points located in the first area (Fig. 3.5). Then using  $A_{\lambda HR^-}$  just obtained before and applying Eq. 3.8b to the points lied in the second area, one can have  $K_{aII}$  readily. Note that  $K_{aIS}$  (and  $K_{aIIS}$ ) determined by this method at two selected wavelengths should be equal.

It is interesting and worthwhile to note that all the above analyses are also valid for the case when two protons are removed simultaneously in each dissociation step

(eg. 3,3',4,4'-benzophenone tetracarboxylic acid). That means Eqs. 3.8a and 3.8b are employed twice<sup>1</sup>.

### 3.3 Time-resolved laser flash photolysis measurements

Transient absorption spectra were obtained by time-resolved laser spectroscopy using a Lambda Physik LPX-120 XeCl-excimer laser (308nm, pulse energy up to 100mJ, pulse width 10ns). The monitoring system includes a xenon lamp 150W (or UV-LED 325nm), a Hamamatsu R928/R955 photomultiplier tube (PMT), a OBB/PTI monochromator model 101/102, and a digital oscilloscope 9410A LeCroy. Sometimes, oscilloscope-probe PM8943 was employed in supporting for the detection if necessary.

Figure 3.6 illustrates energetics of the commercial XeCl-excimer laser and the excimer, XeCl\*, which is produced by a series of reactions.<sup>[51]</sup> A big advantage of this excimer laser in that its short excitation UV-wavelength, 308nm, lies in a region of electromagnetic spectrum absorbed by a very wide range of materials.<sup>[52]</sup>

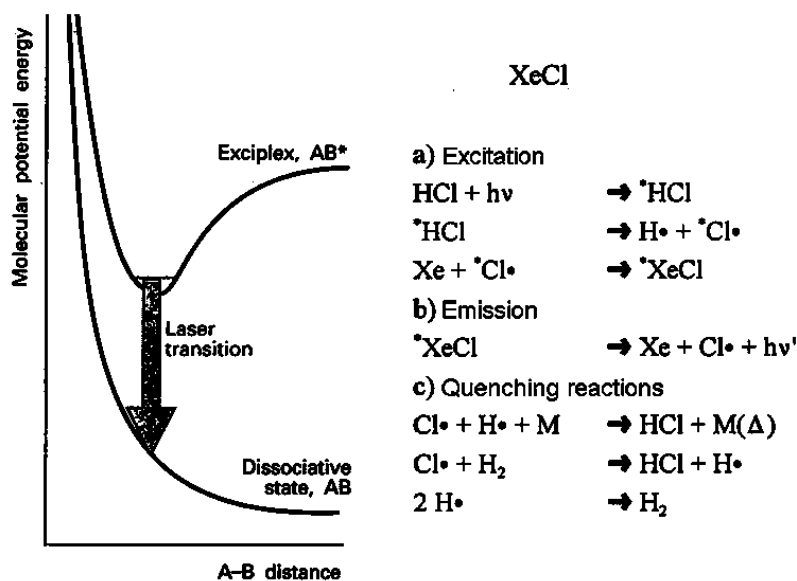


Fig. 3.6: Illustration of four-state energetics of XeCl-excimer laser and the excimer, XeCl\*, which is generated by a series of reactions.

It is worth to first check the corresponding profile to the whole set-up of the Xe-lamp being used in the laser flash measurements. This is shown in Figure 3.7.

<sup>1</sup> Assumed that  $K_{a1} = K_{a2} = K_{aI}$  and  $K_{a3} = K_{a4} = K_{aII}$

It is seen from Fig. 3.7 that the response intensity of the Xe-lamp make it perfect

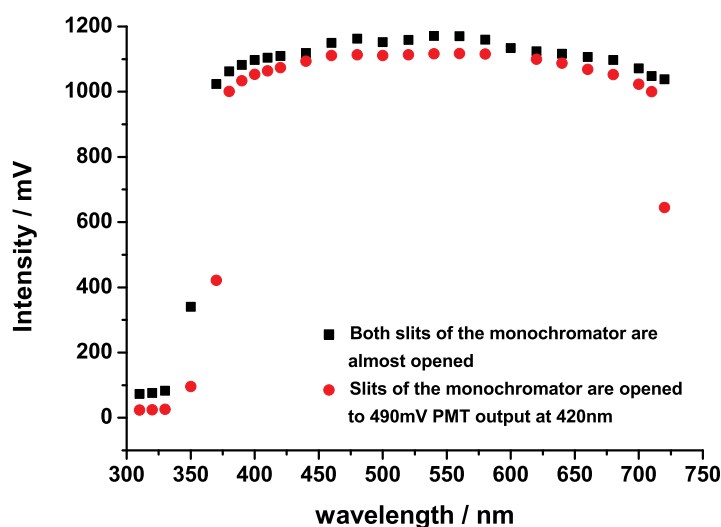


Fig. 3.7: The 150W Xe-lamp intensity response profile, monitored at 800V input for R928-PMT, of the cuvette that contained only water.

in irradiation between 370nm and 720nm. Therefore, usually for the trace of the transient absorption below 370nm other observation sources (eg. UV-LED 325nm and R955-PMT) should be employed. As will be discussed in the *Results and Discussion* chapter, for instance, a home-built UV-LED developed by S. Landgraf with the irradiation wavelength of 325nm is employed instead.

Otherwise, combining the monitoring system which mentioned above, with an oscilloscope probe could be used for detecting such low signals. Here as an example, an experimental procedure which dealing with oscilloscope probe is described in details. Basically to display and measure small voltage signals, which are out of oscilloscope readout, the oscilloscope must have enough gain or sensitivity. For this reason, a 1:1 active voltage probe would be used, Figure 3.8. That is the oscilloscope-probe PM8943 complete kit including a field-effect transistor (FET) tip synchronized an amplifier box (d.c. offset  $\pm 5V$  using for compensation). However, two problems may arise when using this probe. Since the probe becomes a part of the PMT-circuit, it introduces resistive, capacitive, and inductive loading to the circuit. This in turn can result in significant measurement errors. Another disadvantage (tradeoff) is the limited input dynamic range ( $\pm 0.6V$ ) of the probe. Consequently, in order to achieve accurate replication of signal, manufacture's strict instructions must be kept in one's mind as follows:

- Set  $1M\Omega$  FET-probe and dc-mode. Controls to adjust dc-offset voltage at probe

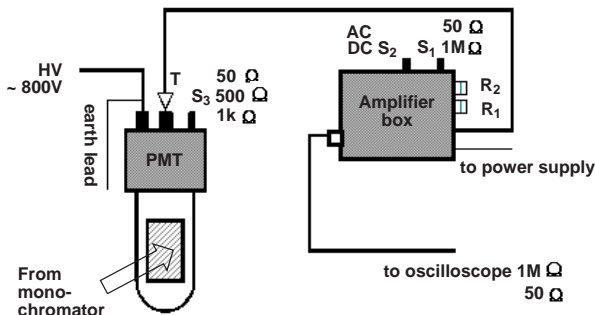


Fig. 3.8: The PMT synchronized an oscilloscope-probe arrangement. R = offset-control; S = switch; T = FET-probe tip.

output to 0V (maximum range:  $\pm 5V$ ).

- Set the R928-PMT at  $500\Omega$ ; oscilloscope at  $1M\Omega$  and  $100mV/div$  sensitivity.
- Display a dark-line as a zero reference.
- Move the bright-line to the former zero-position using offset controls. This adjustment may be facilitated by increasing the Y-sensitivity of the oscilloscope.
- Shift the bright-line to a convenient place on the screen (the shifting must be in the limited dynamic range of the oscilloscope-probe,  $\pm 600mV$ ) and doing measurements.

Testing the oscilloscope-probe PM8943 following these steps was done with the solution of BPTC ( $1 \times 10^{-4}M$ ) in water at  $pH=12.0$ ,  $\lambda_{obs} = 550nm$ . The actual lifetimes of BPTC, which are determined by either using the probe ( ${}^3\tau_0 = 1.74\mu s$ ) or not ( ${}^3\tau_0 = 1.80\mu s$ ), remain „unchanged” (Fig. 3.9).

A generally schematic illustration of the time-resolved laser flash photolysis apparatus can be found in Figure 3.10.

### 3.3.1 Triplet-triplet (T-T) or transient absorption (TA) spectra

In order to avoid the triplet-triplet annihilation, some testing had been done preliminarily. The resulting analytic concentration of BPTC in appropriate buffer solutions was  $1 \times 10^{-4}M$ . That of DP in buffer solutions was  $7 \times 10^{-5}M$  ( $pH < 6$ ),  $1 \times 10^{-3}M$  ( $pH = 6.0$ ) and  $2 \times 10^{-3}M$  ( $pH > 6$ ), see section 3.3.3 for more detail. All solutions were treated identically and de-aerated by bubbling with high purity argon for at least 15min. The irradiation was carried out in a 1x1-cm rectangular quartz cell with a numbers of averages depending on the stable of the samples (e.g. BPTC samples, 150-200 avers., and DP samples, 30-60 avers.).

Laser flash photolysis of BPTC ( $1 \times 10^{-4}M$ ) in aqueous solutions at  $pH=2.0$  and

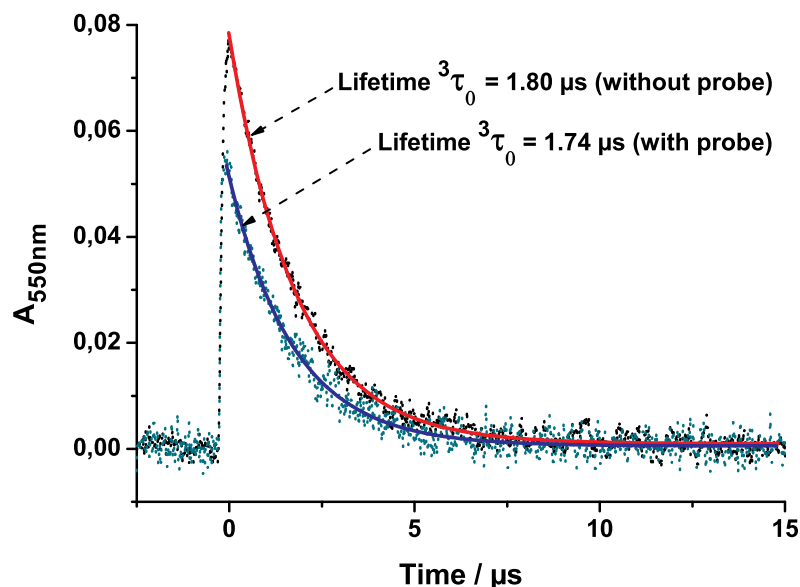


Fig. 3.9: Decay profiles of BPTC ( $1 \times 10^{-4} \text{M}$ ) in water at  $\text{pH}=12.0$ ,  $\lambda_{\text{obs}} = 550 \text{nm}$ .

Upper curves: monitored without probe at  $500 \Omega$  PMT-resistor. Dot-line: experimental; Solid line: exponential fit.

Lower curves: monitored with probe at  $5 \text{k}\Omega$  PMT-resistor;  $1 \text{M}\Omega$  oscilloscope inputs and  $1 \text{M}\Omega$  probe. Dot-line: experimental; Solid line: exponential fit.

$\text{pH}=12.0$  gives the spectra presented in Fig. 3.11. As seen TA spectra of BPTC shows a strong peak at  $\lambda_{\text{max}}=590 \text{nm}$  in water at  $\text{pH}=2.0$ , shifting to  $\lambda_{\text{max}}=550 \text{nm}$  at  $\text{pH}=12.0$ .

### 3.3.2 Determination of $\text{p}K_{\text{a}}^*$ by means of T-T absorption titration method.

T-T absorption (of lowest or local triplet excited state) titration for determining  $K_{\text{a}}^*$ -values was introduced by Jackson and Porter.<sup>[53]</sup> It becomes the most commonly used technique to obtain  $K_{\text{a}}^*$ -values directly. Due to the longer lifetime ( $\mu\text{s}$  time-scale) of the triplet state, this method involves the assumptions that proton transfer in the excited state is very fast and that the protolytic reaction may be attained during the lifetime of the excited state. However, there is a drawback in that a plot of measured absorbances vs.  $\text{pH}$  sometimes does not show inflection points clearly. This is also a problem for the compounds that govern more than one  $K_{\text{a}}$ -value.

For BPTC, from two  $\text{p}K_{\text{a}}$  values in the ground state it is expected that there will be two  $\text{p}K_{\text{a}}^*$ -values as well. Additionally, from T-T absorption spectra of BPTC

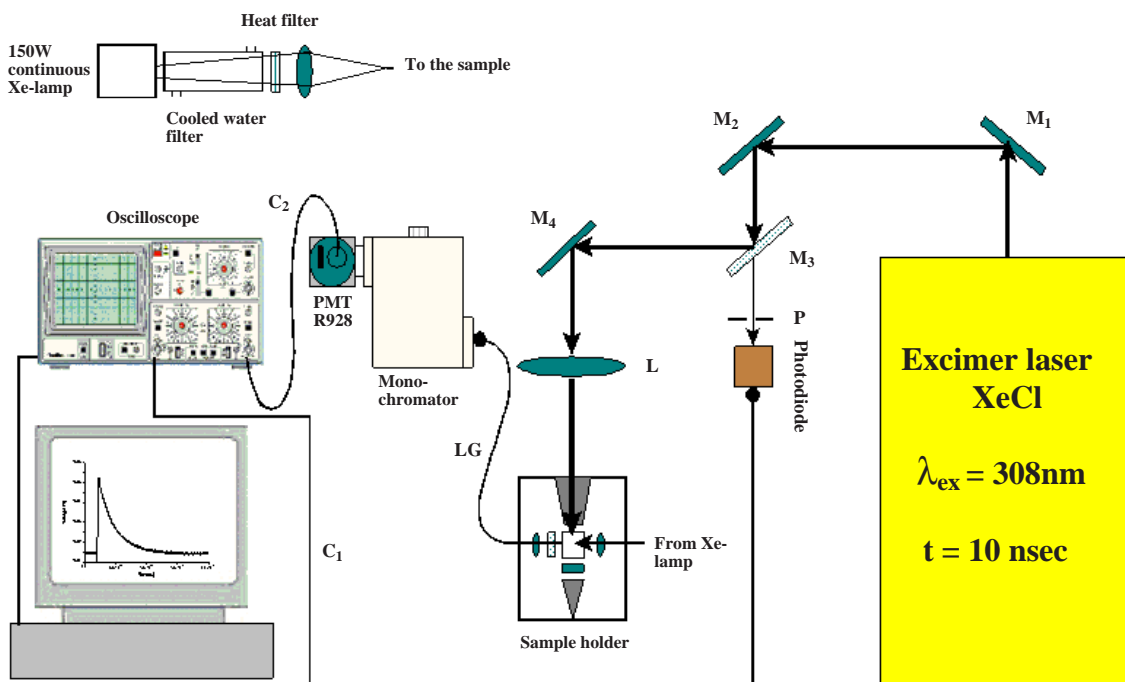


Fig. 3.10: The laser flash photolysis apparatus. M = mirror; P = Pinhole; L = Lens; LG = Light guide ( $260\text{nm} < \lambda \leq 720\text{nm}$ ); C = Cable.

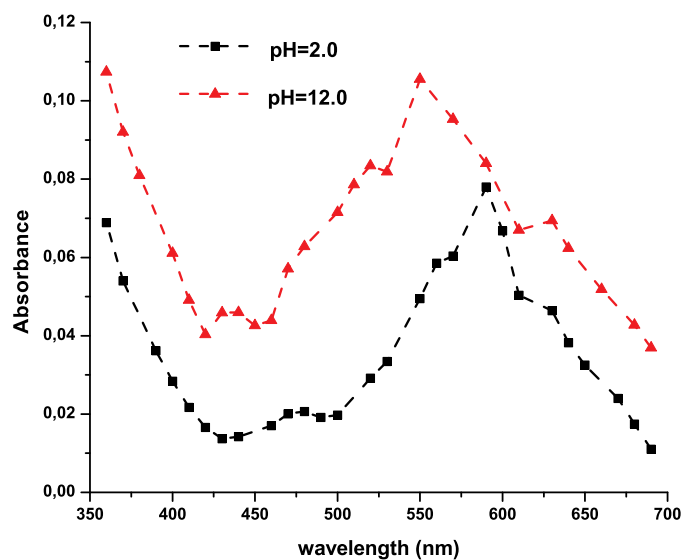


Fig. 3.11: Transient absorption spectra of BPTC ( $1 \times 10^{-4}\text{M}$ ) at pH=2.0 and pH=12.0, monitored by transient absorbances at 590nm and at 550nm between 360 and 690nm, obtained right after the laser flash.

### 3. Experimental

at two limiting case,  $\text{pH}=2.0$  and  $\text{pH}=12.0$  (Fig. 3.11), it can be deduced that molecular coefficients  $\epsilon_{3R^{2-}} > \epsilon_{3H_2R}$  at any wavelength. Both cause the difficulties to obtain the inflection points. Indeed, from the titration curve,  $A_{590nm}$  or  $A_{590nm}$  vs.  $\text{pH}$ , it is problematic to find two  $pK_a^*$ -values. This problem may be overcome

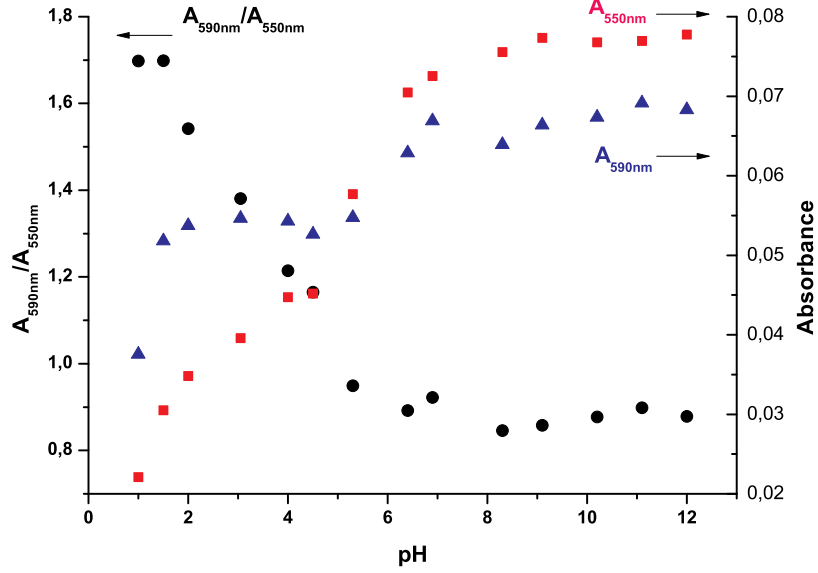


Fig. 3.12: T-T absorption monitored by the transient absorbances at 590nm and 550nm, obtained right after the laser flash; and absorption ratio titration,  $A_{590nm}/A_{550nm}$ .

by measuring the ratio of the absorptions at two different wavelengths („signal to noise”). By selecting signal/noise approach it can be found that the changes in the titration curve ( $A_{590nm}/A_{550nm}$ , Fig. 3.11) is much clearer between  $\text{pH} \approx 2 - 6$ .

With author’s best knowledge, then the below equation may be used to obtain  $pK_a^*$ -values:

$$\frac{\text{signal}}{\text{noise}} = \sum_i f_i \times (\text{signal/noise})_i \quad (3.9)$$

here  $f_i$  is the fraction of the specie  $i$  in equilibrium. As will be discussed in more details in the *Results and Discussion* section, for BPTC, we have:

$$\frac{A_{590nm}}{A_{550nm}} = A = \frac{P_1[H^+]^4 + P_2[H^+]^2K_{aI}^{*2} + P_3K_{aI}^{*2}K_{aII}^{*2}}{[H^+]^4 + [H^+]^2K_{aI}^{*2} + K_{aI}^{*2}K_{aII}^{*2}} \quad (3.10)$$

where  $P_i = (\text{signal/noise})_i$ . By choosing appropriate  $\text{pH}$  in which only one specie, assumed, is present,  $P_i$  can be determined. Finally, by a fitting procedure  $K_{aI}^*$  and  $K_{aII}^*$  can be calculated. (Further details of the short MATLAB<sup>®</sup> program dealing

with this fitting procedure that written can be found in Appendix.)

### 3.3.3 Quenching experiments

**Quenching experiments of triplet BPTC.** A 0.01M stock solution of BPTC ( $M = 358.261 \text{ gmol}^{-1}$ ) was prepared in doubly distilled water. To make the sample for the quenching experiment, 100  $\mu\text{L}$  of the BPTC (0.01M) stock solution was pipetted into a 10mL-volumetric flask yielding an analytic BPTC concentration of  $1 \times 10^{-4}\text{M}$ . Then, the required weight or volume of the stock solution<sup>2</sup> of quencher was added and that flask was filled up to 10 mL with the appropriate buffer solution. If necessary, the ultrasonic bath would be used to get the final sample solution which dissolved completely. All of the samples were treated identically and placed in a 1x1-cm sealed quartz cuvette and deoxygenated through argon bubbling for 15 min. After that the irradiation was carried out.

**Quenching experiments of triplet DP.** The same procedure as BPTC samples was done when preparing an analytic DP concentration ( $7 \times 10^{-5}\text{M}$ ) at  $pH < 6$  from the DP ( $7 \times 10^{-3}\text{M}$ ) stock solution. A stock solution of DP  $1 \times 10^{-3}\text{M}$  at  $pH = 6$  or  $2 \times 10^{-3}\text{M}$  at  $pH > 6$  was prepared in appropriate buffer solutions directly. The required amount of quencher was weighted put into a 10 mL-volumetric flask, then, that flask was filled up to 10 mL with the appropriate stock solution of DP. After that, the same processes as that of preparing BPTC samples was applied for the next steps.

### 3.3.4 Radical absorption spectra

Usually radicals are long-lived transients compared to their parent triplets. To obtain the absorption spectrum of radical that required the depletion of triplet, the highest concentration of quencher of which it is soluble has been used. Alternatively to be better, one is also able to get radical absorption spectrum by delaying observation a bit after irradiation at which the triplet had decayed completely.

## 3.4 Cyclic voltammetry (CV)

Cyclic voltammetric measurements were performed with an Autolab-PGES AUT 73227 potentiostat (Metrohm). A three-electrode cell configuration was used: a Pt counter electrode, a Ag/AgCl reference electrode and a glassy carbon working electrode (0.03  $\text{cm}^2$  area). The working electrode was polished with diamond paste

---

<sup>2</sup> Require the same buffer solution as the one used to dilute.

in water after each single scan to remove possible follow-up products of the oxidative/reductive process on the electrode surface. The background current was always subtracted from the current response for further calculation.  $K_3[Fe(CN)_6]$  is known

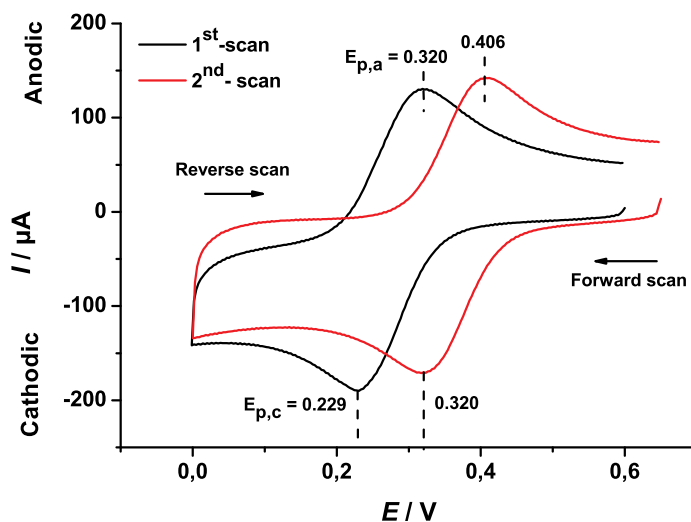


Fig. 3.13: Cyclic voltammogram of  $K_3Fe(CN)_6$  (5mM) in  $KNO_3$  (0.1M) vs.  $Ag/AgCl$ . Scan initiated in negative direction at 100 mV/s. Glassy carbon electrode, area =  $0.03cm^2$ .

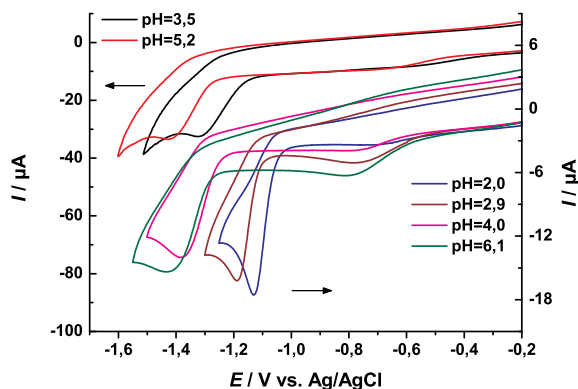
as a standard substance for a testing measurement of the whole CV-set up. Figure 3.13 shows the typical cyclic voltammogram of  $K_3[Fe(CN)_6]$  vs.  $Ag/AgCl$  in water. For such a reversible system, the position of the peaks on the potential axis ( $E_p$ ) is related to the formal potential of the redox process. The formal potential for  $K_3[Fe(CN)_6]$  is centered between  $E_{p,a}$  and  $E_{p,c}$ :

$$E^0 = \frac{E_{p,a} + E_{p,c}}{2} = \frac{0.320 + 0.229}{2} = +0.275 \text{ V} \quad (3.11)$$

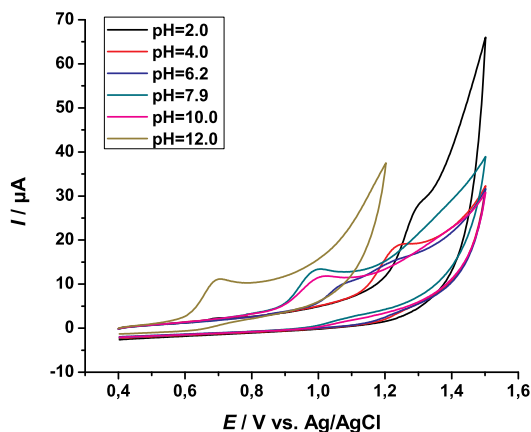
For the second checking after a series of measurements, this value was found to be shifted to +0.363V. Thus, it is important to know how much the potential of the reference electrode changed in order to compare the previous results and the current ones. Furthermore, the value  $E^0$  vs. NHE of the  $[Fe(CN)_6]^{3-}/[Fe(CN)_6]^{4-}$  couple reported in literature is +0.36V. Hence, the potential of the reference electrode,  $Ag/AgCl/0.1M KNO_3$ , used in this work (i.e. for the first series of measurements) is of 85mV vs. NHE. Obviously, changing the electrolyte, its concentration and experimental conditions alter the electrode potential.

The CV-measurements of fluorophores, amino acids and DNA bases used in this

work response as irreversible systems, Fig. 3.14. For such systems, thanks to the help of T. Soomro the apparent standard potentials of the corresponding redox couples were calculated.



(a) Cyclic voltammograms of dipyrindyl (1mM) at 0.1V/s as a function of pH. Curves of pH=3.5 and 5.2 obtained in the second series of measurements



(b) Cyclic voltammograms of thymine (1mM) at 0.1V/s as a function of pH

Fig. 3.14: Cyclic voltammograms of dipyrindyl and thymine as functions of pH

## 3.5 Data evaluation

### 3.5.1 Stern-Volmer relation

Obtaining the laser-flash photolysis data were performed with the help of programs developed by S. Landgraf: LD-CALC2 (version 2.03/32006) for recording

data from the oscilloscope and SHANDLER (version 1.31B/Mar05) for converting data to *ASCII* files which then can be imported to commercial softwares, e.g. OriginPro™ (version 8.0) or MATLAB® (version, up to now, R2010b), for further calculation.

The oscilloscope is triggered by the signal given by a photodiode (cf. Fig. 3.10). Figure 3.15 shows the photodiode response to laser pulses of the whole set-up, half-width 97.5ns, and TA signal profile, half-width 1.47 $\mu$ s. The decay of the trigger signal compared to that of TA signal is around 7%. It is worth noting that if the decay of the trigger signal is rather large (ca. >20% relative to TA signal), a more complex method to analyze the experimental signal has to be carried out (e.g. deconvolution) to get the real signal of TA.

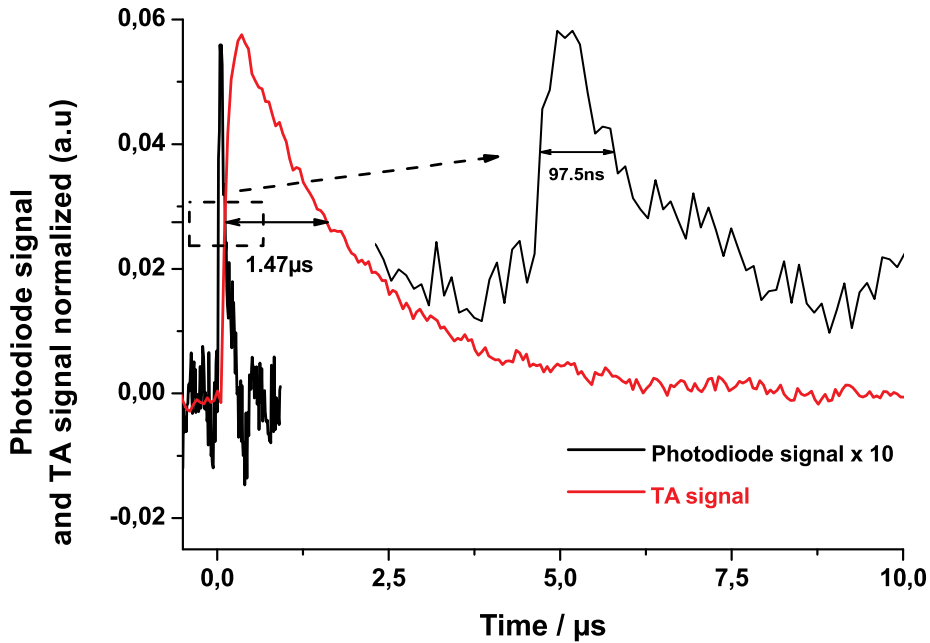


Fig. 3.15: Photodiode response to laser pulses and TA signal profile

Figure 3.16 represents a typical laser-flash photolysis data detected. The transient absorption, then, obtained by Eq. 3.12.

$$\log\left(\frac{U_0}{U_t}\right) = \log\left(\frac{I_0}{I_t}\right) = A_t \quad (3.12)$$

As mentioned earlier, according to the investigated experiments which had been done before, since appropriated concentrations of the fluorophores employed, the triplet-triplet annihilation is negligible. The interaction of the triplet with quencher

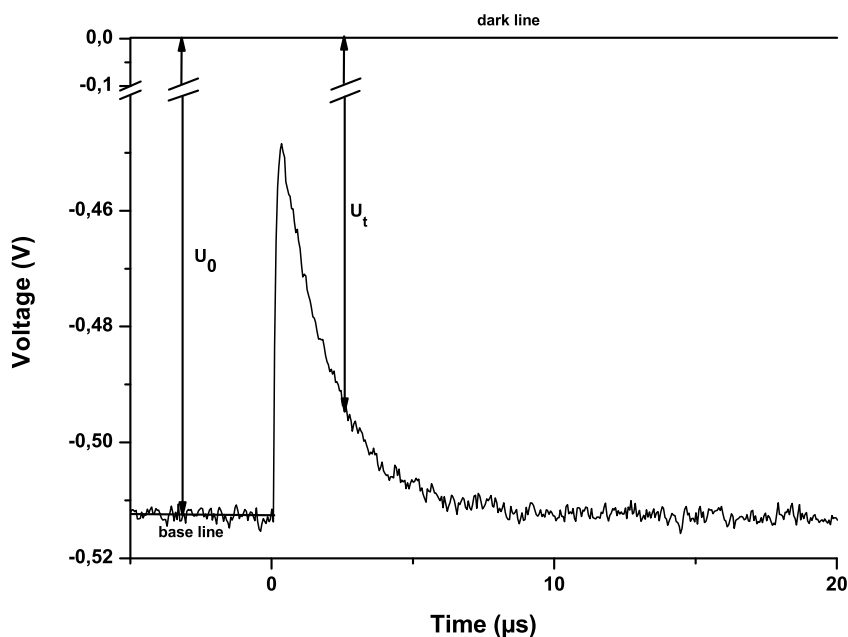
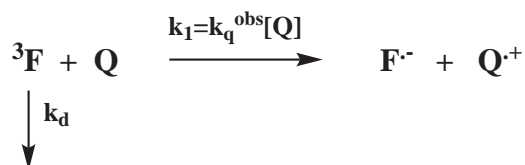


Fig. 3.16: Typical transient absorption obtained by the laser-flash photolysis.

is of pseudo first-order reaction. With these assumptions, some of the most encountered to laser flash photolysis kinetic cases are considered:

(1) When the triplet decay is supposed to be a first-order reaction in the presence of quencher, Q (Scheme 3.1):



Schema 3.1: The first kinetic case consider

The kinetic law reads as

$$\ln \frac{C_t}{C_0} = -k_{\text{obs}} t \quad (3.13)$$

with  $C_0$  and  $C_t$  are the concentrations of the triplet at time 0,  $t$ , respectively; Or if it is expressed in terms of absorbance ( $A$ ):

$$\ln \frac{A_t}{A_0} = -k_{\text{obs}} t \quad (3.14)$$

$A_0$  and  $A_t$  are, respectively, the absorbance at time 0 and  $t$ . Thereupon, the observed

### 3. Experimental

---

quenching rate constant,  $k_q^{obs}$ , is obtained by monitoring the triplet decay at fixed wavelengths applying the Stern-Volmer relation, 3.15a or 3.15b:

$$k_{obs} = k_d + k_q^{obs}[Q] \quad (3.15a)$$

$$\frac{{}^3\tau_0}{3\tau} = 1 + {}^3\tau_0 k_q^{obs}[Q] \quad (3.15b)$$

here  $k_d$  is the decay rate constant of the triplet;  $k_q^{obs}$  is the observed quenching rate constant.  ${}^3\tau_0 = \frac{1}{k_d}$  is the lifetime of the triplet in the absence of quencher;  $3\tau = \frac{1}{k_{obs}}$  is actual lifetime of the triplet in the presence of quencher.

(2) When the triplet disappearance is supposed to be a second-order reaction (with the rate constant  $k_2$ ) in the presence of quencher:

The kinetic law reads as

$$\frac{1}{C_t} - \frac{1}{C_0} = k_2 t \quad (3.16)$$

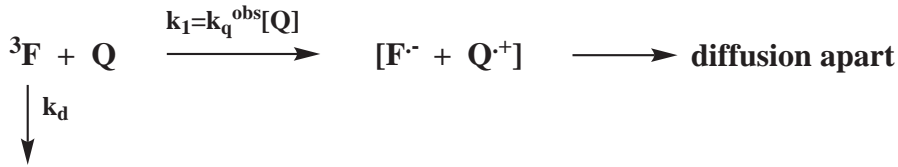
Or if it is expressed in terms of absorbance:

$$\frac{1}{A_t} - \frac{1}{A_0} = \frac{k_2}{\epsilon} \frac{1}{l} t \quad (3.17)$$

From this equation  $k_2/\epsilon$  can be measured ( $l=1\text{cm}$ ).  $\epsilon$  is the molar absorption coefficient of the triplet.

(3) When the system shows a combination of parallel reactions, a first-order decay process and first-order growth of radicals (with the rate constant,  $k_1 = k_q^{obs}[Q]$ ), Scheme 3.2. <sup>[54]</sup>

The sign of such a system is illustrated in Fig. 3.17. Moreover, adding an increase of the quencher concentration will yield an increase absorbance of radicals at the longer time (see more comments in the *Results and Discussion* chapter).



Schema 3.2: The third kinetic case consider

For the sake of simplicity,  $F$  and  $R$  are, respectively, written instead of  ${}^3F$  and  $F\cdot$ . The first order kinetic law is applied to  $[F]$  as follows:

$$\frac{d[F]}{dt} = -k_{obs}[F] \quad (3.18)$$

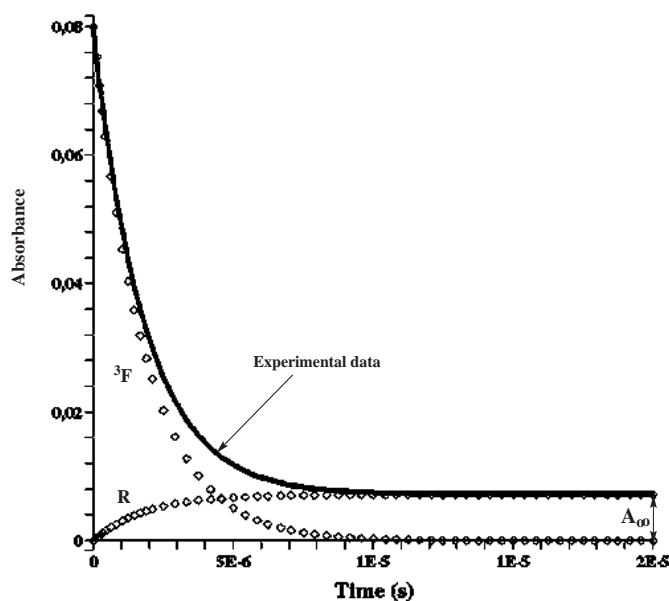


Fig. 3.17: Demonstration of experimental data (solid line) resulting from the addition of transient absorbance due to  ${}^3\text{F}$  (dotted line) and the free radical anion R (dotted line)

with

$$k_{obs} = k_d + k_q^{obs}[Q] = k_d + k_1$$

Equation 3.18 is expressed in terms of absorbance ( $A$ ).

$$\ln \frac{A_t^F}{A_0^F} = -k_{obs}t \quad (3.19)$$

The change of radical concentration is related to the variation in  $[F]$  by the equation

$$d[R] = -\frac{k_q^{obs}[Q]}{k_{obs}}d[F] \quad (3.20)$$

Integrating leads to

$$[R]_t - [R]_0 = -\frac{k_q^{obs}[Q]}{k_{obs}}([F]_t - [F]_0) \quad (3.21)$$

### 3. Experimental

---

From Eq. 3.21, the following expressions are extracted:

$$[R]_0 = 0 \quad (3.22a)$$

$$[R]_t = -\frac{k_q^{obs}[Q]}{k_{obs}}([F]_t - [F]_0) \quad (3.22b)$$

$$[R]_\infty = \frac{k_q^{obs}[Q]}{k_{obs}}[F]_0 \quad (3.22c)$$

Combining Eqs. 3.22a, 3.22b and 3.22c leads to

$$\ln \frac{[R]_\infty}{[R]_\infty - [R]_t} = k_{obs}t \quad (3.23a)$$

$$\ln \frac{A_\infty^R}{A_\infty^R - A_t^R} = k_{obs}t \quad (3.23b)$$

From the Lambert-Beer law one always has:

$$A^F + A^R = A_t \quad (3.24)$$

Finally, the combination of Eqs. 3.23a, 3.23b and 3.24 one gets the kinetic expression:

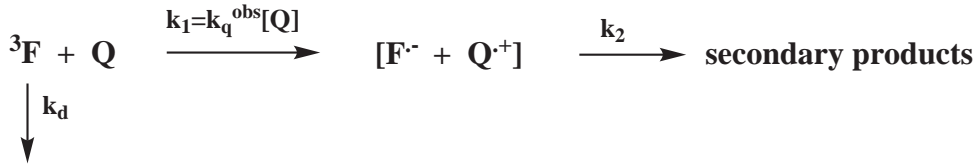
$$\ln \frac{A_t - A_\infty}{A_0 - A_\infty} = -k_{obs}t \quad (3.25)$$

where  $A_0$ ,  $A_t$  and  $A_\infty$  are the absorbance at time 0,  $t$  and infinity, respectively.

Using  $k_{obs}$  obtained from 3.25 and employing 3.15b with various concentrations of the quencher gives the  $k_q^{obs}$  values.

(4) When the system shows a combined first-order decay process, a first order growth of radicals and an overlap by their simultaneous second-order decay (with the rate constant  $k_2$ ), Scheme 3.3.<sup>[55]</sup>

The sign of such a system is illustrated in Fig. 3.18.



Scheme 3.3: The fourth kinetic case consider

The time resolved absorbance for such a system is expressed by Eq. 3.26.

$$\frac{dA}{dt} = \frac{dA^F}{dt} + \frac{dA^R}{dt} \quad (3.26)$$

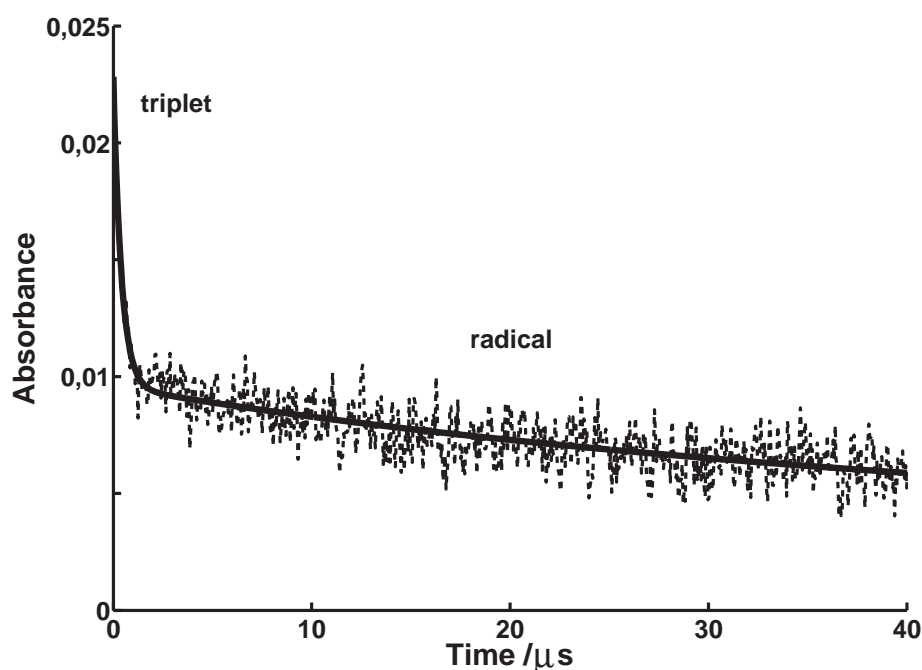


Fig. 3.18: Demonstration of the experimental data from BPTC ( $1 \times 10^{-4}\text{M}$ ) + Thy ( $4.5 \times 10^{-4}\text{M}$ ) system ( $\lambda_{obs} = 590\text{nm}$ ) at  $\text{pH}=2.0$  (dashed line) and simulation (solid line) resulting from the fourth kinetic case considered.

and,

$$\frac{d[F]}{dt} = -(k_d + k_1)[F] \quad (3.27a)$$

$$\frac{d[R]}{dt} = k_1[F] - k_2[R]^2 \quad (3.27b)$$

Note that dealing with these differential equations is not a easy task, here the simulation is carried out to obtain  $k_1$  thanks to the MATLAB<sup>®</sup> program developed by D. Kattinig (further details can be found in Appendix).

Finally, taking  $k_1$  obtained from this simulation one gets a  $k_q^{obs}$ -value relied on the relation  $k_1 = k_q^{obs}[Q]$ .

### 3.5.2 pH-dependence of the observed quenching rate constant $k_q^{obs}$

pH-dependence of  $k_q^{obs}$  can be treated as a summation of  $k_{qi}$  (the „intrinsic” quenching rate constant) multiplied by the fraction of the corresponding species according to the suggestion of Yurkovskaya et al..<sup>[56]</sup>

### 3. Experimental

---

With the assumption that a polyprotic acid symbolized by  $H_nA$ , initial concentration  $C_0$ , can undergo  $n$ -proton dissociation in water and form the corresponding base conjugates. Each step has its own dissociation constant,  $K_{aj}$ ,  $j = 1, \dots, n$ . The fraction of each specie is given by Eq. 3.28.

$$[H_{n-k}A]/C_0 = \left( [H^+]^{n-k} \prod_{j=0}^k K_{aj} \right) / \left( \sum_{k=0}^n [H^+]^{n-k} \prod_{j=0}^k K_{aj} \right) \quad (3.28)$$

with  $0 \leq j \leq k$ ;  $0 \leq k \leq n$ ;  $K_{a0} = 1$ .

For example, triplet DP has  $pK_a^* = 5.8$ ,<sup>[11]</sup> while thymine has a  $pK_a = 9.9$ .<sup>[44]</sup> The pH-dependence of the observed quenching rate constant  $k_q^{obs}$  for the reaction of triplet DP with thymine is divided into three regions based on  $pK_a$  values. Each main pair of reactants is characterized by the so-called intrinsic quenching rate constant  $k_{qi}$  ( $i = 1...3$ ).

$$\begin{array}{lll} \text{pH} < 5.8 & {}^3\text{DPH}^+ \text{ and ThyH} & k_{q1} \\ 5.8 < \text{pH} < 9.9 & {}^3\text{DP} \text{ and ThyH} & k_{q2} \\ 9.9 < \text{pH} & {}^3\text{DP} \text{ and Thy}^- & k_{q3} \end{array}$$

Thus,  $k_q^{obs}$  can be expressed by following equation:

$$\begin{aligned} k_q^{obs} = & k_{q1} \frac{[H^+]}{[H^+] + K_a^*} \times \frac{[H^+]}{[H^+] + K_a} + k_{q2} \frac{K_a^*}{[H^+] + K_a^*} \times \frac{[H^+]}{[H^+] + K_a} \\ & + k_{q3} \frac{K_a^*}{[H^+] + K_a^*} \times \frac{K_a}{[H^+] + K_a} \end{aligned} \quad (3.29)$$

It is seen in Eq. 3.29 that its all parameters are known but  $k_{qi}$ . Here this simple mathematic exercise (the multiple regression) is solved readily and gives the intrinsic values,  $k_{qi}$ . Nevertheless, for a convenience in dealing with all of the quenching data a short MATLAB<sup>®</sup> program was written employing the multiple regression (more details can be found in Appendix).

4

## Results and Discussion

Since in the aqueous solution all neutral fluorophores and quenchers undergo their protonations or deprotonations depending on pH of the medium, it is important to know  $pK_a$ -values of the compounds. Because  $pK_a$ s of BPTC are, at present, unknown, an effort has been made to determine BPTC's  $pK_a$ -values in both ground and triplet excited states.

Afterwards, kinetic results of the photoreactions between 2,2'-dipyridyl and thymine, thymidine in the solution of different pH carried out by time-resolved laser spectroscopy are given. Besides, electrochemical results of DP and thymine are also demonstrated. Combining them together, the feasible reaction pathway has been proposed.

Subsequently, it is devoted to the laser-flash photolysis experiments in aqueous solution of triplet 3,3',4,4'-benzophenone tetracarboxylic acid with various amino acids, alanine, histidine and methionine, and DNA bases, adenine, adenosine, thymine and thymidine. Together, the experimental observations are interpreted in detail. In particular, a possible reaction scheme of the photoreaction of BPTC and thymine is established based on the result of oxidizing thymine.

## 4.1 Determination of $pK_a$ s of BPTC

$pK_a$ -values of BPTC are determined by UV-VIS spectroscopic method with two wavelengths chosen at 257.5nm and 287.5 nm. Plots of absorbances at these two wavelengths with pH, Fig. 4.1, show the important changes between pH=2.6 and 6.7. Absorption spectra of BPTC ( $4 \times 10^{-5}$ M) and the absorption diagram in this pH region can be found in Fig. 4.2. Two linear segments observed, Fig. 4.2(b),

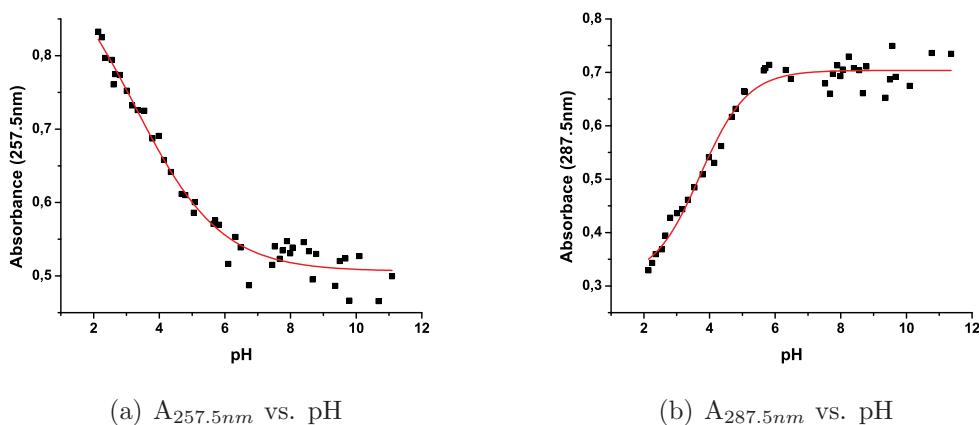
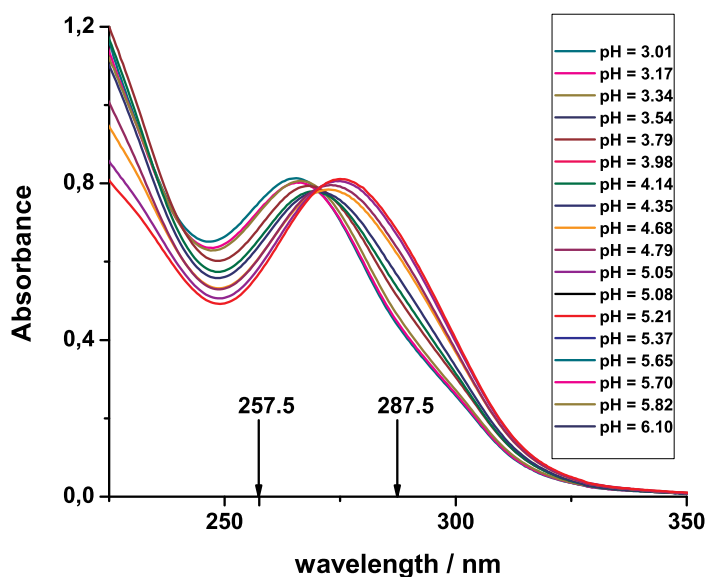
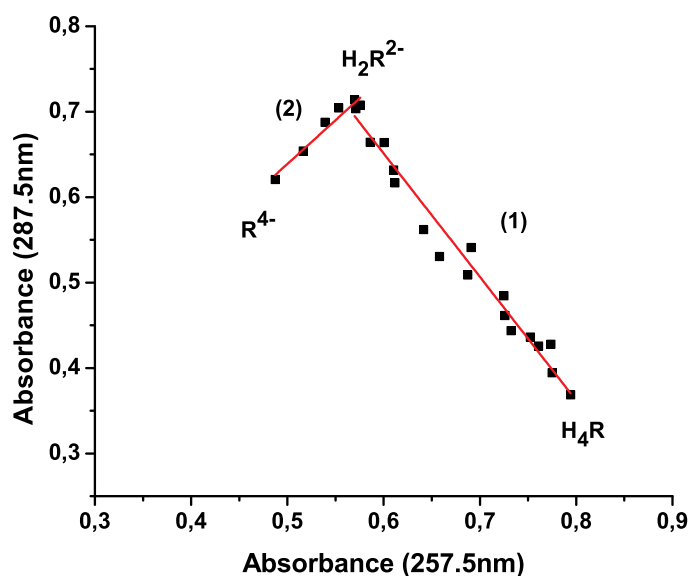


Fig. 4.1: Absorbance values at 257.5nm and 287.5nm as functions of pH.

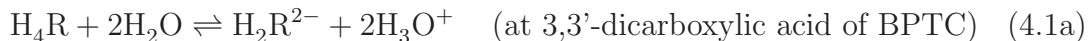
(a) Absorption spectra of BPTC ( $4 \times 10^{-5}\text{M}$ ) at pH=3.01–6.10

(b) Absorption diagram (pH-range: 3.01-6.10). (1): where Eq. 4.1a predominates. (2): where Eq. 4.1b dominates.

Fig. 4.2: Absorption spectra of BPTC ( $4 \times 10^{-5}\text{M}$ ) at pH=3.01–6.10 and A-diagram.

together with the structure of BPTC (indicated as  $\text{H}_4\text{R}$ ) suggest that it possesses two stages of dissociation in each of which two protons are removed simultaneously.

Hence, for BPTC, the acid-base equilibria write as:



The reaction described in Eq. 4.1a predominates in the pH range of 2.6-4.4 (Fig. 4.2, the first solid line), and the second deprotonation reaction given in Eq. 4.1b occurs between pH=4.7-6.7 (Fig. 4.2, the second straight line).

To obtain  $K_{aI}$ , the first straight line can be treated by the following equation:

$$(A_\lambda - A_{\lambda H_4R}) \times 10^{-pH} = -K_{aI} \times A_\lambda + K_{aI} A_{\lambda H_2R^{2-}} \quad (4.2)$$

where  $A_\lambda$  is the experimental absorbance at the selected wavelength (i.e. 257.5 or 287.5nm);  $A_{\lambda H_4R}$  is the absorbance of  $\text{H}_4\text{R}$  (i.e. at pH=2.1), and  $A_{\lambda H_2R^{2-}}$  being that of  $\text{H}_2\text{R}^{2-}$ .

By linear regression applied to Eq. 4.2 at 257.5 and 287.5nm,  $K_{aI}$ s are calculated from slope of the plot of  $(A_\lambda - A_{\lambda H_4R}) \times 10^{-pH}$  vs.  $A_\lambda$  and yielding the values of  $A_{\lambda H_2R^{2-}}$ . They are tabulated in Tab. 4.1.

To attain  $K_{aII}$ s, the points located in the second solid line can be evaluated in a similar way, employing this equation:

$$(A_\lambda - A_{\lambda H_2R^{2-}}) \times 10^{-pH} = -K_{aII} \times A_\lambda + K_{aII} A_{\lambda R^{4-}} \quad (4.3)$$

Note, here, that  $A_{\lambda H_2R^{2-}}$  at 257.5 or 287.5nm is known;  $A_{\lambda R^{4-}}$  is the absorbance of  $\text{R}^{4-}$  (i.e. at pH=13.0). Resulting values of  $K_{aII}$  and  $A_{\lambda R^{4-}}$  are listed in Tab. 4.1.

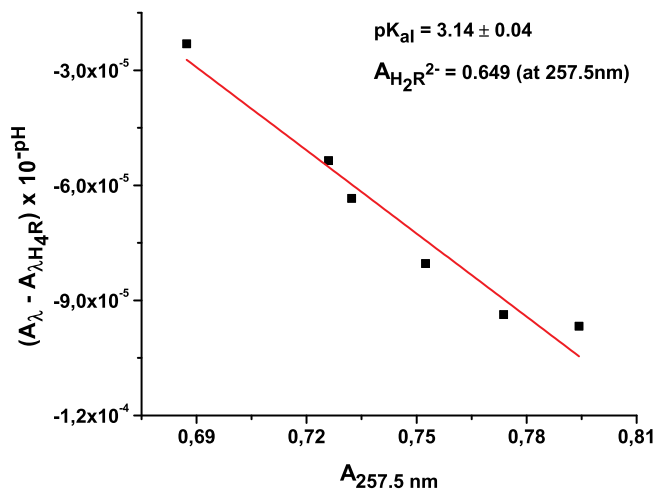
Tab. 4.1: Experimental ionization constant of BPTC determined by UV-VIS spectrometry.

$\lambda$ (nm)	$pK_{aI}$	$pK_{aII}$	$A_{\lambda H_2R^{2-}}$	$A_{\lambda R^{4-}}$ (cal.)	$A_{\lambda R^{4-}}$ (exp.) <sup>a</sup>	Error <sup>b</sup>
257.5	3.14±0.04	5.24±0.03	0.649	0.487	0.527	-7.6%
287.5	3.25±0.04	5.00±0.05	0.572	0.740	0.680	+8.8%
average	3.20±0.04	5.12±0.05				

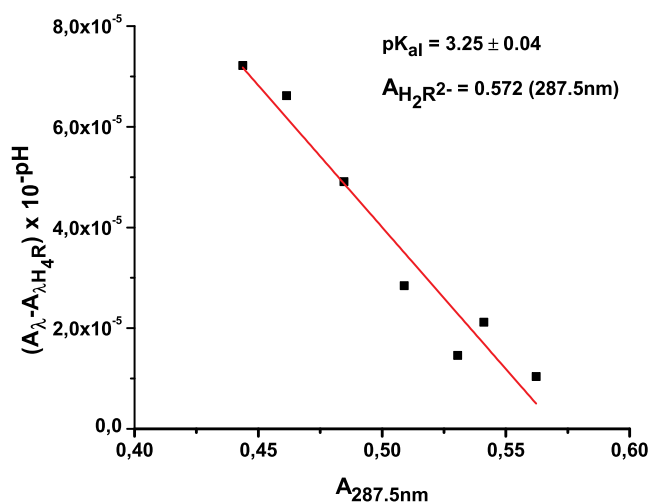
<sup>a</sup> measured at pH=13.0

<sup>b</sup> relative error of  $A_{\lambda R^{4-}}$  calculated to experimental.

There is a good agreement (error < 10%) between the calculated values of  $A_{\lambda R^{4-}}$  and those obtained experimentally (i.e. at pH=13.0), which demonstrates the accuracy of the method carried out for estimating the  $pK_a$ -values of BPTC.



(a) Determination of the  $pK_{aI}$  at 257.5nm

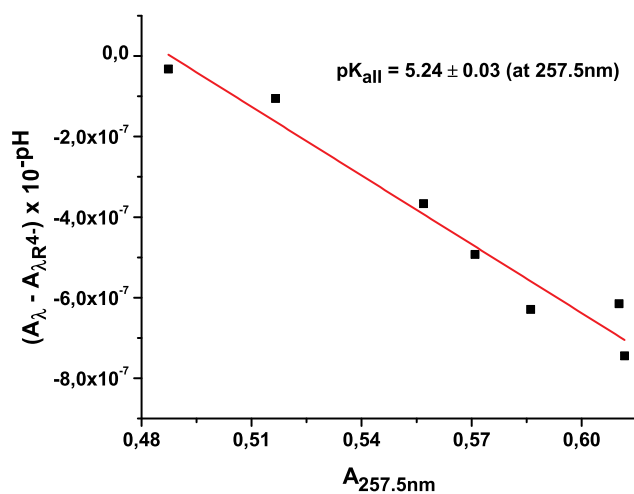


(b) Determination of the  $pK_{aI}$  at 287.5nm

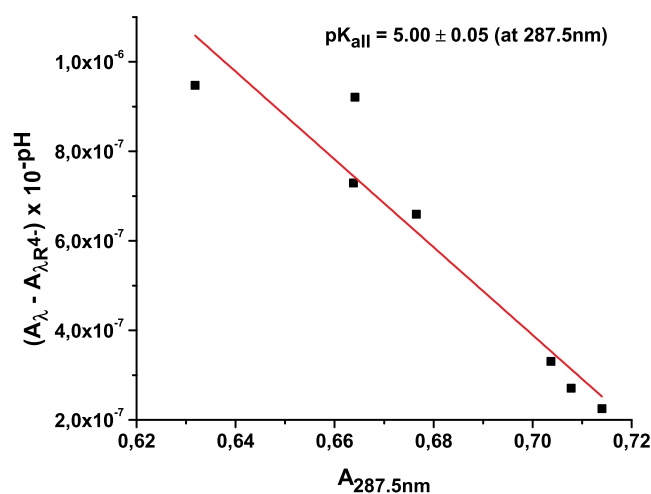
Fig. 4.3: Determination of the  $pK_{aI}$  of BPTC in water. Graphic representation of Eq. 4.2 at 257.5nm and 287.5nm.

## 4.2 Determination of $pK_a^*$ of triplet BPTC

Any time when a compound possesses more than one  $pK_a$  values, it requires a complicated analysis to obtain them. BPTC has two  $pK_a$ s in the ground state, it is also expected two values in the triplet excited state. With this assumption,



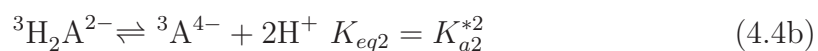
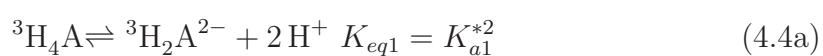
(a) Determination of the  $pK_{aII}$  at 257.5nm



(b) Determination of the  $pK_{aII}$  at 287.5nm

Fig. 4.4: Determination of the  $pK_{aII}$  of BPTC in water. Graphic representation of Eq. 4.3 at 257.5nm and 287.5nm.

acid-base equilibria for triplet BPTC can be write as follows:



Here  $K_{eq}$  stands for the equilibrium constant of BPTC in the triplet excited state. It leads to assume:

$$[{}^3\text{H}_3\text{A}^-] \approx 0 \text{ and } [{}^3\text{HA}^{3-}] \approx 0$$

Recall Eq. 3.10, to get  $pK_a^*$ -values, firstly,  $P_i$  needs to be chosen at appropriate pH. From the T-T absorption titration, Fig. 3.12, that measured  $A_{590nm}/A_{550nm}$  ratio against pH,  $P_i$ -values are collected and brought in Tab. 4.2. Secondly, it requires to know fractions of species in equilibrium. Simply, from Eq. 3.28 we can write:

$${}^3[\text{H}_4\text{A}]/C_0 = \frac{[\text{H}^+]^4}{[\text{H}^+]^4 + [\text{H}^+]^2 K_{a1}^{*2} + K_{a1}^{*2} K_{a2}^{*2}} \quad (4.5a)$$

$${}^3[\text{H}_2\text{A}^{2-}]/C_0 = \frac{[\text{H}^+]^2 K_{a1}^{*2}}{[\text{H}^+]^4 + [\text{H}^+]^2 K_{a1}^{*2} + K_{a1}^{*2} K_{a2}^{*2}} \quad (4.5b)$$

$${}^3[\text{A}^{4-}]/C_0 = \frac{K_{a1}^{*2} K_{a2}^{*2}}{[\text{H}^+]^4 + [\text{H}^+]^2 K_{a1}^{*2} + K_{a1}^{*2} K_{a2}^{*2}} \quad (4.5c)$$

Hence, employing the fitting procedure on Eq. 3.10 with known parameters,  $A$ ,  $P_i$  and  $[\text{H}]^+$ , gives  $pK_a^*$ -values. The idea of the fitting program is that doing fit<sup>1</sup> data for several times with randomly selected starting condition ( $K_{aI}$  and  $K_{aII}$  being initial values) to validate the fit and estimate unknown parameters,  $K_{aI}^*$  and  $K_{aII}^*$  (see more in Appendix). The results are tabulated in Tab. 4.2 and depicted in Fig. 4.5.

Tab. 4.2: Results of  $pK_a^*$ -values.

$P_i$	Value	Taken	$pK_{aI}^*$	$pK_{aII}^*$
$P_1$	1.7	at pH=2.0	2.1±0.2	4.7±0.2
$P_2$	1.3	at pH=3.4		
$P_3$	0.9	at pH=12.0		

### 4.3 Quenching results of triplet DP

In aqueous solution, the reactive species can be either protonated, neutral or deprotonated forms depending on pH. The  $pK_a$ -values that used as boundaries to divide

<sup>1</sup> MATLAB<sup>®</sup> toolbox provides a non-linear fit function for doing this.

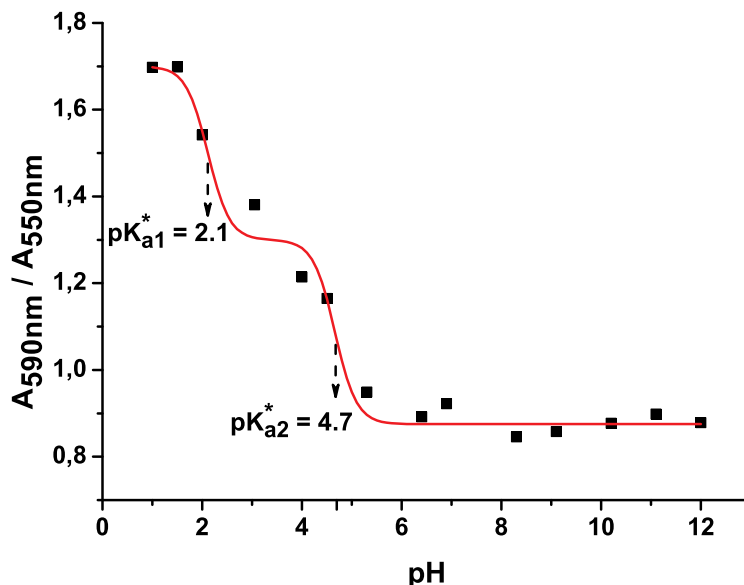


Fig. 4.5: Determination of  $pK_a^*$ s of triplet BPTC

these pH-regions and corresponding reactants can be found in Tabs. 3.1 and 4.3.

Kinetic traces of DP-triplet are measured at a wavelength of 325nm where DP-triplet absorbs much more than its radicals.<sup>[9]</sup> The decay of the neutral state  $^3DP$  (at pH=12.0) obeys the first order kinetic law with  $k_d = 2.1 \times 10^4 s^{-1}$ , while the protonated state  $^3DPH^+$  (at pH=2.0) shows an admixture of first-order,  $k_d = 2.5 \times 10^4 s^{-1}$ , and second-order,  $k_2/\epsilon = 5.4 \times 10^5 cms^{-1}$ , disappearances. These observations are in agreement with reported data.<sup>[9]</sup> In the presence of quencher, the decay of DP-triplet follows a pseudo first-order reaction with  $k_1 = k_q^{obs} C_0$ . Where  $k_q^{obs}$  is extracted from Stern-Volmer plot (Eq. 3.15a or 3.15b).

### 4.3.1 Results of quenching by Thymine

In the presence of thymine, the actual lifetime of the triplet DP is decreased. The time evolution of  $^3DP$  with an increase in concentration of thymine in water at pH=2.0 and Stern-Volmer relation are shown in Figure 4.6 as an example. The nature of the species that participate in the quenching reaction is listed in Table 4.3 (see more in Scheme 4.1 and Fig. 4.7). Furthermore, the pH-dependence of the observed quenching rate constant,  $k_q^{obs}$ , is treated by Eq. 3.29 and is presented in Fig. 4.8. It is found that the turning-points of this titration curve (pH $\approx$ 5.8 and 9.9) coincide well with the (de)protonation of dipyridyl and thymine. This fact indicates the quenching process is influenced by the protonation states of the

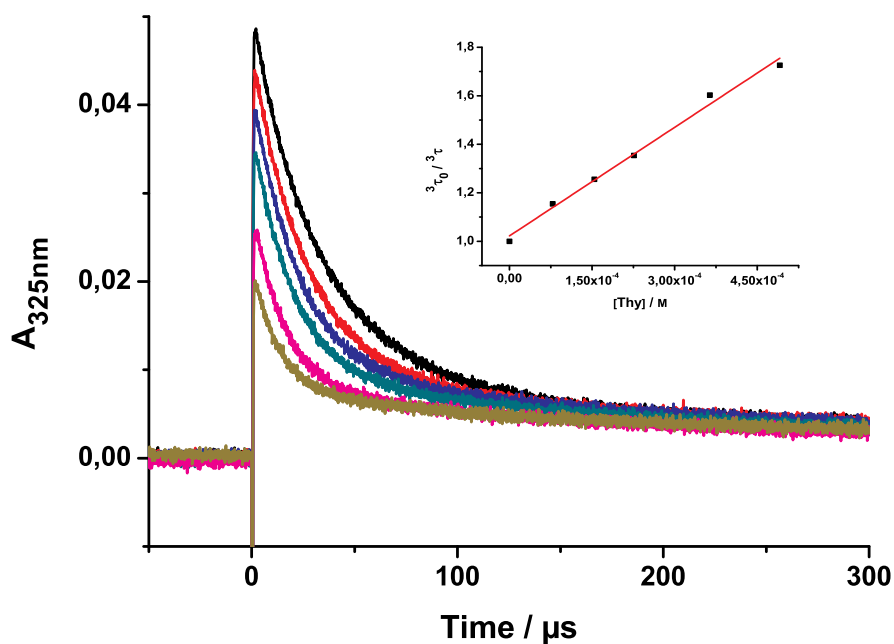
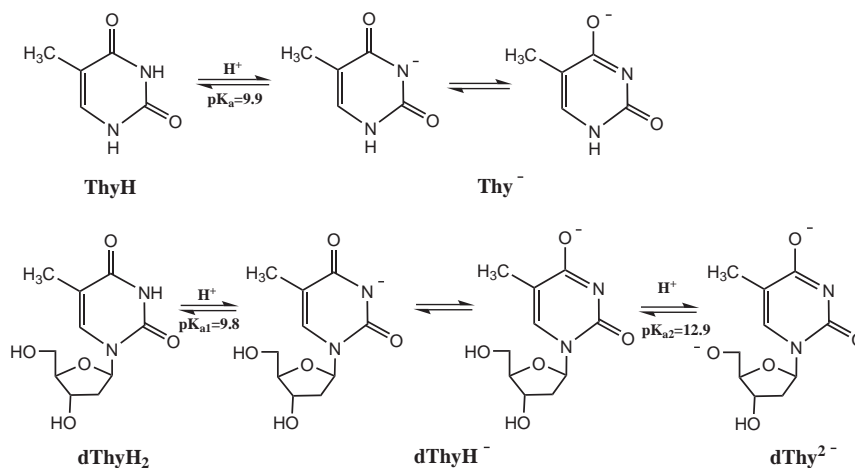


Fig. 4.6: Decays ( $\lambda_{\text{obs}}=325\text{nm}$ ) of triplet DP ( $2 \times 10^{-3}\text{M}$ ) + Thy (concentration increasing from top to bottom: 0 -  $4.9 \times 10^{-4}\text{M}$ ) in water at  $\text{pH}=12.0$ . Insert: Stern-Volmer plot from Eqs. 3.14 and 3.15b.



Schema 4.1: Equilibria of Thy and dThy in aqueous solution.

reactants. Three pH-regions can be distinguished as:  $\text{pH} < 5.8$ ;  $5.8 < \text{pH} < 9.9$ ; and  $\text{pH} > 9.9$ .

At  $\text{pH} > 9.9$ , the triplet dipyridyl and thymine exist, respectively, in the neutral,  ${}^3\text{DP}$ , and deprotonated, Thy<sup>-</sup>, forms. It is clear from the kinetic data (Fig. 4.6) that the primary photochemical reaction between  ${}^3\text{DP}$  and thymine is electron transfer.

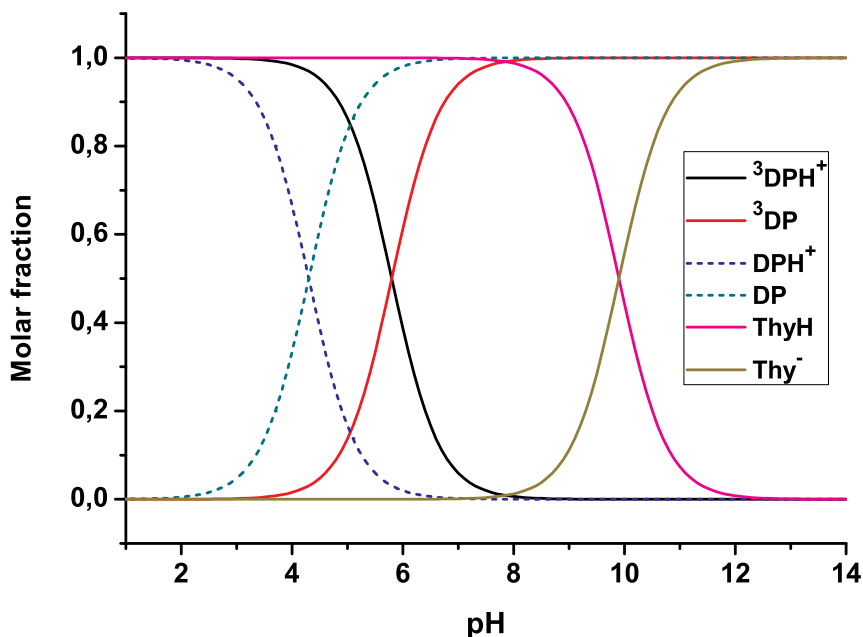
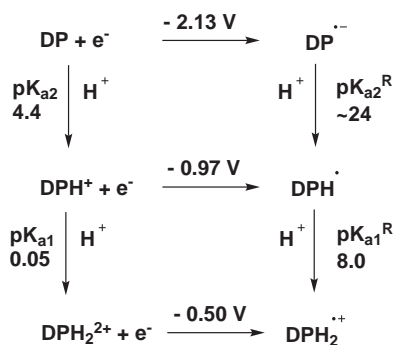
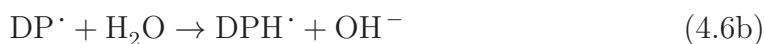
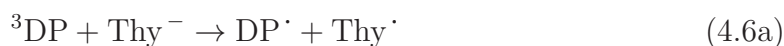


Fig. 4.7: Molar fractions of triplet DP, DP and thymine in water.



Schema 4.2:  $pK_a$ -values and redox potentials (vs. NHE) of dipyridyl.<sup>[57]</sup>

The radical anion formed,  $\text{DP}^{\cdot-}$ , is a strong base ( $pK_{\text{a},\text{DPH}^{\cdot}} \approx 24$ )<sup>[57]</sup> which is protonated immediately.<sup>[10]</sup>



On the other hand, it is concluded that the reactivity of triplet dipyridyl and thymine is highest in this range of pH (see Fig. ?? and Tab. 4.3).

Between  $5.8 < \text{pH} < 9.9$ , both triplet dipyridyl and thymine are in the neutral

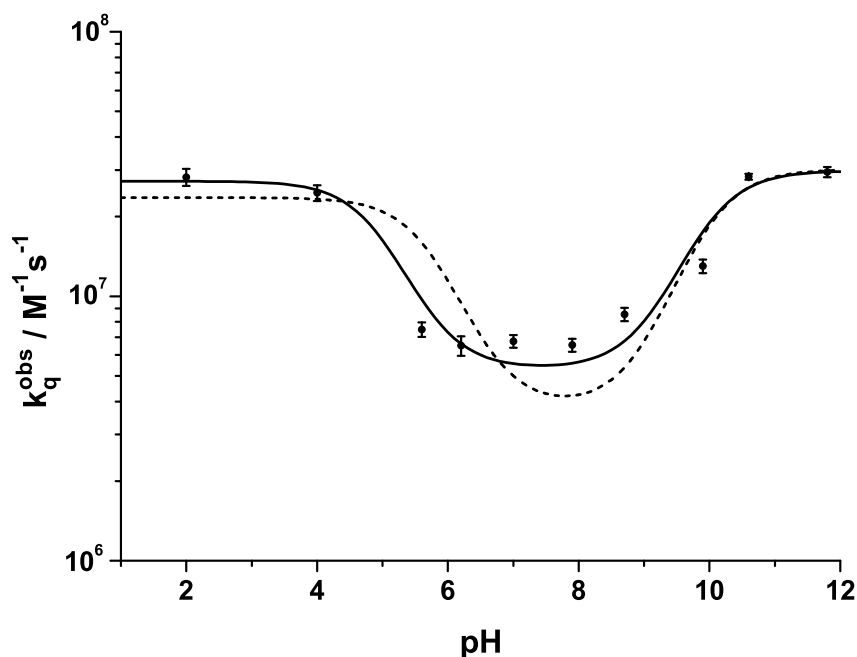


Fig. 4.8: pH-dependence of the observed quenching rate constants  $k_q^{obs}$  for the reaction between triplet DP and Thy. The dashed line is the simulation according to Eq. 3.29 with  $pK_{a,DPH^+}^T = 5.8$ . While the solid line is that with  $pK_{a,DPH^+}^T = 5.0$ . See Tab. 4.3 for parameters.

states. The species resulting from the reduction of DP would expect to be observed was the neutral radical  $DPH\cdot$  ( $\lambda_{max}=365$  and  $470\text{nm}^{[9]}$ ). However, it could not be detected in our experiments and this has been attributed to the in-stability of radical ions. The nature of the primary photochemical step between  ${}^3DP$  and ThyH would take place, perhaps, in a similar way (hydrogen abstraction) to that of triplet dipyrindyl and N-acetyl tyrosine suggested by Tsentalovich et al..<sup>[9]</sup>



At  $\text{pH} < 5.8$ , the triplet dipyrindyl and thymine exist in  ${}^3DPH^+$  and ThyH states, respectively. The transient absorption spectrum obtained at  $2\mu\text{s}$  after irradiation of the solution of DP ( $7.0 \times 10^{-5}\text{M}$ ) and Thy ( $7.5 \times 10^{-3}\text{M}$ ) at  $\text{pH}=2.0$  is shown in Fig. 4.9. This spectrum, which is similar to that of the cation radical  $DPH_2^{\cdot+}$  ( $\lambda_{max}=370\text{nm}$ ),<sup>[10]</sup> indicates that the reaction yields the  $DPH_2^{\cdot+}$  species. The formation of this long-lived radical may be explained by the different mechanisms of which the same radical cation is generated in the reduction process: (i) Hydrogen atom transfer; (ii) Proton coupled electron transfer (PCET) by means of either con-

#### 4. Results and Discussion

Tab. 4.3: Quenching rate constants of triplet DP by quenchers ( $k_{qi}$ )

Quencher	pH region	Main reactant pair	$k_{qi}$	$10^{-7} \times k_{qi} / \text{M}^{-1}\text{s}^{-1a}$	
Thymine	pH<5.8	$^3\text{DPH}^+$ and ThyH	$k_{q1}$	2.4	2.7
	5.8<pH<9.9	$^3\text{DP}$ and ThyH	$k_{q2}$	0.38	0.53
	9.9<pH	$^3\text{DP}$ and Thy $^-$	$k_{q3}$	3.0	3.0
Thymidine	pH<5.8	$^3\text{DPH}^+$ and dThyH $_2$	$k_{q1}$	0.41	0.29
	5.8<pH<9.8	$^3\text{DP}$ and dThyH $_2$	$k_{q2}$	1.0	1.0
	9.8<pH<12.9	$^3\text{DP}$ and dThyH $^-$	$k_{q3}$	0.43	0.44
	12.9<pH	$^3\text{DP}$ and dThy $^{2-}$	$k_{q4}$	0.0052 $^b$	0

<sup>a</sup>  $k_{qi}$ -values in the left and right hand sides resulted from simulations with  $pK_{a,\text{DPH}^+}^T = 5.8$  and  $5.0$  respectively.

<sup>b</sup>  $k_{q5}$  is small implies that the deprotonation of the deoxyribose group of dThy does not affect the quenching reaction.

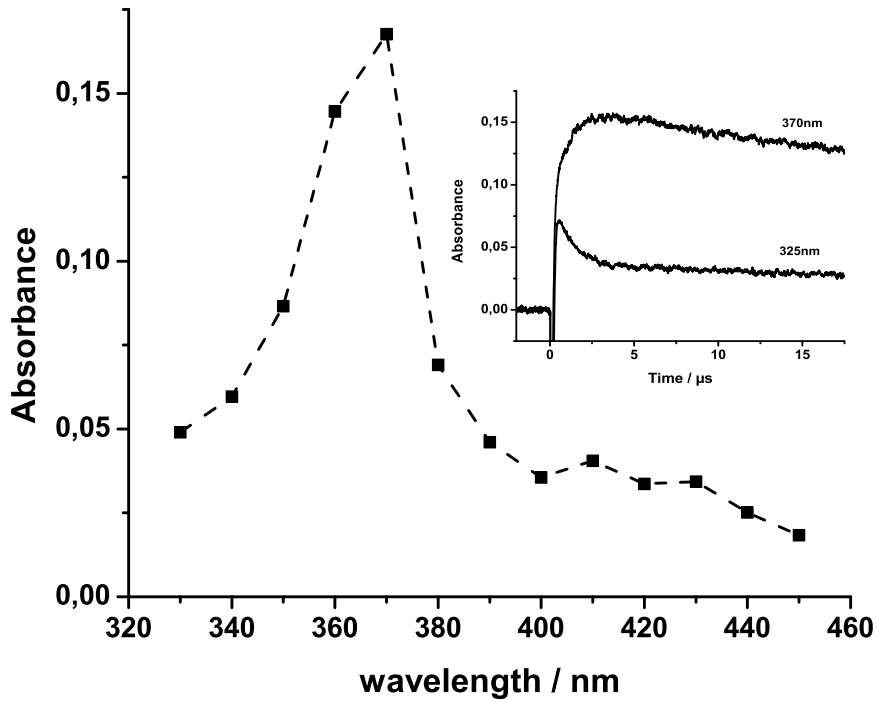


Fig. 4.9: Transient absorption spectrum obtained at  $2\mu\text{s}$  after irradiation of DP ( $7.0 \times 10^{-5}\text{M}$ )+Thy ( $7.5 \times 10^{-3}\text{M}$ ) at pH=2.0. Insert: Decay profiles observed at  $\lambda_{obs}=325\text{nm}$  and  $370\text{nm}$

certed (CPET) pathway or step-wise pathway, electron transfer followed by proton transfer (ETPT) or proton transfer followed by electron transfer (PTET). Noting that regardless of the activation energy barrier, case (i) and case (ii) are equal.<sup>[10]</sup> Moreover, the PTET-mechanism can be ruled out since thymine would prefer its deprotonation at  $\text{pH} > pK_{a,\text{Thy}} = 9.9$ . As will be discussed later, the possibility of the favorable pathway will be evaluated by the reaction driving force which is calculated based on the electrochemical results.

Otherwise, it can be seen that the rate constant of thymine with  $\text{DPH}^+$  is higher than that with  ${}^3\text{DP}$  (see Fig. ?? and Tab. 4.3). The interpretation of this behavior is related to the dissociation constant of the neutral radical  $\text{DPH}^\cdot$  ( $pK_{a,\text{DPH}^\cdot} \approx 24$ ) and the equilibrium constant of triplet dipyridyl ( $pK_a^* = 5.8$ ) according to Chibisov (see section 2.3.3).<sup>[35]</sup> When  $pK_{a,\text{DPH}^\cdot} > pK_a^*$ , then  $k_{q1} > k_{q2}$  (see Tab. 4.3).

### 4.3.2 Results of quenching by Thymidine

The initial reactive species existing in solution at different pH are shown in Tab. 4.3 (see more in Scheme 4.1). Decays of DP-triplet and Stern-Volmer plot in the presence of dThy are demonstrated in Figure 4.10. Besides, the pH-dependence of the quenching rate constant,  $k_q^{\text{obs}}$ , can be expressed by the following Eq. 4.8<sup>[56]</sup> and is presented in Fig. 4.11.

$$\begin{aligned}
 k_q^{\text{obs}} = & k_{q1} \frac{[\text{H}^+]^3}{([\text{H}^+] + K_a^*)([\text{H}^+]^2 + K_{a1}[\text{H}^+] + K_{a1}K_{a2})} \\
 & + k_{q2} \frac{K_a^*[\text{H}^+]^2}{([\text{H}^+] + K_a^*)([\text{H}^+]^2 + K_{a1}[\text{H}^+] + K_{a1}K_{a2})} \\
 & + k_{q3} \frac{K_a^*K_{a1}[\text{H}^+]}{([\text{H}^+] + K_a^*)([\text{H}^+]^2 + K_{a1}[\text{H}^+] + K_{a1}K_{a2})} \\
 & + k_{q4} \frac{K_a^*K_{a1}K_{a2}}{([\text{H}^+] + K_a^*)([\text{H}^+]^2 + K_{a1}[\text{H}^+] + K_{a1}K_{a2})} \quad (4.8)
 \end{aligned}$$

The main reactions at each pH region and their corresponding quenching rate constants,  $k_{qi}$ , obtained by least-square fitting (solid line, Fig. 4.11), are summarized in Tab. 4.3. It is important to note that,  $k_{q3} = 5.2 \times 10^4 \text{M}^{-1}\text{s}^{-1}$  is about 2 orders of magnitude lower than others. This implies its small contribution to the overall quenching rate constant. In other words, the protonation state of the deoxyribose group ( $pK_{a2} = 12.9$ ) of dThy does not much influence the quenching reaction. Note that  $pK_{a,\text{Thy}} \approx pK_{a1,\text{dThy}}$  (see Tab. 3.1), therefore, similar pH-divided regions and mechanisms to that of triplet dipyridyl-thymine reaction are predicted for the quenching reaction of triplet dipyridyl by thymidine.

In contrast, the DP-triplet quenching rate constants (see Tab. 4.3) for thymidine show a different behavior compared with those for thymine. The source of this behavior is, at present, not clear.

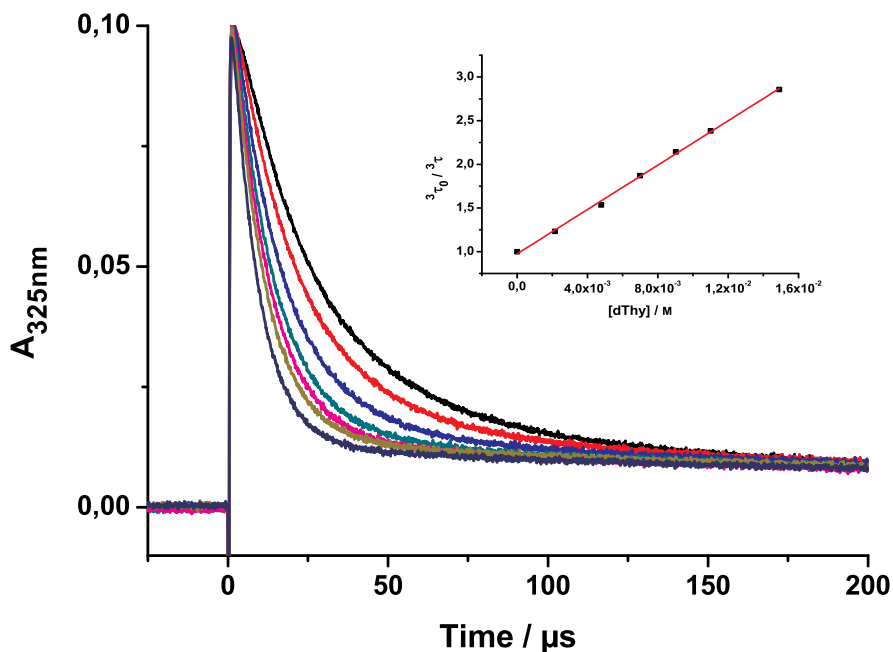


Fig. 4.10: Decays ( $\lambda_{\text{obs}}=325\text{nm}$ ) for DP+dThy system in water at pH=2.0. Concentration of dThy increases from top to bottom: 0 -  $1.5 \times 10^{-2}\text{M}$ . Insert: Stern-Volmer plot from Eqs. 3.14 and 3.15b.

### 4.3.3 CV results of DP

As mentioned earlier, to check the feasible mechanism that the reaction between thymine (thymidine) and triplet dipyridyl would proceed, the pH-dependent redox potentials of DP and thymine have been investigated at  $\text{pH} < 7$ . An attempt was also made to measure the oxidation potential of thymidine at  $\text{pH} < 7$ . Unfortunately, it is not possible because thymidine is not easy to be oxidized.

Figure 4.12 shows the variation of the apparent standard reduction potential of DP,  $E_{\text{ap,DP}}^0$ , with pH. As seen in Fig. 4.12, the apparent standard reduction potential of DP is assigned to be constant (within experimental error,  $\pm 20\text{mV}$ ) between the pH-ranges of 2.0-3.0 and 4.0-6.0 as well. A change of  $E_{\text{ap,DP}}^0$  occurs at  $\text{pH} \approx 3 - 4$  corresponding to the deprotonation of  $\text{DPH}^+$  to the neutral DP. This is reasonable because dipyridyl has a  $pK_a$  value of 4.3. Accordingly the following

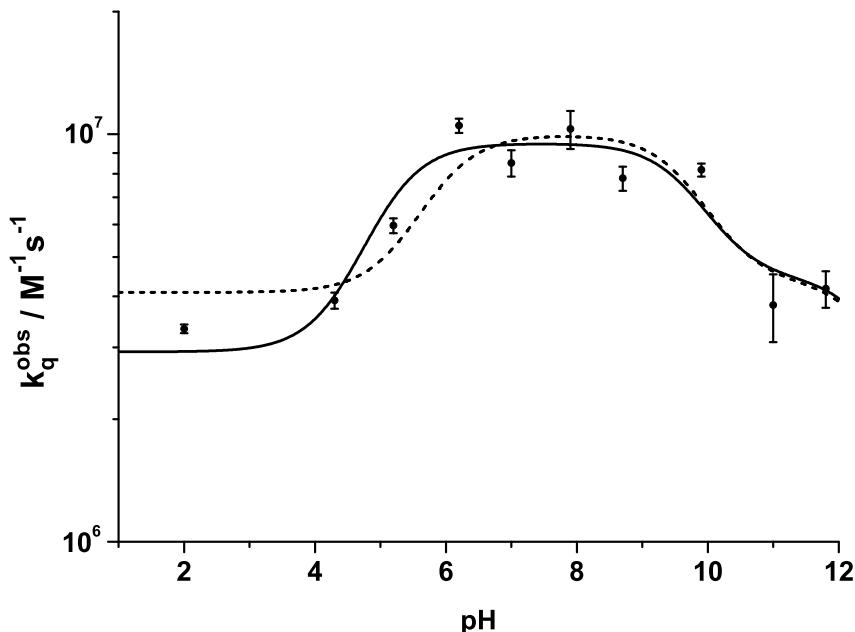


Fig. 4.11: pH-dependence of the observed quenching rate constant  $k_q^{obs}$  for the reaction of triplet DP with dThy. The dashed line is the simulation according to Eq. 4.8 with  $pK_{a,DPH^+}^T = 5.8$ . While the solid line is that with  $pK_{a,DPH^+}^T = 5.0$ . See Tab. 4.3 for parameters.

value is determined,  $E_{DPH^+}^0 = E_{ap,DPH^+}^0 = -1.22V$  vs. Ag/AgCl (taken at pH=2.0). This value is comparable with the published one,  $E_{DPH^+}^0 = -0.97V$  vs. NHE by Krishnan et al.<sup>[57]</sup> (cf. Scheme 4.2) using pulse-radiolysis technique.

#### 4.3.4 CV results of Thymine

In Figure 4.13, pH-dependence of the apparent standard oxidation potential of thymine is given. It shows a linear variation of  $E_{ap,Thy}^0$  with pH characterized by a slope of  $-55.2 \pm 2.7$  mV per pH-unit. Note that this is a sign of proton coupled electron transfer of which possible pathways are depicted in Scheme 4.3. As a consequence, the following values are estimated (for more details see section 2.5.2):  $E_{ThyH^+/ThyH}^0 = E_{ETPT}^0 = 1.27V$ ;  $E_{Thy^{\cdot-},H^+/ThyH}^0 = E_{CPET}^0 = 1.45V$ . From knowing of redox potentials of dipyridyl and thymine, it is allowed to calculate the reaction driving forces ( $-\Delta G^0$ ) which correspond to the different mechanisms predicted as

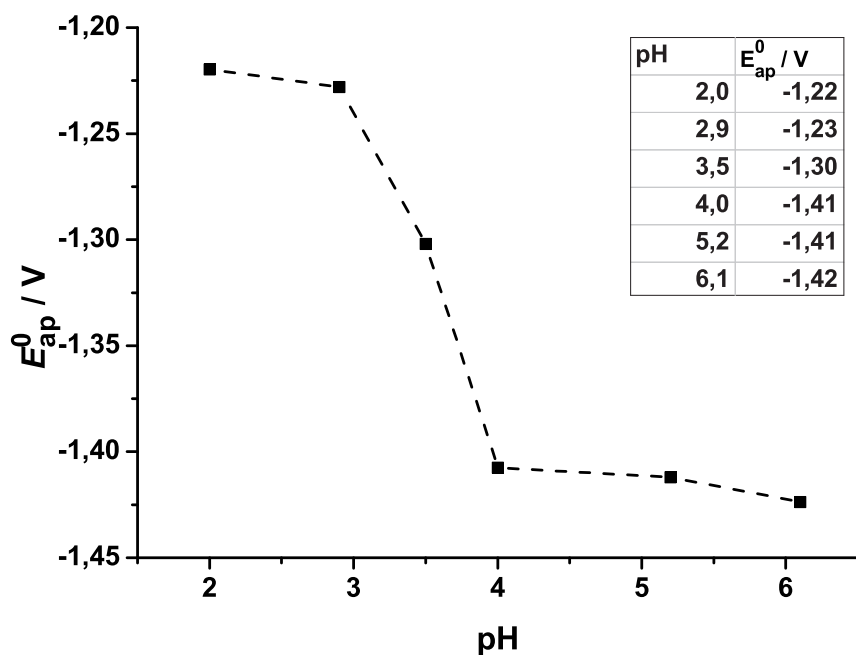
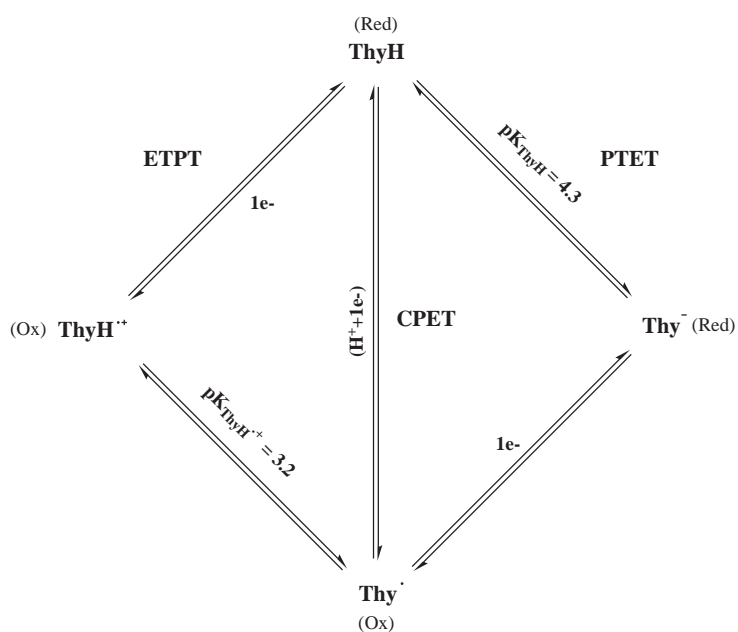


Fig. 4.12: Variation of the apparent standard reduction potential (vs. Ag/AgCl) of DP (1mM) with pH.



Schema 4.3: Demonstration of PCET-pathways for the oxidation of thymine

follows:

$$-\Delta G_{ETPT}^0 = -F(E_{ETPT}^0 - E_{DPH+}^0) + E_T = E_T - 240.3 \text{ (kJmol}^{-1}\text{)} \quad (4.9a)$$

$$-\Delta G_{CPET}^0 = -F(E_{CPET}^0 - E_{DPH+}^0) + E_T = E_T - 257.7 \text{ (kJmol}^{-1}\text{)} \quad (4.9b)$$

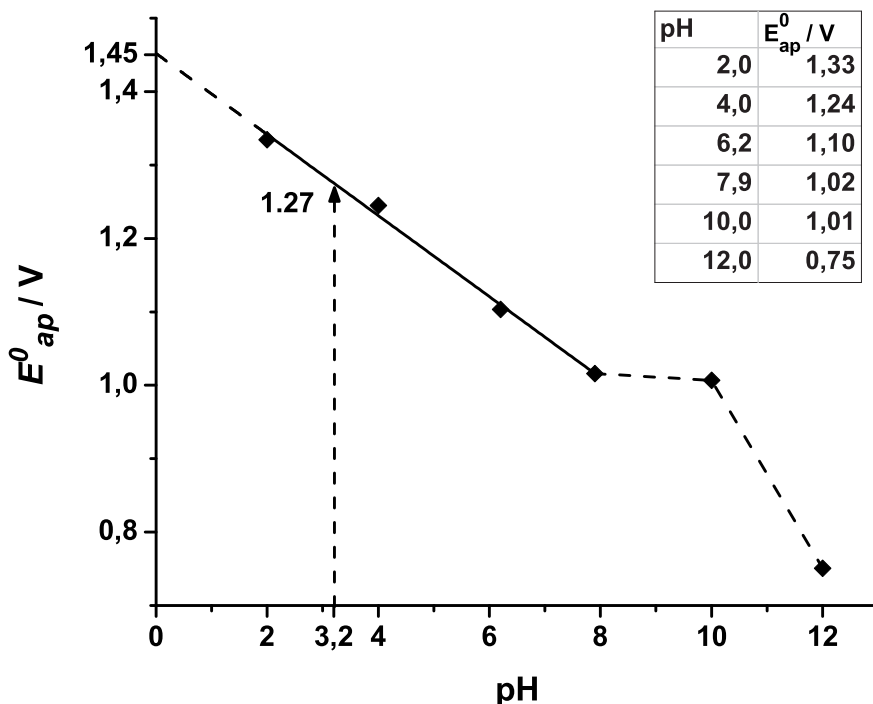
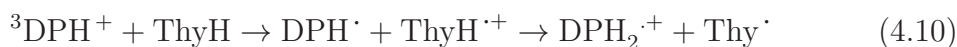


Fig. 4.13: The apparent standard oxidation potential (vs. Ag/AgCl) of thymine (1mM) as a function of pH. Solid line: linear fit, slope =  $-55.2 \pm 2.7$  mV/pH. Dashed line (pH<2): extrapolated from fitting.

Where  $E_T$  is the triplet energy<sup>2</sup>. Thus, a comparison of the reaction driving forces ( $-\Delta G_{ETPT}^0 > -\Delta G_{CPET}^0$ , Fig. 4.14) leads to postulate that the primary photoreaction between thymine (and thymidine) and triplet dipyrindyl at pH<5.8 is an electron transfer followed by proton transfer reaction.



## 4.4 Quenching results of triplet BPTC

### 4.4.1 T-T absorption spectra

The spectra shown in Figure 3.11 are very similar to the triplet spectra of benzophenone and 4-BC.<sup>[59]</sup> It is safe to assign those to T-T absorption spectra of BPTC. From this results, we have chosen 590nm and 550nm as observation wavelengths for kinetic traces of all quenching experiments in the acid media and in the basic media,

<sup>2</sup>  $E_T=282$  kJmol<sup>-1</sup> in cyclohexane<sup>[58]</sup>. If it is assumed that  $E_T$  does not change much from cyclohexane to water,  $-\Delta G_{ETPT}^0 = 41.7$  kJmol<sup>-1</sup> and  $-\Delta G_{CPET}^0 = 24.3$  kJmol<sup>-1</sup>.

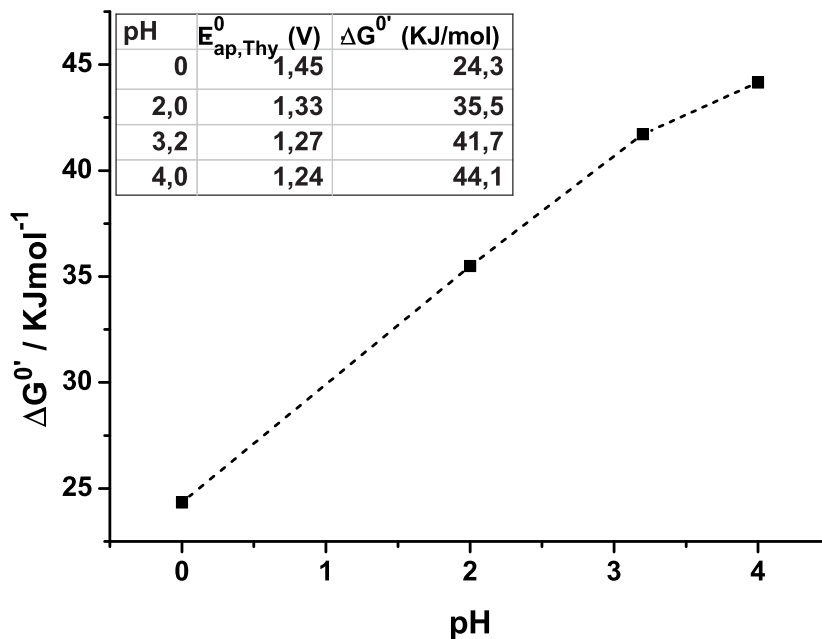


Fig. 4.14: The variation of the driving force with pH for  ${}^3\text{DPH}^+ + \text{ThyH}$  reaction. Calculated with the triplet energy  $E_{\text{T}} = 282 \text{ kJmol}^{-1}$ ,  $E_{\text{DPH}^+}^0 = -1.22\text{V}$ .

respectively.

The decay of triplet BPTC, observed at both wavelengths  $\lambda_{\text{max}} = 590\text{nm}$  and  $\lambda_{\text{max}} = 550\text{nm}$  in water, follows a first-order kinetics with  $k_d = (5 - 7) \times 10^5 \text{ s}^{-1}$  in agreement with reported values.<sup>[60,61]</sup> Figure 4.15 demonstrates the molar fractions of triplet BPTC and BPTC in water.

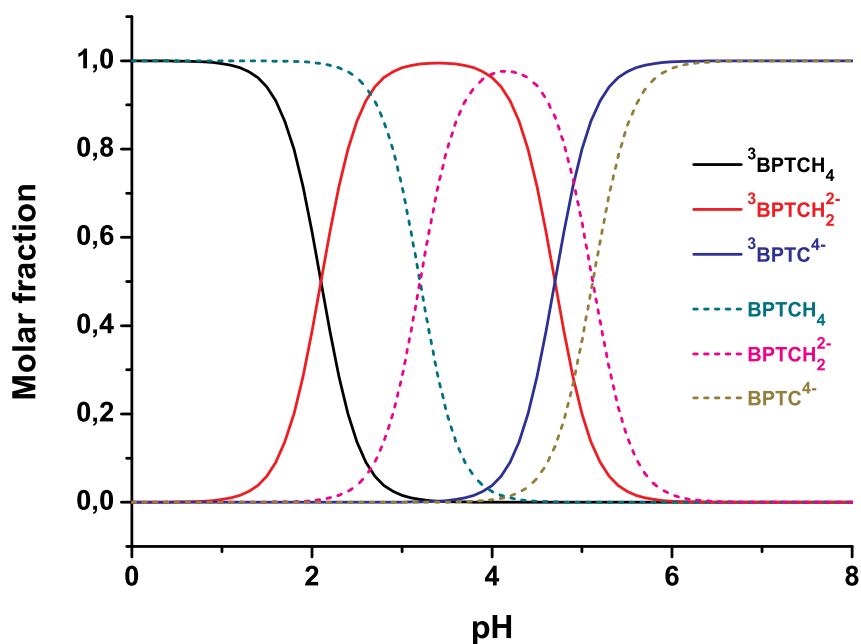
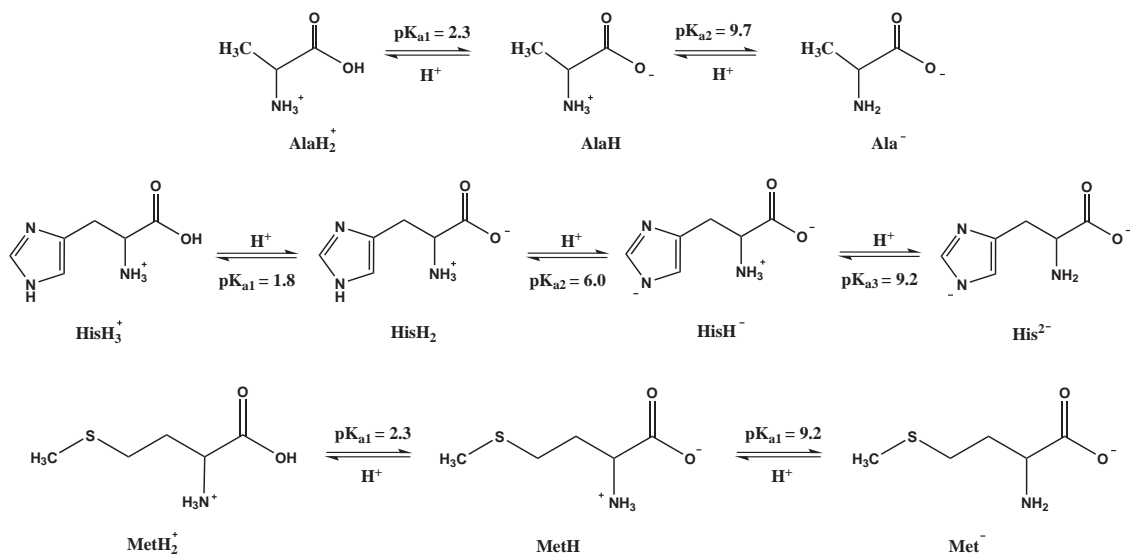


Fig. 4.15: Molar fractions of triplet BPTC and BPTC in water.

#### 4.4.2 Results of quenching by Alanine



Schema 4.4: Equilibria of Ala, His and Met in aqueous solution.

In Figure 4.16 the decays of triplet BPTC with increase concentration of Ala at pH=11.9 is presented. Figure 4.17 gives the transient absorption spectra of BPTC

ketyl radical anion (BPTC $\cdot^-$ ) attained at  $\lambda_{obs}=630\text{nm}$ . Although the absorption of this radical (in ms time-scale) is small, it confirms that electron transfer from Ala to triplet BPTC occurs, followed by fast diffusion apart. Quenching rate constants of triplet BPTC by alanine are found as  $1.9 \times 10^5 - 1.6 \times 10^7 \text{M}^{-1}\text{s}^{-1}$ .

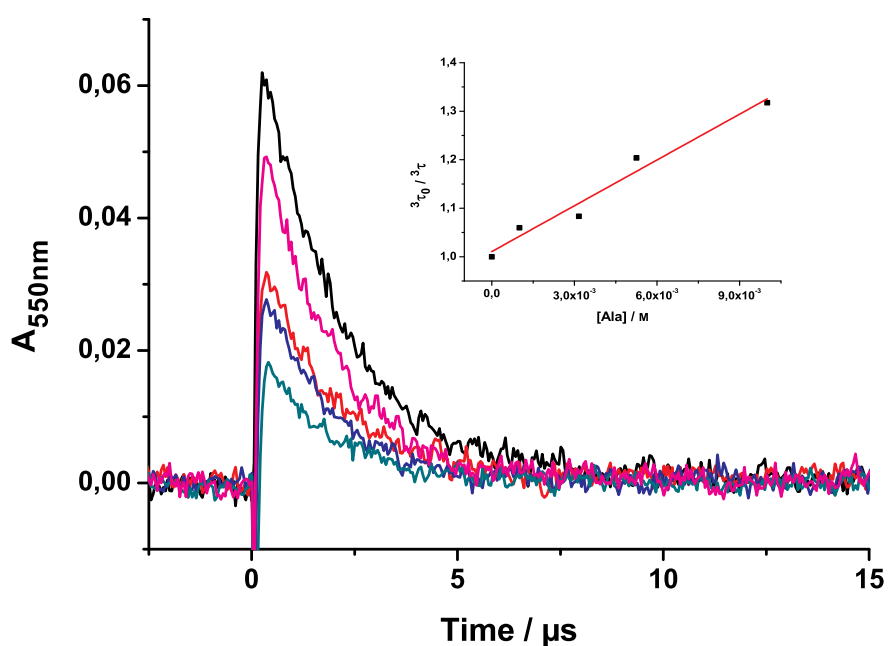


Fig. 4.16: Decay profiles ( $\lambda_{obs}=550\text{nm}$ ) for BPTC+Ala system in water pH=11.9. Concentration of Ala increases from top to bottom: 0 -  $1 \times 10^{-3}\text{M}$ . Insert: Stern-Volmer plot from Eqs. 3.25 and 3.15b.

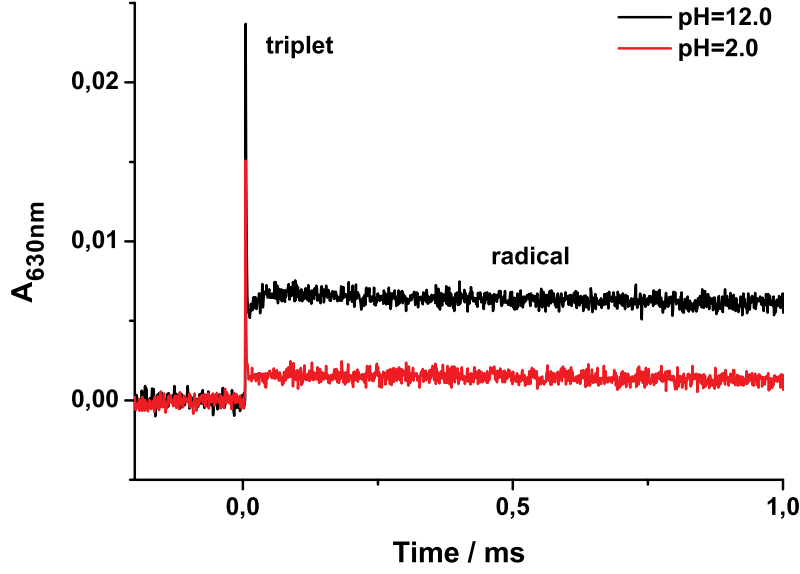


Fig. 4.17: TA spectra ( $\lambda_{obs}=630\text{nm}$ ) for BPTC ( $1 \times 10^{-4}\text{M}$ ) + Ala ( $5 \times 10^{-2}\text{M}$ ) systems in water at  $\text{pH}=2.0$  and  $11.9$ , monitored right after the laser-flash.

The pH-dependence of the observed quenching rate constant  $k_q^{obs}$  can be simulated according to the expression in Eq. 4.11 (see Tabs. 3.1 and 4.4 for parameters).

$$\begin{aligned}
 k_q^{obs} = & k_{q1} \frac{[H^+]^4}{[H^+]^4 + [H^+]^2 K_{a1}^{*2} + K_{a1}^{*2} K_{a2}^{*2}} \frac{[H^+]^2}{[H^+]^2 + [H^+] K_{a1} + K_{a1} K_{a2}} \\
 & + k_{q2} \frac{[H^+]^2 K_{a1}^{*2}}{[H^+]^4 + [H^+]^2 K_{a1}^{*2} + K_{a1}^{*2} K_{a2}^{*2}} \frac{[H^+]^2}{[H^+]^2 + [H^+] K_{a1} + K_{a1} K_{a2}} \\
 & + k_{q3} \frac{[H^+]^2 K_{a1}^{*2}}{[H^+]^4 + [H^+]^2 K_{a1}^{*2} + K_{a1}^{*2} K_{a2}^{*2}} \frac{[H^+] K_{a1}}{[H^+]^2 + [H^+] K_{a1} + K_{a1} K_{a2}} \\
 & + k_{q4} \frac{K_{a1}^{*2} K_{a2}^{*2}}{[H^+]^4 + [H^+]^2 K_{a1}^{*2} + K_{a1}^{*2} K_{a2}^{*2}} \frac{[H^+] K_{a1}}{[H^+]^2 + [H^+] K_{a1} + K_{a1} K_{a2}} \\
 & + k_{q5} \frac{K_{a1}^{*2} K_{a2}^{*2}}{[H^+]^4 + [H^+]^2 K_{a1}^{*2} + K_{a1}^{*2} K_{a2}^{*2}} \frac{K_{a1} K_{a2}}{[H^+]^2 + [H^+] K_{a1} + K_{a1} K_{a2}} \quad (4.11)
 \end{aligned}$$

Intrinsic rate constants obtained from the best fit (solid line, Fig. 4.18) are summarized in Tab. 4.4. It is seen that  $k_{q2}$ ,  $k_{q4} = 0$  implies no quenching reaction of triplet BPTC by  $\text{AlaH}_2^+$  and by  $\text{AlaH}$ . However, in solutions  $\text{pH}>9$  interestingly,  $k_q^{obs}$  increases with pH when deprotonated  $\text{Ala}^-$  becomes dominated by the equilibrium Eq. 4.12. This can be assigned to a greater reactivity of the electron rich  $\text{Ala}^-$  with triplet BPTC.



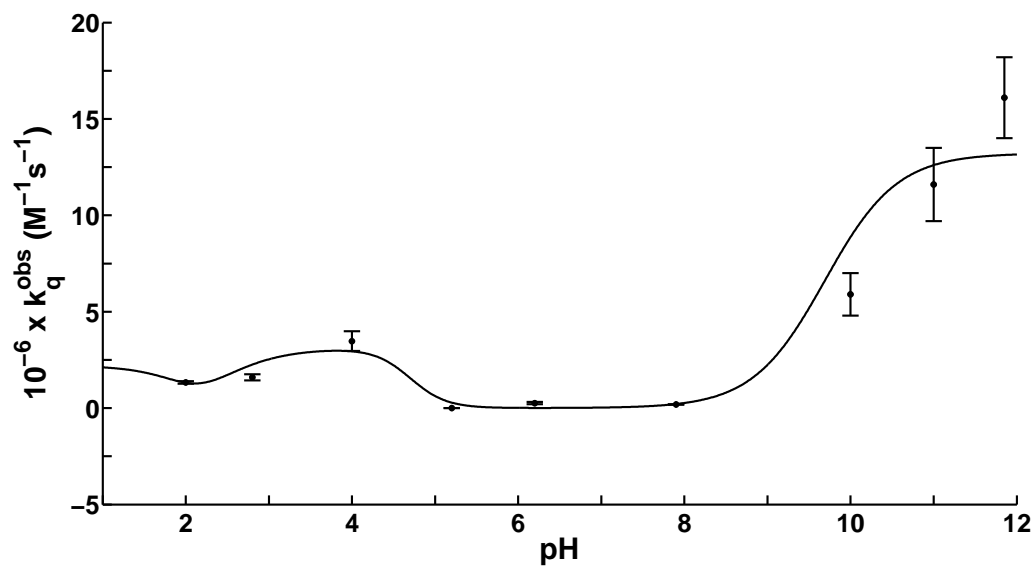


Fig. 4.18: pH-dependence of the observed quenching rate constant  $k_q^{obs}$  for the reaction of triplet BPTC with Ala. Solid line is the simulation from Eq. 4.11.

Tab. 4.4: Quenching rate constants of triplet BPTC by quenchers ( $k_{qi}$ )

Quencher	pH region	Main reactant pair	$k_{qi}$	$k_{qi}(M^{-1}s^{-1})$
Alanine	pH<2.1	${}^3\text{BPTCH}_4$ and $\text{AlaH}_2^+$	$k_{q1}$	$2.2 \times 10^6$
	2.1<pH<2.3	${}^3\text{BPTCH}_2^{2-}$ and $\text{AlaH}_2^+$	$k_{q2}$	0
	2.3<pH<4.7	${}^3\text{BPTCH}_2^{2-}$ and $\text{AlaH}$	$k_{q3}$	$3.1 \times 10^6$
	4.7<pH<9.7	${}^3\text{BPTC}^{4-}$ and $\text{AlaH}$	$k_{q4}$	0
	9.7<pH	${}^3\text{BPTC}^{4-}$ and $\text{Ala}^-$	$k_{q5}$	$1.3 \times 10^7$
Histidine	pH<1.8	${}^3\text{BPTCH}_4$ and $\text{HisH}_3^+$	$k_{q1}$	0
	1.8<pH<2.1	${}^3\text{BPTCH}_4$ and $\text{HisH}_2$	$k_{q2}$	0
	2.1<pH<4.7	${}^3\text{BPTCH}_2^{2-}$ and $\text{HisH}_2$	$k_{q3}$	$5.5 \times 10^8$
	4.7<pH<6.0	${}^3\text{BPTC}^{4-}$ and $\text{HisH}_2$	$k_{q4}$	$8.1 \times 10^8$
	6.0<pH<9.2	${}^3\text{BPTC}^{4-}$ and $\text{HisH}^-$	$k_{q5}$	$7.7 \times 10^8$
	9.2<pH	${}^3\text{BPTC}^{4-}$ and $\text{His}^{2-}$	$k_{q6}$	$3.3 \times 10^8$
Methionine	pH<2.1	${}^3\text{BPTCH}_4$ and $\text{MetH}_2^+$	$k_{q1}$	$3.0 \times 10^9$
	2.1<pH<2.3	${}^3\text{BPTCH}_2^{2-}$ and $\text{MetH}_2^+$	$k_{q2}$	$2.6 \times 10^{10}$
	2.3<pH<4.7	${}^3\text{BPTCH}_2^{2-}$ and $\text{MetH}$	$k_{q3}$	$4.3 \times 10^9$
	4.7<pH<9.2	${}^3\text{BPTC}^{4-}$ and $\text{MetH}$	$k_{q4}$	$2.3 \times 10^9$
	9.2<pH	${}^3\text{BPTC}^{4-}$ and $\text{Met}^-$	$k_{q5}$	$6.8 \times 10^8$
Adenine	pH<2.1	${}^3\text{BPTCH}_4$ and $\text{AdeH}_2^+$	$k_{q1}$	0
	2.1<pH<4.2	${}^3\text{BPTCH}_2^{2-}$ and $\text{AdeH}_2^+$	$k_{q2}$	$8.4 \times 10^9$
	4.2<pH<4.7	${}^3\text{BPTCH}_2^{2-}$ and $\text{AdeH}$	$k_{q3}$	$2.0 \times 10^9$
	4.7<pH<9.9	${}^3\text{BPTC}^{4-}$ and $\text{AdeH}$	$k_{q4}$	$2.3 \times 10^9$
	9.9<pH	${}^3\text{BPTC}^{4-}$ and $\text{Ade}^-$	$k_{q5}$	$4.7 \times 10^8$
Adenosine	pH<2.1	${}^3\text{BPTCH}_4$ and $\text{dAdeH}_2^+$	$k_{q1}$	$4.8 \times 10^9$
	2.1<pH<3.5	${}^3\text{BPTCH}_2^{2-}$ and $\text{dAdeH}_2^+$	$k_{q2}$	$6.8 \times 10^9$
	3.5<pH<4.7	${}^3\text{BPTCH}_2^{2-}$ and $\text{dAdeH}$	$k_{q3}$	$4.0 \times 10^9$
	4.7<pH<12.5	${}^3\text{BPTC}^{4-}$ and $\text{dAdeH}$	$k_{q4}$	$6.2 \times 10^8$
	12.5<pH	${}^3\text{BPTC}^{4-}$ and $\text{dAde}^-$	$k_{q5}$	$4.5 \times 10^7$
Thymine	pH<2.1	${}^3\text{BPTCH}_4$ and $\text{ThyH}$	$k_{q1}$	$3.5 \times 10^9$
	2.1<pH<4.7	${}^3\text{BPTCH}_2^{2-}$ and $\text{ThyH}$	$k_{q2}$	$2.5 \times 10^9$
	4.7<pH<9.9	${}^3\text{BPTC}^{4-}$ and $\text{ThyH}$	$k_{q3}$	$1.0 \times 10^9$
	9.9<pH	${}^3\text{BPTC}^{4-}$ and $\text{Thy}^-$	$k_{q4}$	0
Thymidine	pH<2.1	${}^3\text{BPTCH}_4$ and $\text{dThyH}_2$	$k_{q1}$	$6.6 \times 10^9$
	2.1<pH<4.7	${}^3\text{BPTCH}_2^{2-}$ and $\text{dThyH}_2$	$k_{q2}$	$2.5 \times 10^9$
	4.7<pH<9.8	${}^3\text{BPTC}^{4-}$ and $\text{dThyH}_2$	$k_{q3}$	$4.0 \times 10^8$
	9.8<pH<12.9	${}^3\text{BPTC}^{4-}$ and $\text{dThyH}^-$	$k_{q4}$	$3.1 \times 10^8$
	12.9<pH	${}^3\text{BPTC}^{4-}$ and $\text{dThy}^{2-}$	$k_{q5}$	$0^a$

<sup>a</sup>  $k_{q5} = 0$  implies that the deprotonation of the deoxyribose group of dThy does not affect the quenching process.

### 4.4.3 Results of quenching by Histidine

Time-profiles of triplet BPTC in the presence of His in water at pH=6.2 are demonstrated in Figure 4.19. It is seen in Fig. 4.19 that at the beginning of irradiation the transient absorbance decreases but increases at a longer time (at ca.  $2.5 \mu\text{s}$ ). This clearly indicates an overlap of the triplet decay and growth of the radical (i.e. the third kinetic case consider, see section 3.5.1).

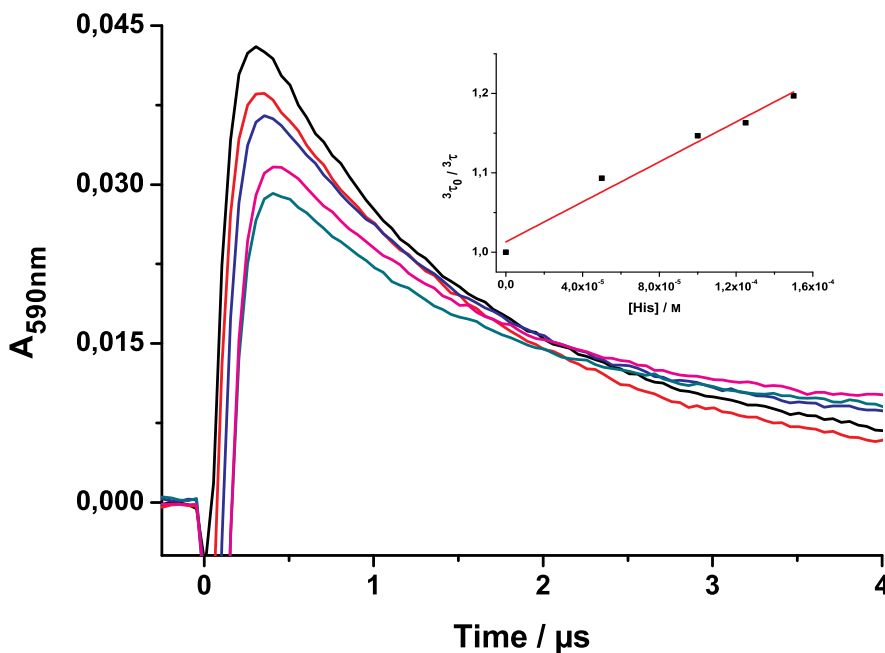


Fig. 4.19: Decay profiles ( $\lambda_{obs}=590\text{nm}$ ) for BPTC+His system in water at pH=6.2. Concentration of His increases from top to bottom: 0 -  $1.5 \times 10^{-4}\text{M}$ . Insert: Stern-Volmer plot from Eqs. 3.25 and 3.15b.

$$\begin{aligned}
 k_q^{obs} = & k_{q1} \frac{[H^+]^4}{[H^+]^4 + [H^+]^2 K_{a1}^{*2} + K_{a1}^{*2} K_{a2}^{*2}} \times \frac{[H^+]^3}{[H^+]^3 + [H^+]^2 K_{a1} + [H^+] K_{a1} K_{a2} + K_{a1} K_{a2} K_{a3}} \\
 & + k_{q2} \frac{[H^+]^4}{[H^+]^4 + [H^+]^2 K_{a1}^{*2} + K_{a1}^{*2} K_{a2}^{*2}} \times \frac{[H^+]^2 K_{a1}}{[H^+]^3 + [H^+]^2 K_{a1} + [H^+] K_{a1} K_{a2} + K_{a1} K_{a2} K_{a3}} \\
 & + k_{q3} \frac{[H^+]^2 K_{a1}^{*2}}{[H^+]^4 + [H^+]^2 K_{a1}^{*2} + K_{a1}^{*2} K_{a2}^{*2}} \times \frac{[H^+]^2 K_{a1}}{[H^+]^3 + [H^+]^2 K_{a1} + [H^+] K_{a1} K_{a2} + K_{a1} K_{a2} K_{a3}} \\
 & + k_{q4} \frac{K_{a1}^{*2} K_{a2}^{*2}}{[H^+]^4 + [H^+]^2 K_{a1}^{*2} + K_{a1}^{*2} K_{a2}^{*2}} \times \frac{[H^+]^2 K_{a1}}{[H^+]^3 + [H^+]^2 K_{a1} + [H^+] K_{a1} K_{a2} + K_{a1} K_{a2} K_{a3}} \\
 & + k_{q5} \frac{K_{a1}^{*2} K_{a2}^{*2}}{[H^+]^4 + [H^+]^2 K_{a1}^{*2} + K_{a1}^{*2} K_{a2}^{*2}} \times \frac{[H^+] K_{a1} K_{a2}}{[H^+]^3 + [H^+]^2 K_{a1} + [H^+] K_{a1} K_{a2} + K_{a1} K_{a2} K_{a3}} \\
 & + k_{q6} \frac{K_{a1}^{*2} K_{a2}^{*2}}{[H^+]^4 + [H^+]^2 K_{a1}^{*2} + K_{a1}^{*2} K_{a2}^{*2}} \times \frac{K_{a1} K_{a2} K_{a3}}{[H^+]^3 + [H^+]^2 K_{a1} + [H^+] K_{a1} K_{a2} + K_{a1} K_{a2} K_{a3}} \quad (4.13)
 \end{aligned}$$

Together with the appearance of  $\text{BPTC}^{\cdot-}$  at  $\lambda_{obs}=630\text{nm}$  (in a separate experiment) means electron transfer from His to triplet BPTC and then fast escape of radical ions from the charge-transfer complex would be followed. Quenching rate constants are in the range of  $8.7 \times 10^7 - 7.7 \times 10^8 \text{M}^{-1}\text{s}^{-1}$ .

All reactant species presented in the solution at different pH are listed in Tab. 4.4 (see also in Fig. 4.15 and Scheme 4.4). pH-dependence of the observed quenching rate constant  $k_q^{obs}$  can be expressed by Eq. 4.13 (see Tabs. 3.1 and 4.4 for

parameters). This is shown in Figure 4.20, whose parameters obtained from the best fit (solid line, Fig. 4.20) is also summarized in Tab. 4.4. It can be found

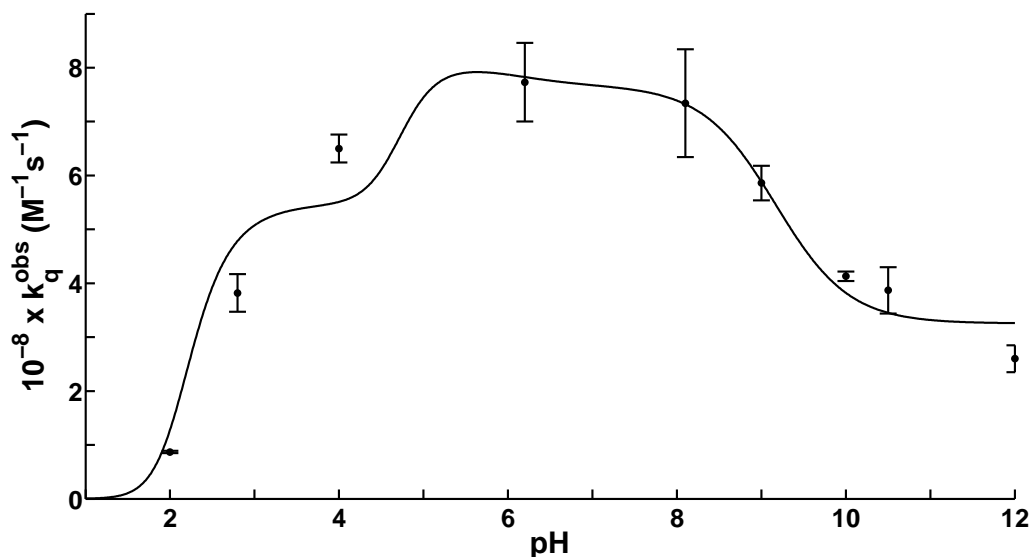
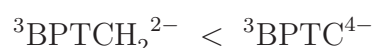


Fig. 4.20: pH-dependence of the observed quenching rate constant  $k_q^{obs}$  for the reaction of triplet BPTC with His. Solid line is the simulation from Eq. 4.13.

that  $k_{q1}, k_{q2} = 0$  means no quenching reaction of  ${}^3\text{BPTCH}_4$  by  $\text{HisH}_3^+$  or by  $\text{HisH}_2$  under strong acidic solutions ( $\text{pH} < 2$ ). In the pH range of 2–6, the increase of  $k_q^{obs}$  is explained by the consecutive acid-base equilibria established, Eqs. 4.4a and 4.4b. Therefore, it is also interesting to notice that rate constants between  $\text{HisH}_2$  and triplet BPTC tends to be:



Theoretically more negative net charge the reduction would be more difficult and the quenching rate constant becomes lower but, here, this is not the case. Further decrease of  $k_q^{obs}$  at  $\text{pH} > 6$  is caused by the shift of  $\text{HisH}^-$  equilibrium towards its dianionic form, Equation 4.14. Due to a coulombic repulsion effect the rate constants get smaller.



#### 4.4.4 Results of quenching by Methionine

Met can exist in protonated, neutral or deprotonated forms depending on the pH of the solution (see Tab. 4.4, Fig. 4.15 and Scheme 4.4). In the presence of Met the lifetime of the triplet BPTC is decreased and the longer-lived transient  $\text{BPTC}^{\cdot-}$

appears,  $\lambda_{max}=630\text{nm}$ . The decays and Stern-Volmer plot for this system in the solution of  $\text{pH}=3.4$  are presented in Fig. 4.21. The formation of ketyl radical anion implies that the photochemical primary step is an electron transfer accompanied by fast diffusion out of the charge-transfer complex. The pH-dependence of the

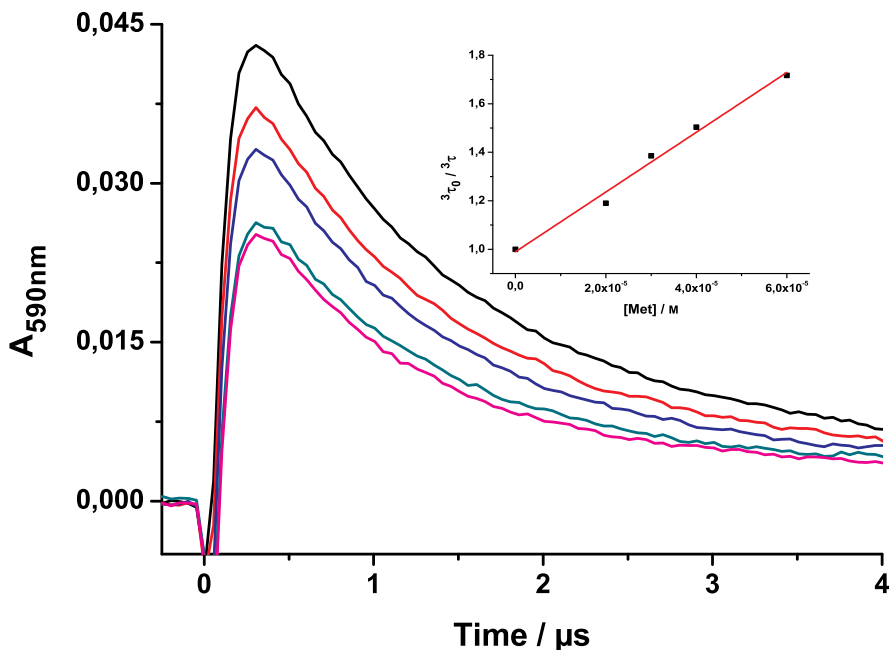


Fig. 4.21: Decay profiles ( $\lambda_{obs}=590\text{nm}$ ) for BPTC+Met system in water at  $\text{pH}=3.4$ . Concentration of Met increases from top to bottom:  $0 - 6 \times 10^{-5}\text{M}$ . Insert: Stern-Volmer plot from Eqs. 3.25 and 3.15b.

observed quenching rate constant  $k_q^{obs}$  is simulated according to Eq. 4.11 (similar to the case of Ala) and is shown in Figure 4.22 (see Tabs. 3.1 and 4.4 for parameters). It is worth to note that, for methionine, there are two electron-donor centers at the sulfur atom and nitrogen atom. In fact,  $k_q^{obs}$  varied at  $\text{pH}>4.7$  indicates the state of protonation of the amine group rather than sulfur moiety influences the quenching rate of the triplet BPTC.

Figure 4.22 demonstrates a maximum of  $k_q^{obs}$  at  $\text{pH}\approx 2.2$ . The increase of  $k_q^{obs}$  up to  $\text{pH}\approx 2.2$  can be explained by a shift of the triplet BPTC equilibrium towards its dianionic form,<sup>[10]</sup> Equation 4.4a. The highest quenching rate constant, here, can be attributed to the molecular net charge of the reactants,  ${}^3\text{BPTCH}_2^{2-} + \text{MetH}_2^+$  (coulombic interaction). The further decrease of  $k_q^{obs}$  at  $\text{pH}\approx 2.8-5$  is caused by a

drop of the  $\text{MetH}_2^+$  concentration followed by equilibrium Equation 4.15:



After reaching a plateau (clearly in the simulation) in the pH-region of 5-8,  $k_q^{obs}$  slightly decreases, which corresponds to the deprotonation of the amine group ( $pK_{a2} = 9.2$ ).

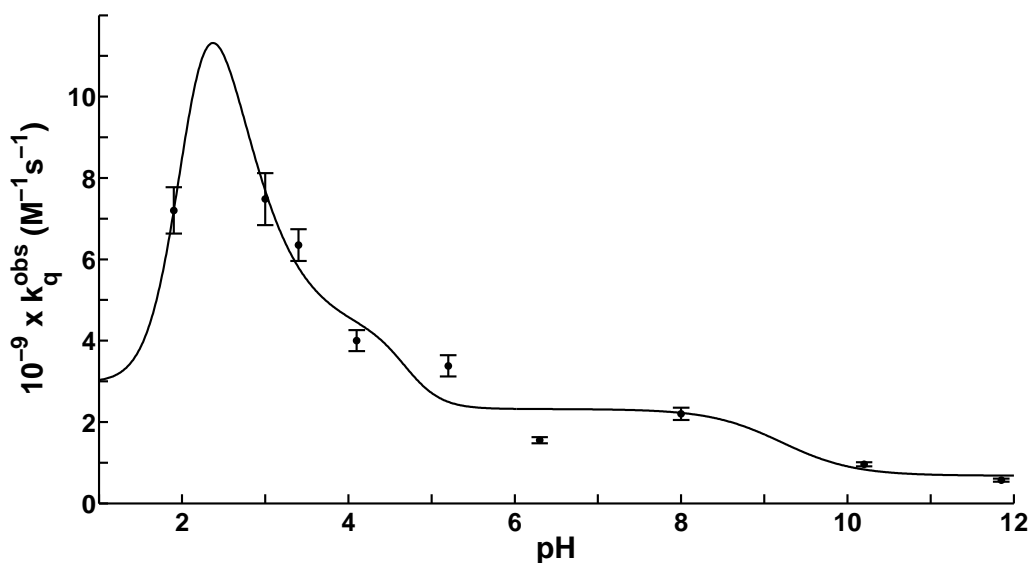
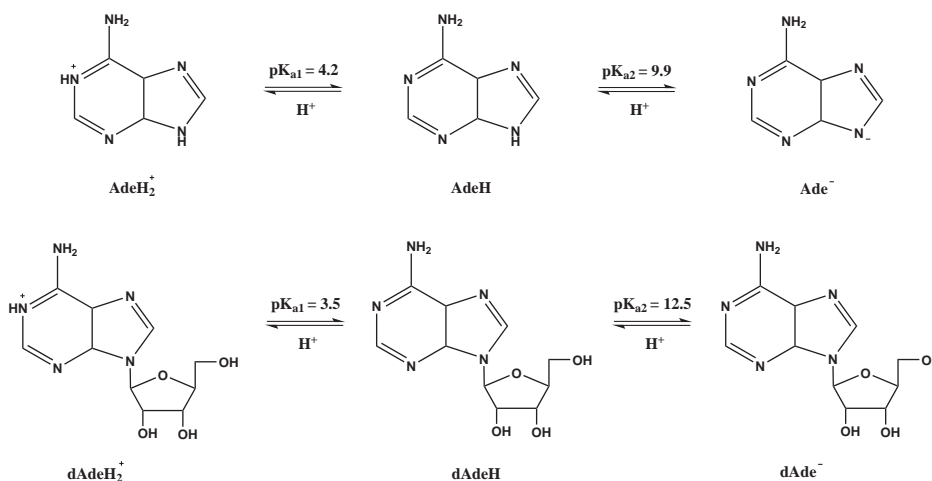


Fig. 4.22: pH-dependence of the observed quenching rate constant  $k_q^{obs}$  for the reaction of BPTC triplet with Met. Solid line is the simulation from Eq. 4.11.

#### 4.4.5 Results of quenching by Adenine

The decay profiles at pH=4.0 and Stern-Volmer plot of the quenching of triplet BPTC by Ade are represented in Figure 4.23. The formation of the long-lived transient  $\text{BPTC}^-$  (shown in Fig. 4.23 at time ca.  $2.5 \mu\text{s}$  or from separate experiments) is observed in the whole range of pH. This leads to conclude that an electron transfer reaction from Ade to triplet BPTC is followed by fast diffusion of the reactants. The pH-dependence of the observed quenching rate constant  $k_q^{obs}$  is also described by Equation 4.11 and is presented in Figure 4.24 (see Tables 3.1 and 4.4 also in Scheme 4.5 for parameters).

It is seen that  $k_{q1} = 0$  implies no quenching reaction of triplet BPTC by  $\text{AdeH}_2^+$



Schema 4.5: Equilibria of Ade and dAde in aqueous solution.

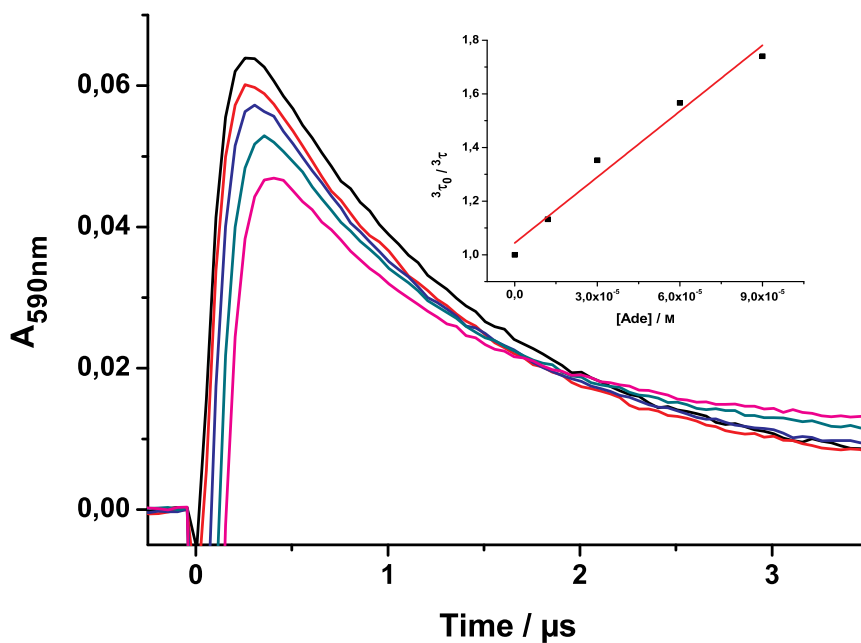


Fig. 4.23: Decay profiles ( $\lambda_{obs}=590\text{nm}$ ) for BPTC+Ade system in water at pH=4.0. Concentration of Ade increases from top to bottom: 0 -  $9 \times 10^{-5}\text{M}$ . Insert: Stern-Volmer plot from Eqs. 3.25 and 3.15b.

under strong acidic conditions (pH<2). At pH>2, a similar interpretation to the quenching reaction by methionine mentioned earlier (see the text) remains valuable to explain for the change of  $k_q^{obs}$  with pH.

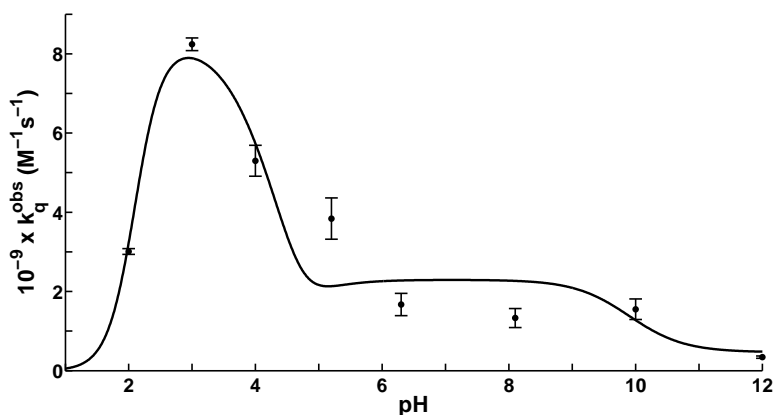


Fig. 4.24: pH-dependence of the observed quenching rate constant  $k_q^{obs}$  for the reaction of triplet BPTC with Ade. The solid line is the simulation from Eq. 4.11.

#### 4.4.6 Results of quenching by Adenosine

In Figure 4.25 the time evolution and kinetic analysis for the quenching of triplet BPTC by dAde at pH=4.0 is given. Undoubtedly, this is the third kinetic case consider (see section 3.5.1) because the total radical absorbance increases slightly (at time ca. 3  $\mu$ s) with concentration of dAde. Together with the observation of BPTC $^{\cdot-}$  at  $\lambda_{obs}$ =630nm leads to the conclusion that electron transfer from dAde to triplet BPTC occurs followed by fast diffusion step. The pH-dependence of the observed quenching rate constant  $k_q^{obs}$  is expressed by Equation 4.11 (see Tables 3.1 and 4.4 also in Scheme 4.5 for parameters). Values obtained from the best fit (solid line, Figure 4.26) are summarized in Table 4.4. Once again, a similar explanation, to that of the quenching reaction by adenine, for the variation of the observed quenching rate constant  $k_q^{obs}$  with pH is used.

#### 4.4.7 Results of quenching by Thymine

The lifetime of the triplet BPTC is decreased and the long-lived transient BPTC $^{\cdot-}$  ( $\lambda_{max}$ =630nm) appears, when thymine is present. The formation of ketyl radical anion implies that the photochemical primary step is an electron transfer. In the range of pH=2.0-10.0, we found that the transient kinetics for this system correspond to the fourth kinetic case consider (see section 3.5.1). Data analysis for this system in the solution pH=8.0 is presented in Figures 4.27 and 4.28. It can be seen that the total radical absorbance is high ( $A_{radical}^{\infty}/A_{triplet}^0 = 0.28$  at [Thy]= $6 \times 10^{-4}$ M, Fig. 4.27) due to the high radical quantum yield of BPTC $^{\cdot-}$  at pH=8.0. Plotting  $k_1$  vs. [Thy] at pH=8.0 (Fig. 4.28) gives a good linearity and zero

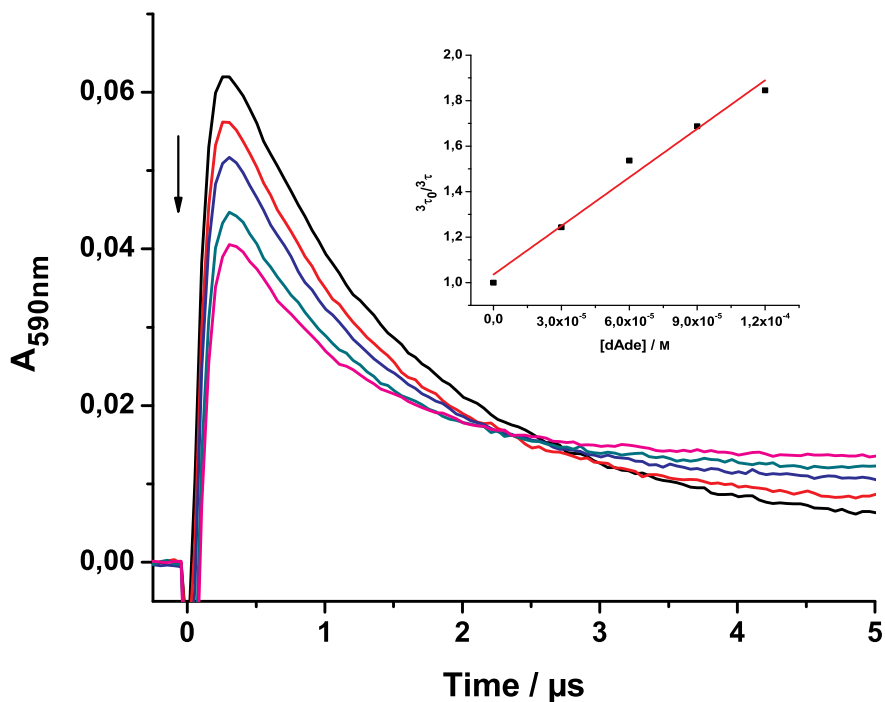


Fig. 4.25: Decay profiles ( $\lambda_{obs}=590\text{nm}$ ) for BPTC+dAde system in water at pH=4.0. Concentration of dAde increases from top to bottom: 0 -  $1.2 \times 10^{-4}\text{M}$ . Insert: Stern-Volmer plot from Eqs. 3.25 and 3.15b.

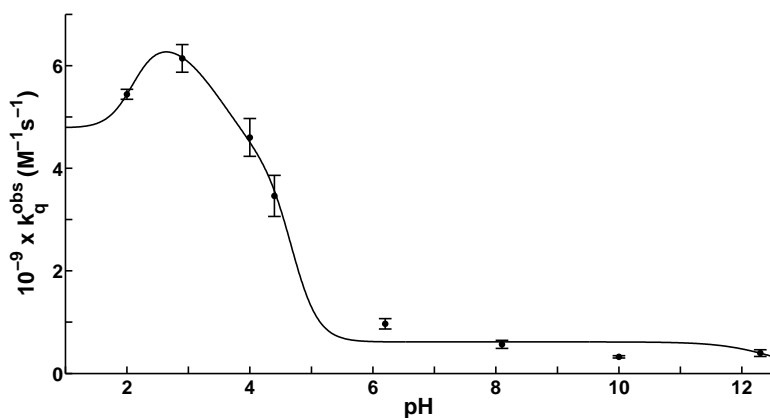


Fig. 4.26: pH-dependence of the observed quenching rate constant  $k_q^{obs}$  for the reaction of triplet BPTC with dAde. Solid line is the simulation from Eq. 4.11.

intercept, which shows an accuracy of the analyzed model. The spectrum of  $\text{BPTC}^{\cdot-}$  over the range of 610-660nm was obtained by laser flash irradiation to the solution of BPTC ( $1.0 \times 10^{-4} \text{molL}^{-1}$ ) and thymine ( $1.5 \times 10^{-2} \text{molL}^{-1}$ ), Fig. 4.29.  $\text{BPTC}^{\cdot-}$

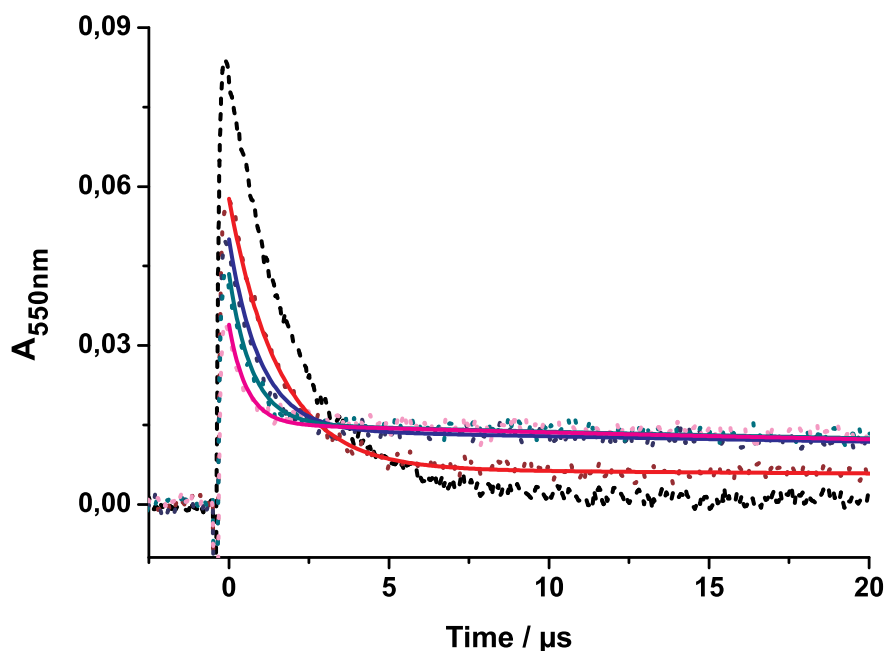


Fig. 4.27: Decays ( $\lambda_{obs}=550\text{nm}$ ) of triplet BPTC ( $1 \times 10^{-4}\text{molL}^{-1}$ ) + thymine (concentration increase from top to bottom: 0 -  $1.5 \times 10^{-4}\text{M}$ ) in water at  $\text{pH}=8.0$ . Experimental: dashed lines; simulation with Eq. 3.26: solid lines.

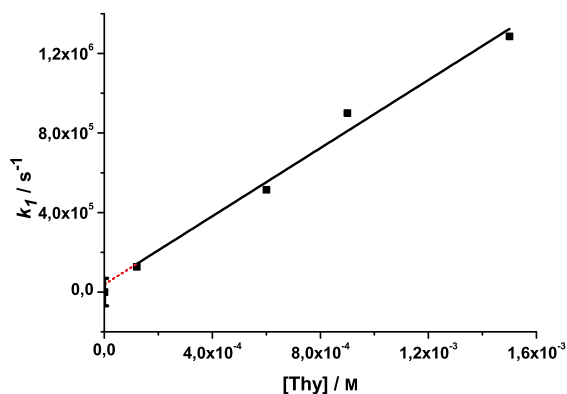


Fig. 4.28:  $k_1$  vs.  $[\text{Thy}]$  plot for the BPTC+Thy system in water at  $\text{pH}=8.0$ .

absorbs at  $\lambda_{\text{max}}=630\text{nm}$  and the decay monitored at  $\lambda_{\text{obs}}=630\text{nm}$  obeys a second-order kinetic law ( $k_2/\epsilon_{\text{BPTC}^-} = 3 \times 10^5\text{cm}^{-1}$ ). Indeed, Inbar et al.<sup>[59]</sup> has reported that the pinacol yield of the  $4\text{-BC}^{\cdot-} + 4\text{-BC}^{\cdot-}$  reaction is minor. This leads to the postulation that after an initial electron transfer followed by proton transfer, ketyl radicals ( $\text{BPTCH}^{\cdot}$ ) are formed, which dissociate into free radical ions and thereafter

randomly encounter to undergo the pinacol reaction ( $\text{BPTCH}\cdot + \text{BPTCH}\cdot$ ).

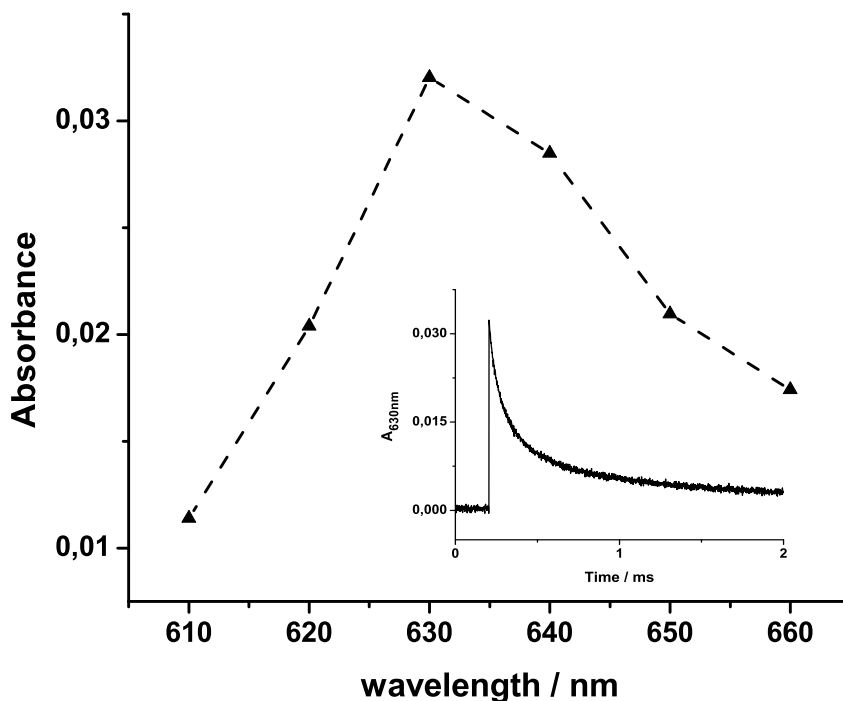
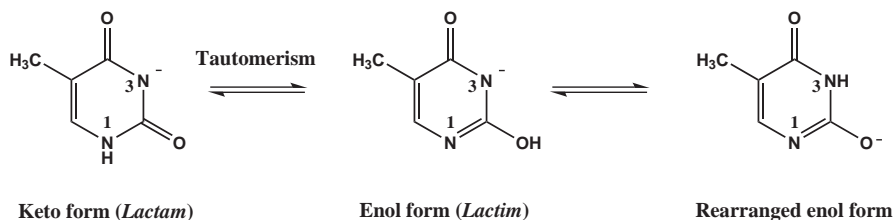


Fig. 4.29: BPTC ketyl radical anion spectrum in the presence of thymine ( $1.5 \times 10^{-2} \text{ molL}^{-1}$ ) at  $\text{pH}=2.0$ . Insert: Decay profile ( $\lambda_{\text{obs}}=630\text{nm}$ ) of  $\text{BPTC}\cdot^-$ , which form the pinacol after the fast protonation of  $\text{BPTC}\cdot^-$  to  $\text{BPTCH}\cdot$ .

On the other hand, the formation of  $\text{BPTC}\cdot^-$  could not be observed at  $\text{pH}=12.0$ , even at high concentrations of thymine ( $[\text{Thy}]=1.5 \times 10^{-2} \text{ molL}^{-1}$ ). This can be explained by a keto-enol tautomerism of  $\text{Thy}^-$ , Scheme 4.6, which significantly changes the chemical properties of  $\text{Thy}^-$ . Therefore, no quenching reaction of triplet BPTC by  $\text{Thy}^-$  occurs.



Scheme 4.6: Tautomerism at  $\text{pH}>10$ .

The pH-dependence of the observed quenching rate constants  $k_q^{\text{obs}}$  is simulated

by Eq. 4.17 and is shown in Fig. 4.30.

$$\begin{aligned}
 k_q^{obs} = & k_{q1} \frac{[H^+]^4}{[H^+]^4 + [H^+]^2 K_{a1}^{*2} + K_{a1}^{*2} K_{a2}^{*2}} \frac{[H^+]}{[H^+] + K_a} \\
 & + k_{q2} \frac{[H^+]^2 K_{a1}^{*2}}{[H^+]^4 + [H^+]^2 K_{a1}^{*2} + K_{a1}^{*2} K_{a2}^{*2}} \frac{[H^+]}{[H^+] + K_a} \\
 & + k_{q3} \frac{K_{a1}^{*2} K_{a2}^{*2}}{[H^+]^4 + [H^+]^2 K_{a1}^{*2} + K_{a1}^{*2} K_{a2}^{*2}} \frac{[H^+]}{[H^+] + K_a}
 \end{aligned} \tag{4.17}$$

Fig. 4.30 shows a continuous downhill and flat behavior of  $k_q^{obs}$ . The decrease of  $k_q^{obs}$

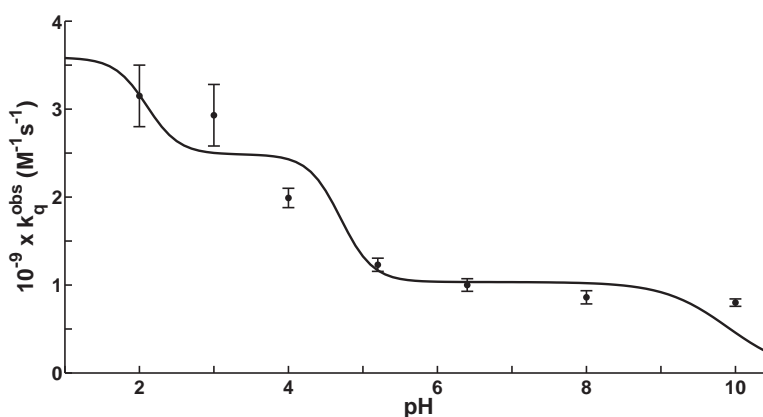


Fig. 4.30: pH-dependence of the observed quenching rate constants  $k_q^{obs}$  for the reaction of triplet BPTC with thymine. The solid line is the simulation according to Equation 4.17.

with pH is characterized by two changes (at  $\text{pH} \approx 2.1$  and  $4.7$ ) which coincide well with the two-deprotonation stages of triplet BPTC. Moreover,  $k_q^{obs}$  reaches plateaus in the regions,

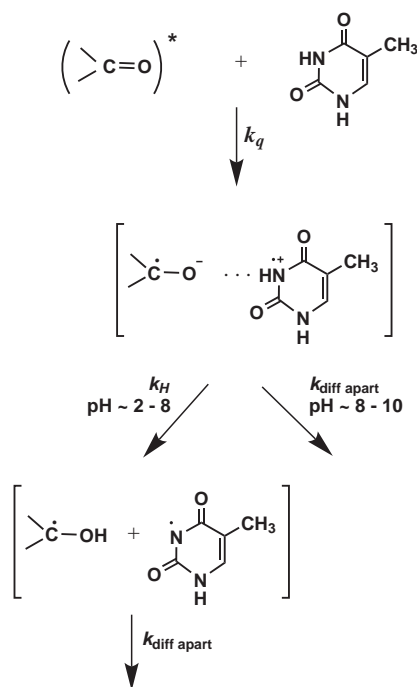
$$\begin{aligned}
 3.0 < \text{pH} < 4.0 & \text{ (} {}^3\text{BPTCH}_2^{2-} + \text{ThyH) and} \\
 6.0 < \text{pH} < 8.0 & \text{ (} {}^3\text{BPTC}^{4-} + \text{ThyH)}
 \end{aligned}$$

which are attributed to the equilibria of the corresponding reactant pairs. Note that in the range of  $\text{pH} < pK_a$ , thymine exists in the neutral form while triplet BPTC shows two steps of deprotonation ( $pK_{a1}^* = 2.1$  and  $pK_{a2}^* = 4.7$ ). Therefore, it is allowed to predict the chemical reactivity between triplet BPTC and ThyH with the order:



Perhaps, for more negative net charge the reduction is more difficult and the quenching rate constant becomes lower.

Closing the kinetic analysis, one question remains related to the quenching reactions of triplet BPTC by thymine at pH=2.0-10.0. Is electron transfer followed by proton transfer? In order to check the favorable pathway, the pH-dependent result of the oxidation potential of thymine by the cyclic voltammetry is applied once again. We knew, from the section 4.3.4, at  $\text{pH} \leq 8.0$  an one proton coupled one electron transfer during the oxidation of thymine. This observation and the above kinetic analysis suggest that the possible pathway of the quenching reaction of triplet BPTC by thymine between pH 2.0-8.0 is an initial electron transfer followed by proton transfer (Scheme 4.7). At pH around 8.0-10.0, a simple electron transfer mechanism might take place in competition.



Scheme 4.7: Quenching reaction of triplet BPTC by thymine

#### 4.4.8 Results of quenching by Thymidine

When thymidine is present with increase concentration, the appearance of  $\text{BPTC}^{\cdot-}$  at  $\lambda_{obs}=630\text{nm}$ , which then decays according to second-order kinetics in ms time-scale (for the whole range of  $\text{pH}=2.0-12.0$ ), is observed. This is interpreted by an electron transfer mechanism from dThy to triplet BPTC forming the radical pair followed by fast escape of these radical ions from the charge-transfer successor complex. Thereafter, depending on pH of the solution, the pinacol reactions,

BPTCH $\cdot$ +BPTCH $\cdot$ , BPTCH $\cdot$ +BPTC $\cdot^-$  or BPTC $\cdot^-$ +BPTC $\cdot^-$ , occur. Note that unlike thymine a keto-enol tautomerism is no longer possible due to the deoxyribose group of dThy.

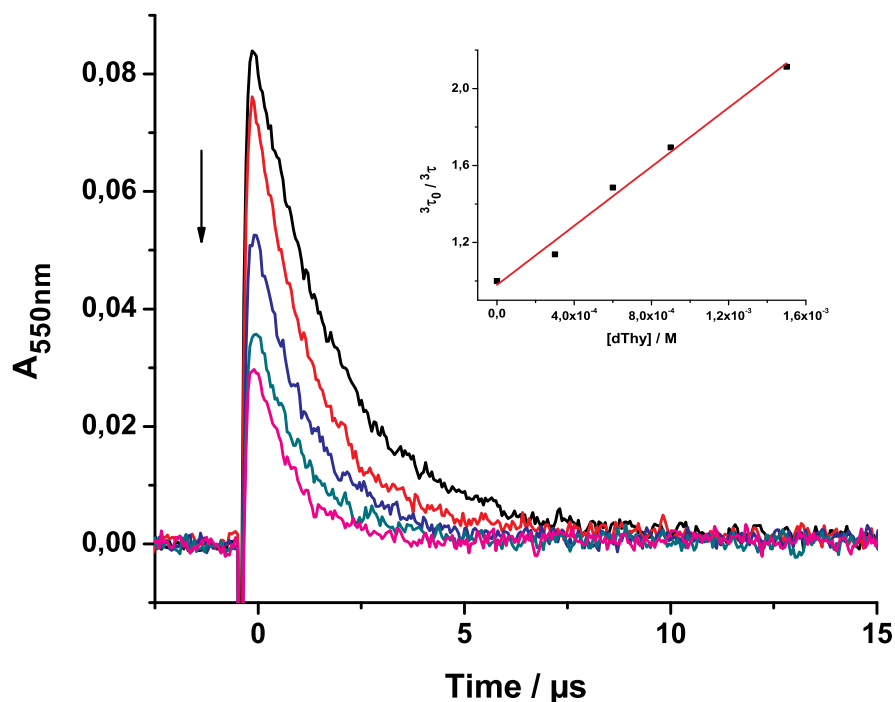


Fig. 4.31: Decay profile ( $\lambda_{obs}=550\text{nm}$ ) for BPTC+dThy system in water pH=8.0. Concentration of dThy increases from top to bottom: 0 -  $1.5 \times 10^{-3}\text{M}$ . Insert: Stern-Volmer plot from Eqs. 3.25 and 3.15b.

The pH-dependence of the observed quenching rate constant  $k_q^{obs}$  can be expressed by Equation 4.18 and is presented in Figure 4.32 (see Tables 3.1 and 4.4 for parameters). The main reactions at each pH region and their corresponding quenching rate constants,  $k_{qi}$ , obtained by the best fit (solid line, Figure 4.32), are summarized in Table 4.4. Note also that  $k_{q5} = 0$  implies the deprotonation of the deoxyribose group ( $pK_a = 12.9$ ) of dThy do not influence much the overall quenching rate constant,  $k_q^{obs}$ . Therefore, similar explanations, like the quenching reaction with thymine for pH<10 and that with methionine for pH> 10, are given for the

variation of the observed quenching rate constants  $k_q^{obs}$  with pH.

$$\begin{aligned}
 k_q^{obs} = & k_{q1} \frac{[H^+]^4}{[H^+]^4 + [H^+]^2 K_{a1}^{*2} + K_{a1}^{*2} K_{a2}^{*2}} \times \frac{[H^+]^2}{[H^+]^2 + [H^+] K_{a1} + K_{a1} K_{a2}} \\
 & + k_{q2} \frac{[H^+]^2 K_{a1}^{*2}}{[H^+]^4 + [H^+]^2 K_{a1}^{*2} + K_{a1}^{*2} K_{a2}^{*2}} \times \frac{[H^+]^2}{[H^+]^2 + [H^+] K_{a1} + K_{a1} K_{a2}} \\
 & + k_{q3} \frac{K_{a1}^{*2} K_{a2}^{*2}}{[H^+]^4 + [H^+]^2 K_{a1}^{*2} + K_{a1}^{*2} K_{a2}^{*2}} \times \frac{[H^+]^2}{[H^+]^2 + [H^+] K_{a1} + K_{a1} K_{a2}} \\
 & + k_{q4} \frac{K_{a1}^{*2} K_{a2}^{*2}}{[H^+]^4 + [H^+]^2 K_{a1}^{*2} + K_{a1}^{*2} K_{a2}^{*2}} \times \frac{[H^+] K_{a1}}{[H^+]^2 + [H^+] K_{a1} + K_{a1} K_{a2}} \\
 & + k_{q5} \frac{K_{a1}^{*2} K_{a2}^{*2}}{[H^+]^4 + [H^+]^2 K_{a1}^{*2} + K_{a1}^{*2} K_{a2}^{*2}} \times \frac{K_{a1} K_{a2}}{[H^+]^2 + [H^+] K_{a1} + K_{a1} K_{a2}} \quad (4.18)
 \end{aligned}$$

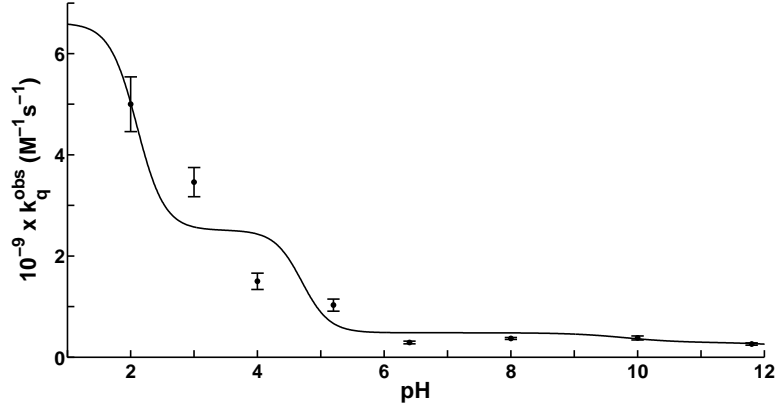


Fig. 4.32: pH-dependence of the observed quenching rate constant  $k_q^{obs}$  for the reaction of triplet BPTC with dThy. Solid line is the simulation from Eq. 4.18.

#### 4.4.9 CV results of BPTC

In Figure 4.13, pH-dependence of the apparent standard reduction potential of BPTC is given. It shows a linear variation of  $E_{ap,BPTC}^0$  with pH characterized by a slope of  $-27.8 \pm 2.4$  mV per pH-unit.

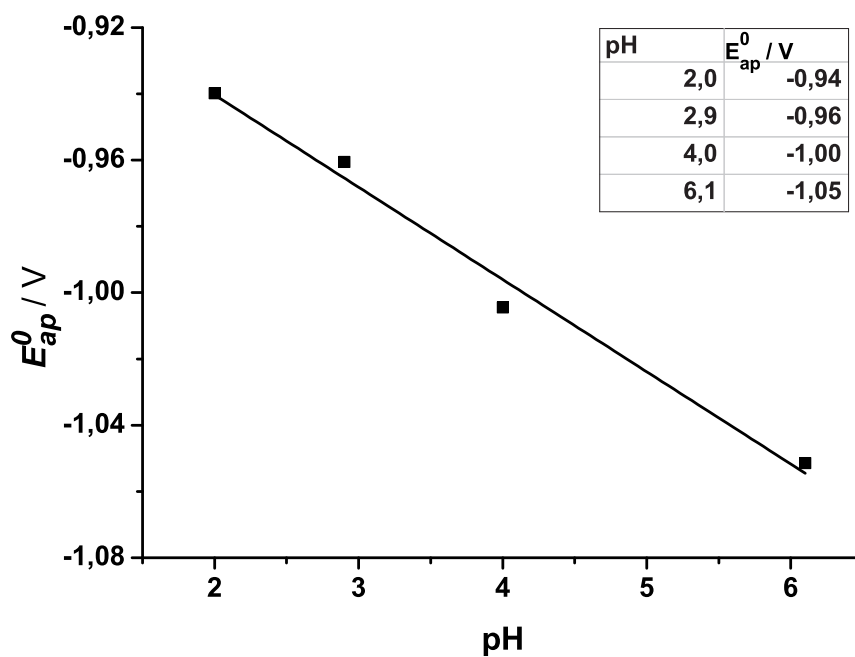


Fig. 4.33: The apparent standard reduction potential (vs. Ag/AgCl) of BPTC (1mM) as a function of pH. Solid line: linear fit, slope =  $-27.8 \pm 2.4$  mV/pH.



**5**

## **Conclusions and Outlook**

## 5.1 Conclusions

The photoinduced electron transfer in aqueous solution of different pH has been studied extensively in the course of this thesis. The fluorophores are two well known types, aza-aromatic (i.e. 2,2'-dipyridyl) and carbonyl aromatic (i.e. 3,3',4,4'-benzophenone tetracarboxylic acid), which are suitable for photochemical reactions. DNA-bases, adenine, adenosine, thymine and thymidine, are the first class of quenchers. Three representative amino acids, the simplest - alanine, aromatic - histidine and sulfur-containing - methionine, are under investigation.

Depending on the pH of the solution, all fluorophores and quenchers are protonated, neutral or deprotonated states. Applying UV-VIS spectroscopy, we determined that BPTC has two  $pK_a$ -values,  $pK_{aI}=3.20$  and  $pK_{aII}=5.12$ . These values in the triplet excited states are  $pK_{aI}^*=2.1$  and  $pK_{aII}^*=4.7$  estimated by T-T absorption titration, pointing that  ${}^3\text{BPTC}$  is a stronger acid compared to BPTC (ground state).

Quenching reactions between triplet 2,2'-dipyridyl and thymine and thymidine were studied in the whole pH-scale 2.0-12.0. Bimolecular rate constants for quenching by thymine were found to be in the range of  $(0.65 - 3.0) \times 10^7 \text{M}^{-1}\text{s}^{-1}$  depending on pH of solution, these values being  $(0.33 - 1.0) \times 10^7 \text{M}^{-1}\text{s}^{-1}$  for the quenching reactions by thymidine. A relationship between the quenching rate constants and pH has been established over a wide range. Moreover, the formation of the radical cation  $\text{DPH}_2^{\cdot+}$  ( $\lambda_{\text{max}}=370\text{nm}$ ) is observed at  $\text{pH}<5.8$ .

pH-dependent quenching reactions of the triplet state of 3,3',4,4'-benzophenone tetracarboxylic acid by DNA bases and amino acids were investigated in aqueous solution pH 2.0-12.0. BPTC ketyl radical anion,  $\text{BPTC}^{\cdot-}$  ( $\lambda_{\text{max}}=630\text{nm}$ ), is observed in the course of all quenching reactions. Additionally, two kinetic problems which are frequently encountered when analyzing the flash photolysis data have been solved:

- The T-T absorption decay combines with a 1st-order growth of the radicals.
- The T-T absorption decay is overlapped by a 1st-order growth and 2nd-order disappearance of radicals (see the quenching by thymine at  $\text{pH}<10$ ).

Subsequently, bimolecular quenching rate constants by alanine are in the range of  $1.9 \times 10^5 - 1.6 \times 10^7 \text{M}^{-1}\text{s}^{-1}$ . It is found to be higher,  $k_q^{\text{obs}} = 0.87 - 7.7 \times 10^8 \text{M}^{-1}\text{s}^{-1}$  for quenching by histidine. Reaction rate constants are near the diffusion limit for quenching by methionine, adenine, adenosine, thymine and thymidine. The  $k_q^{\text{obs}}$ -pH relation has been provided to all quenchers.

In particular, the apparent standard reduction potential of DP in water was measured by cyclic voltammetry. The resulting values are attributed to be constant

(within experimental error,  $\pm 20\text{mV}$ ) between the pH-ranges of 2.0-3.0 and 4.0-6.0 as well. We estimated  $E_{\text{DPH}^+}^0 = E_{\text{ap,DPH}^+}^0 = -1.22\text{V}$  (taken at pH=2.0) and  $E_{\text{DP}}^0 = E_{\text{ap,DP}}^0 = -1.42\text{V}$  (taken at pH=6.1) vs. Ag/AgCl.

Furthermore, the pH-dependence of the oxidation of thymine was also carried out in water. In contrast to DP, thymine shows a linear variation of the apparent standard potential with  $\text{pH} \leq 8.0$ , which is characterized by a slope of  $-55.2 \pm 2.7$  per pH unit. This indicates a coupling of proton and electron transfer. From these results, it is allowed to establish  $E_{\text{ThyH}^+/\text{ThyH}}^0 = E_{\text{ETPT}}^0 = 1.27$  (calculated at pH=3.2) and  $E_{\text{Thy}\cdot\text{H}^+/\text{ThyH}}^0 = E_{\text{CPET}}^0 = 1.45\text{V}$  (calculated at pH=0) vs. Ag/AgCl. Besides, the apparent standard reduction potential of BPTC in solution  $\text{pH} < 7$  shows a linear variation with a slope of  $-27.8 \pm 2.4$  mv/pH.

The electrochemical results of the oxidation of thymine reveal that  $-\Delta G_{\text{ETPT}}^0 = E_{\text{T}} - 240.3 > -\Delta G_{\text{CPET}}^0 = E_{\text{T}} - 257.7 \text{ kJmol}^{-1}$ . Together with the kinetic analysis of the photoreactions between DP and thymine (thymidine), it is suggested in terms of thermodynamics that an electron transfer followed by proton transfer from thymine (thymidine) to triplet dipyridyl takes place at  $\text{pH} < 5.8$ . Between pH 5.8-9.9 hydrogen abstraction mechanism would prefer. At  $\text{pH} > 9.9$  electron transfer reactions occur.

The observation of the  $\text{BPTC}\cdot^-$  at  $\lambda_{\text{max}}=630\text{nm}$  in all reactions of  $^3\text{BPTC}$  with quenchers confirms that the photochemical primary step is electron transfer. On the other hand, it is postulated that a proton coupled electron transfer by means of step-wise mechanism from thymine to triplet BPTC in the solutions  $\text{pH} \approx 2.0-8.0$  proceeds due to the feature of the oxidation of thymine.

## 5.2 Outlook

Chemically induced dynamic nuclear and electron polarization (CIDNP and CIDEP) techniques have been widely applied to study the chemical reaction mechanism. In addition, chemically kinetic and chemically thermodynamic investigations are also indispensable for this purpose. Both are necessary to provide a detailed information of the reaction mechanism. Although the mechanisms of the reactions between triplet DP, BPTC and thymine are predicted, the kinetic solvent isotope effects should be investigated by both laser-flash photolysis and cyclic voltammetry to strongly support the conclusions.

As found in this research, BPTC is a very good fluorophore initiating reactions with some DNA-bases, and it could also be used for reactions with other nucleobases such as uracil, cytosine, guanine and their nucleosides, uridine, cytidine and guanosine.

Despite the protonation states of the fluorophores and quenchers depend pH of solution, pH-dependent function of the overall quenching rate constant can be established in a similar way to extract a rate constant of each corresponding reactant-pair. This will give an idea about their chemical reactivity and save time for the experimentalist.

## APPENDIX



## Appendix A

### Simulation of the transient absorbance to extract $k_1$ s

```

%%%%%%%%%%%%%%%%%%%%%%%%%%%%%%%%%%%%%%%%%%%%%%%%%%%%%%%%%%%%%%%%%%%%%%%%
%Codes were wirrtten by Dr. Daniel Kattnig
%%%%%%%%%%%%%%%%%%%%%%%%%%%%%%%%%%%%%%%%%%%%%%%%%%%%%%%%%%%%%%%%%%%%%%%%
function [fun,varargout] = dRdt_fun(k1,k2,T0)
% dRdt_fun : rate equation for quenching products
% dRdt_fun(k1,k2,T0) returns a function handle to the rate equation of the
% quenching products assuming a pseudo-first order growth (k1), a second
% order decay (k2), and an initial precursor (triplet) concentration of T0.

fun = @fun12; if nargin >= 2
    varargout{1} = @fun12_jacobian;
end

function dRdt = fun12(t,R)
    dRdt = k1*T0 .* exp(-k1.*t) - k2 .* R.^2;
end

function J = fun12_jacobian(t,R)
    J = -2*k2 .* R;
end

end

%%%%%%%%%%%%%%%%%%%%%%%%%%%%%%%%%%%%%%%%%%%%%%%%%%%%%%%%%%%%%%%%%%%%%%%%
% Simulation of the transient absorbance
%%%%%%%%%%%%%%%%%%%%%%%%%%%%%%%%%%%%%%%%%%%%%%%%%%%%%%%%%%%%%%%%%%%%%%%%
function dA = sim_absorbance(p,t)

k1 = p.k1;

if isfield(p,'tau') && ~isempty(p.tau) && p.tau > 0
    k1 = k1 + 1/p.tau;
end

dRdt = dRdt_fun(k1,p.k2dash*p.dA_Rinf,1); % in units of dA_Rinf

```

```

options = odeset('RelTol',1e-6,'AbsTol',1e-8, ...
    'NonNegative',1);
[t,R] = ode45(dRdt,t,0,options);

dA = p.dA_T0 .* exp(-k1.*t) + p.dA_Rinf .* R;

%%%%%%%%%%%%%%%%%%%%%%%%%%%%%%%%%%%%%%%%%%%%%%%%%%%%%%%%%%%%%%%%%%%%%%%%
%%Fitting the transient absorbance
%%%%%%%%%%%%%%%%%%%%%%%%%%%%%%%%%%%%%%%%%%%%%%%%%%%%%%%%%%%%%%%%%%%%%%%%
function pop = fit_absorbance(t,dA,varargin)

if nargin >= 3 && isstruct(varargin{1})
    p = varargin{1};
    if isempty(p.k1)
        p.k1 = k1_guess(t,dA);
        if isfield(p,'tau') && ~isempty(p.tau) && p.tau > 0
            p.k1 = p.k1 - 1/p.tau;
        end
    end
    if isempty(p.k2dash)
        p.k2dash = k2dash_guess(t,dA);
    end
    % always guess:
    p.dA_T0 = dA(1);
    p.dA_Rinf = mean(dA(end-9:end));
else
    p.k1 = k1_guess(t,dA);           % tunit^-1
    p.dA_T0 = dA(1);                 % depsilon_T T0
    p.dA_Rinf = mean(dA(end-9:end)); % alpha * T0 * depsilon_R
    p.k2dash = k2dash_guess(t,dA);
    % p.tau = 0;
end

parameter_names = {'k1','k2dash','dA_Rinf'}; nr =
length(parameter_names); x0 = zeros(1,nr); for i = 1:nr
    x0(i) = p.(parameter_names{i});
end scale = ones(1,nr);
% lv = x0 > 1e-6;
% scale(lv) = x0(lv);
x0 = x0./scale;

```

```
pop = p;

options = optimset('Display','iter'); x =
lsqnonlin(@fitfun,x0,zeros(1,nr),[],options);

for i = 1:nr
    pop.(parameter_names{i}) = scale(i) * x(i);
end

function residual = fitfun(parameter_values)

    for k = 1:nr
        pop.(parameter_names{k}) = scale(k) * parameter_values(k);
    end

    dA_sim = sim_absorbance(pop,t);
    residual = dA - dA_sim;

end

end

function k2dash = k2dash_guess(t,dA)

% k2dash = (dA(end-100)/dA(end) - 1) / (dA(end-100)*(t(end)-t(end-100)));

n = min(length(t)/4,201); dk = [ones(n,1),t(end-n+1:end)] \
(1./dA(end-n+1:end));

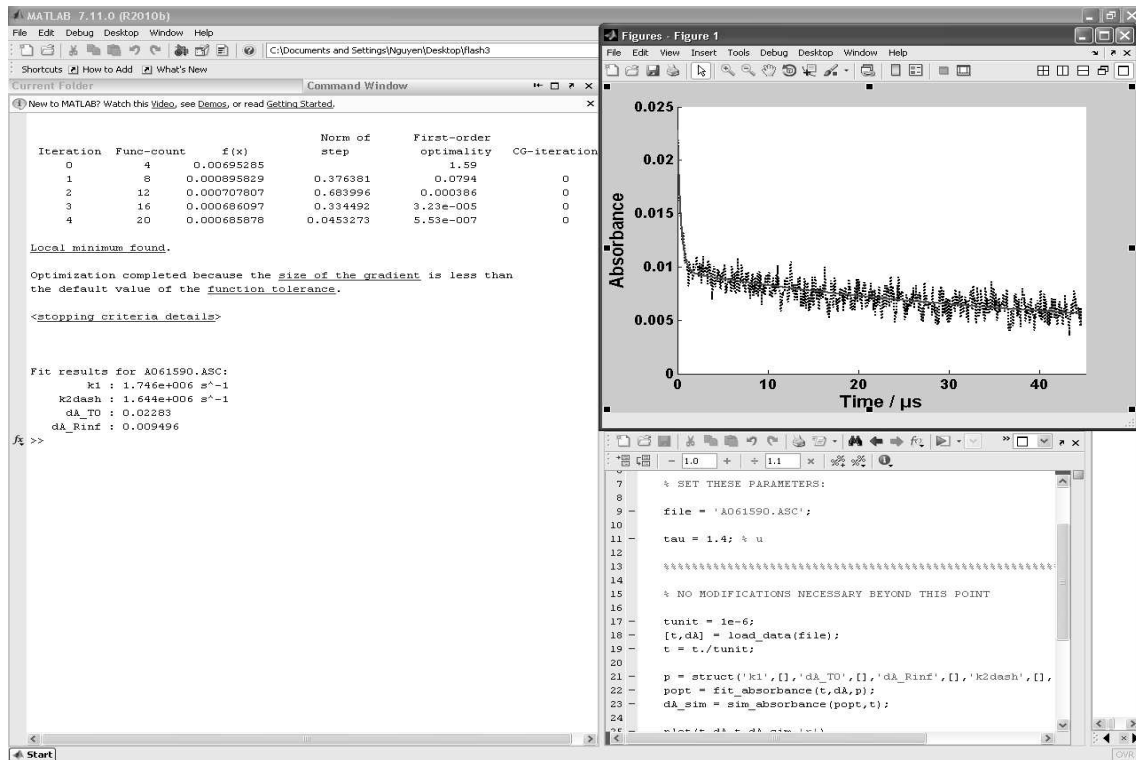
k2dash = max(0,dk(2));

end

function k1 = k1_guess(t,dA)

k1 = log(dA(1)/dA(10))/t(10);

end
```



## Appendix B

### Simulation of the absorbance ratio titration to extract $pK_a^*$ s

```

%Determining pKa values by triplet-triplet absorbance method (curve fit
% of 2 parameters - absorbance ratio function of pH
%%%%%%%%%%%%%%%%%%%%%%%%%%%%%%%%%%%%%%%%%%%%%%%%%%%%%%%%%%%%%%%%%%%%%%%%
clear all
%plot fit
figure(1) clf

%%%%%%%%%%%%%%%%%%%%%%%%%%%%%%%%%%%%%%%%%%%%%%%%%%%%%%%%%%%%%%%%%%%%%%%%
%START inputs
%%%%%%%%%%%%%%%%%%%%%%%%%%%%%%%%%%%%%%%%%%%%%%%%%%%%%%%%%%%%%%%%%%%%%%%%

%pH
x=[1 1.5 2 3.05 4 4.5 5.3 6.4 6.9 8.3 9.1 10.2 11.1 12];

%The measured absorbance ration
y=[1.69809 1.69822 1.54212 1.3807 1.21436 1.16469 0.94922 0.8921
    
```

```

0.92232 0.84599 0.85791 0.87729 0.89859 0.87858];

%Estimate of S/N measurements
% currently set to 10%
dy = y*0.1;

%Formula converted to
% the inline version
func = inline('(1.7*(10.^(-4*x)) + 1.3*p(1)*(10.^(-2*x)) +
0.875*p(2))./((10.^(-4*x)) + p(1)*(10.^(-2*x)) + p(2))','p','x');

%Initial parameter guess
p0 = [10^-6.4 10^-16.64];

%The fit is run a several times.
Nrepeat=50;
%each parameter is varied by a normal distribution with sd*mean
sd = 0.1;

%%%%%%%%%%%%%%%%%%%%%%%%%%%%%%%%%%%%%%%%%%%%%%%%%%%%%%%%%%%%%%%%%%%%%%%%
%END inputs
%%%%%%%%%%%%%%%%%%%%%%%%%%%%%%%%%%%%%%%%%%%%%%%%%%%%%%%%%%%%%%%%%%%%%%%%

for rep =1:Nrepeat
    rep

    %Form the new randomized start vector
    p = [p0(1)*(1+sd*randn), p0(2)*(1+sd*randn)];

    %Do the fit
    [p,r,j] = nlinfit(x,y,func,p);

    %Get parameter errors
    c95 = nlparci(p,r,j);

    %Absorbance-ratio errors (residual)
    [yp, ci] = nlpredci(func,x,p,r,j);

    %Plot the fit
    figure(1)

```

## Appendix

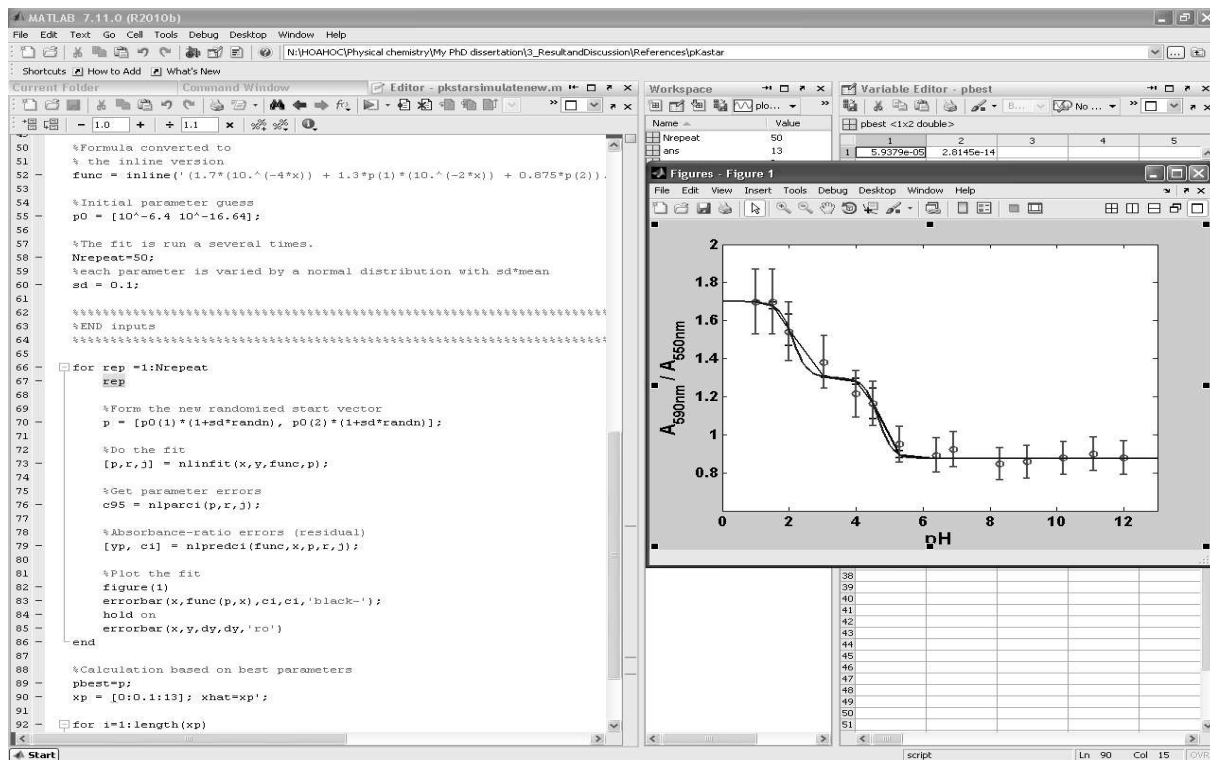
```

errorbar(x,func(p,x),ci,ci,'black-');
hold on
errorbar(x,y,dy,dy,'ro')
end

%Calculation based on best parameters
pbest=p; xp = [1:0.1:10]; xhat=xp';

for i=1:length(xp)
    xp(i);
    yp(i)=(1.7*(10.^(-4*xp(i))) + 1.3*pbest(1)*(10.^(-2*xp(i))) + ...
        0.875*pbest(2))./((10.^(-4*xp(i))) + pbest(1)*(10.^(-2*xp(i))) + pbest(2)));
end
figure(1)
plot(xp,yp,'b')

```



## Appendix C

### pH-dependent function of $k_q^{\text{obs}}$

```

clear clc format short e
%%%%%%%%%%%%%%%%%%%%%%%%%%%%%%%%%%%%%%%%%%%%%%%%%%%%%%%%%%%%%%%%%%%%%%%%
%%SET inputs
x = [2;      3;      4;      5.2;      6.4 ;  8.0  ;  10];
%lamda obs = 590 (pH<7) and lamda obs = 550 (pH>7)
y = [3.15e9; 2.93e9;  1.99e9;  1.23e9;  1e9;  8.6e8;
8.0e8];
%ka_stars  of BPTC
ka_star1 = 10^-2.1; ka_star2 = 10^-4.7;
%ka value of Thymine
ka1 = 10^-9.9;
%%%%%%%%%%%%%%%%%%%%%%%%%%%%%%%%%%%%%%%%%%%%%%%%%%%%%%%%%%%%%%%%%%%%%%%%
%%START
for i=1:length(x)
    x1(i)=10^-x(i);
    x2(i)=x1(i)^4+x1(i)^2*ka_star1^2+ka_star1^2*ka_star2^2;
    x3(i)=x1(i)+ka1;
    x4(i)=x2(i)*x3(i);

    A(i)=x1(i)^5/x4(i);
    B(i)=( ka_star1^2* (x1(i)^3))/x4(i);
    C(i)=( ka_star1^2*ka_star2^2* x1(i))/x4(i);
end

global q

%Estimate parameters
h=[A' B' C']; MAT=h'*h; q = inv(MAT)*h'*y

%Calculate R^2 (correlation coefficient)
yhat = h*q; ymean = sum(y)/length(y);ry1 = y - yhat; ydivmean = y-
ymean; ry2 = ry1.^2; ydivmean2 = ydivmean.^2; r2 =
1-(sum(ry2)/sum(ydivmean2));

%Experimental errors
ry =[3.5e8 3.5e8 1.1e8 7.5e7 7.2e7 7.5e7 4.2e7];

```

```
%[y yhat];
```

```
figure(1)
```

```
plot(x,y,'b.', 'markersize',25)
```

```
xlabel('pH', 'fontsize',18, 'fontweight', 'b'); %Write label for x-axis
```

```
%Write label for y-axis
```

```
ylabel('10-9 x kq{obs}
```

```
(M{-1}s{-1})', 'fontsize',18, 'fontweight', 'b');
```

```
set(findobj('type', 'axes'), 'fontsize',16, 'fontweight', 'b')
```

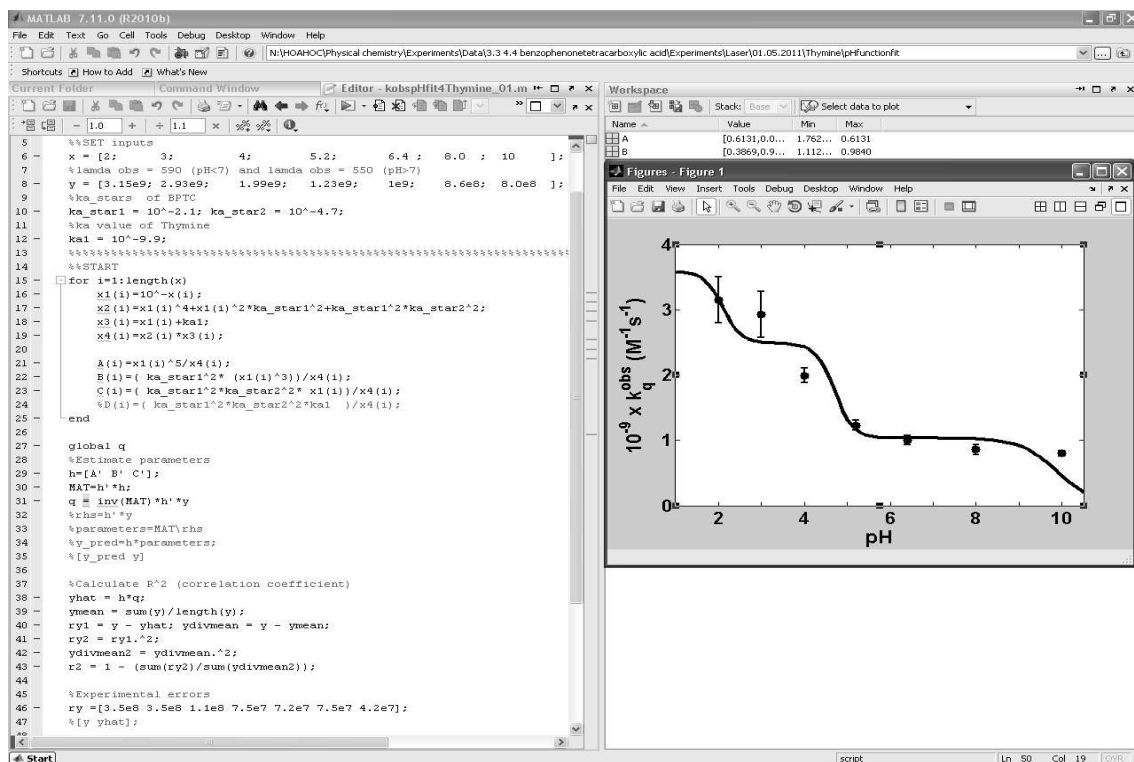
```
hold on
```

```
errorbar(x,y,ry, 'b+', 'LineWidth',2);
```

```
hold on
```

```
pHfunThymine
```

```
hold off
```



# Bibliography

- [1] J.F. Ireland and P.A.H. Wyatt. *Acid-Base Properties of Electronically Excited States of Organic Molecules*. Academic Press, 1976.
- [2] *Handbook of Chemistry and Physics*. CRC Press, 84<sup>th</sup> edition, 2003.
- [3] *LAB tools. Tabellen für das Labor*. Merck, Darmstadt, Germany.
- [4] Bronislaw Marciniak, Krzysztof Bobrowski, and Gordon L. Hug. Quenching of triplet states of aromatic ketones by sulfur-containing amino acids in solution. evidence for electron transfer. *J. Phys. Chem.*, 97:11937–11943, 1993.
- [5] Krzysztof Bobrowski, Gordon L. Hug, Bronislaw Marciniak, and Halina Kozubek. The 4-carboxybenzophenone-sensitized photooxidation of sulfur-containing amino acids in alkaline aqueous solutions. secondary photoreactions kinetics. *J. Phys. Chem.*, 98:537–544, 1994.
- [6] Olga B. Morozova, Sergey E. Korchak, Renad Z. Sagdeev, and Alexandra V. Yurkovskaya. Time-resolved chemically induced dynamic nuclear polarization studies of structure and reactivity of methionine radical cations in aqueous solution as a function of ph. *The Journal of Physical Chemistry A*, 109:10459–10466, 2005.
- [7] Olga B. Morozova, Sergey E. Korchak, Hans-Martin Vieth, and Alexandra V. Yurkovskaya. Photo-cidnp study of transient radicals of met-gly and gly-met peptides in aqueous solution at variable ph. *The Journal of Physical Chemistry B*, 113:7398–7406, 2009.
- [8] Olga B. Morozova, Konstantin L. Ivanov, Alexey S. Kiryutin, Renad Z. Sagdeev, Talea Kchling, Hans-Martin Vieth, and Alexandra V. Yurkovskaya. Time-resolved cidnp: an nmr way to determine the epr parameters of elusive radicals. *Phys. Chem. Chem. Phys.*, 14:6619–6627, 2011.

- [9] Yuri P. Tsentalovich, Olga B. Morozova, Alexandra V. Yurkovskaya, and P. J. Hore. Kinetics and mechanism of the photochemical reaction of 2,2'-dipyridyl with tryptophan in water: Time-resolved cidnp and laser flash photolysis study. *J. Phys. Chem. A*, 103:5362–5368, 1999.
- [10] Yuri P. Tsentalovich, Olga B. Morozova, Alexandra V. Yurkovskaya, P. J. Hore, and Renad Z. Sagdeev. Time-resolved cidnp and laser flash photolysis study of the photoreactions of n-acetyl histidine with 2,2-dipyridyl in aqueous solution. *J. Phys. Chem. A*, 104:6912–6916, 2000.
- [11] Yuri P. Tsentalovich, Olga B. Morozova, Alexandra V. Yurkovskaya, P. J. Hore, and Renad Z. Sagdeev. Time-resolved cidnp and laser flash photolysis study of the photoreactions of n-acetyl histidine with 2,2'-dipyridyl in aqueous solution. *J. Phys. Chem. A*, 104:6912–6916, 2000.
- [12] Olga B. Morozova, Alexandra V. Yurkovskaya, Yuri P. Tsentalovich, Malcolm D. E. Forbes, and Renad Z. Sagdeev. Time-resolved cidnp study of intramolecular charge transfer in the dipeptide tryptophan-tyrosine. *J. Phys. Chem. B*, 106:1455–1460, 2002.
- [13] Olga B. Morozova, Alexandra V. Yurkovskaya, Hans-Martin Vieth, and Renad Z. Sagdeev. Intramolecular electron transfer in tryptophan-tyrosine peptide in photoinduced reaction in aqueous solution. *J. Phys. Chem. B*, 107:1088–1096, 2003.
- [14] Olga B. Morozova, Alexandra V. Yurkovskaya, Renad Z. Sagdeev, K. Hun Mok, and P. J. Hore. Time-resolved cidnp study of native-state bovine and human-lactalbumins. *J. Phys. Chem. B*, 108:15355–15363, 2004.
- [15] Olga B. Morozova, Alexandra V. Yurkovskaya, and Renad Z. Sagdeev. Reversibility of electron transfer in tryptophan-tyrosine peptide in acidic aqueous solution studied by time-resolved cidnp. *J. Phys. Chem. B*, 109:3668–3675, 2005.
- [16] Olga B. Morozova, P. J. Hore, Renad Z. Sagdeev, and Alexandra V. Yurkovskaya. Intramolecular electron transfer in lysozyme studied by time-resolved chemically induced dynamic nuclear polarization. *J. Phys. Chem. B*, 109:21971–21978, 2005.
- [17] R. A. Marcus. Nobel lecture, 1992. Chemistry.

- 
- [18] J. Silverman and R. W. Dodson. The exchange reaction between the two oxidation states of iron in acid solution. *J. Phys. Chem.*, 56:846–852, 1952.
- [19] Francis P. Dwyer and Alan M. Sargeson. The rate of electron transfer between the tris- (ethylenediamine)-cobalt(ii) and cobalt(iii) ions. *J. Phys. Chem.*, 65: 1892–1894, 1961.
- [20] E. Rabinowitch. *Photosynthesis and Related Processes*. Interscience Inc., 1945.
- [21] Gonzalo Angulo. *Experimental observations of non-markovian effects on diffusion-induced photo-induced electron transfer reactions*. PhD thesis, Graz University of Technology, 2003.
- [22] J. Schurr Michael. The role of diffusion in bimolecular solution kinetics. *Biophys. J.*, 10:700–716, 1970.
- [23] Arnulf Rosspeintner. *Experimental observations of diffusionl effects on electron transfer reactions*. PhD thesis, Graz University of Technology, 2008.
- [24] E. Kotomin and V. Kuzovkov. *Modern Aspects of Diffusion-Controlled Reactions*. Elsevier, 1996.
- [25] Peter Atkins and Julio de Paula. *Physical Chemistry*. W. H. Freeman, New York, 8<sup>th</sup> edition, 2006.
- [26] Norman Sutin. Nuclear, electronic, and frequency factors in electron transfer reactions. *Acc. Chem. Res.*, 15:275–282, 1982.
- [27] J. R. Miller, L. T. Calcaterra, and G. L. Closs. Intramolecular long-distance electron transfer in radical anions. the effects of free energy and solvent on the reaction rates. *J. Am. Chem. Soc.*, 106:3047–3049, 1984.
- [28] G. Levich and R. Dogonadze. *Dokl. Akad. Nauk.*, 124:123, 1959.
- [29] I. Rips and J. Jortner. The effect of solvent relaxation dynamics on outer-sphere electron transfer. *Chem. Phys. Lett.*, 133:411–414, 1987.
- [30] H. Huppert, D. Kanety and Edward M. Kosower. Kinetics and mechanism of intramolecular electron transfer in solution. *Faraday Discuss. Chem. Soc.*, 74: 161–175, 1982.

- [31] G. Grampp and K. Rasmussen. Solvent dynamical effects on the electron self-exchange rate of the tempo $\cdot$ /tempo $^+$  couple (tempo = 2,2,6,6-tetramethyl-1-piperidinyloxy radical) part i. esr-linebroadening measurements at  $t = 298$  k. *Phys. Chem. Chem. Phys.*, pages 5546–5549, 2002.
- [32] George J. Kavarnos and Nicholas J. Turro. Photosensitization by reversible electron transfer: theories, experimental evidence, and examples. *Chem. Rev. (Washington, DC, U. S.)*, 86:401–449, 1986.
- [33] Günter Grampp. Lecture course - che.357: Photochemistry, Summer 2009. Graz University of Technology.
- [34] K. K. Rohatgi Mukkerjee. *Fundamentals of Photochemistry*. John Wiley and Sons Inc., New York, 1986.
- [35] A.K Chibisov. Electron transfer in photochemical reactions. *Russ. Chem. Rev.*, 50:615–629, 1981.
- [36] Joseph R. Lakowicz. *Principles of Fluorescence Spectroscopy*. Springer, 2006.
- [37] A. Weller. Electron transfer in photochemical reactions. *Z. Elektrochem.*, 56: 662, 1952.
- [38] Julien Bonin, Cyrille Costentin, Cyril Louault, Marc Robert, Mathilde Routier, and Jean-Michel Saveant. Intrinsic reactivity and driving force dependence in concerted proton and electron transfers to water illustrated by phenol oxidation. *Proc. Natl. Acad. Sci. U. S. A.*, 107:3367–3372, 2010.
- [39] Cyrille Costentin, Marc Robert, Jean-Michel Saveant, and Anne-Lucie Teillout. Concerted proton-coupled electron transfers in aquo/hydroxo/oxo metal complexes: Electrochemistry of [osii(bpy)2py(oh2)]2+ in water. *Proc. Natl. Acad. Sci. U. S. A.*, 106:11829–11836, 2009.
- [40] Martin Sjödin, Stenbjörn Styring, Henriette Wolpher, Yunhua Xu, Licheng Sun, and Leif Hammarström. Switching the redox mechanism: Models for proton-coupled electron transfer from tyrosine and tryptophan. *J. Am. Chem. Soc.*, 127:3855–3863, 2005.
- [41] My Hang V. Huynh and Thomas J. Meyer. Colossal kinetic isotope effects in proton-coupled electron transfer. *Proc. Natl. Acad. Sci. U. S. A.*, 101:13138–13141, 2004.

- 
- [42] Roger L. Lundblad and Fiona M. Macdonald, editors. *Handbook of Biochemistry and Molecular Biology*. CRC Press, 4<sup>th</sup> edition, 2010.
- [43] Robert H. Linnell and A. Kaczmarczyk. Ultraviolet spectra of [ill] compounds. *J. Phys. Chem.*, 65:1196–1200, 1961.
- [44] James J. Christensen, J. Howard Rytting, and Reed M. Izatt. Thermodynamics of proton dissociation in dilute aqueous solution. vii.  $pK$ ,  $\Delta H$ , and  $\Delta S$  values for proton ionization from several pyrimidines and their nucleosides at 25 $^{\circ}$ . *J. Phys. Chem.*, 71:2700–2705, 1967.
- [45] James J. Christensen, J. Howard Rytting, and Reed M. Izatt. Thermodynamic  $pK$ ,  $H$ ,  $S$ , and  $CP$  values for proton dissociation from several purines and their nucleosides in aqueous solution. *Biochemistry*, 9:4907–4913, 1970.
- [46] Francis A. Carey. *Organic Chemistry*. McGraw-Hill, Columbus, 5<sup>th</sup> edition, 2004.
- [47] Douglas A. Skoog, Donald M. West, F. James Holler, and Stanley R. Crouch. *Fundamentals of Analytical Chemistry*. Thomson, Belmont, CA 94002. USA, 8<sup>th</sup> edition, 2004.
- [48] J.N. Butler. *Ionic equilibrium - a mathematical approach*. Addison-Wesley, 1964.
- [49] Heinz-Helmut Perkampus. *UV-VIS Spectroscopy and Its Applications*. Translated by H. Charlotte Grinter and Dr.T.L. Threlfall. Springer, Berlin, 1992.
- [50] S. E. Blanco, M. C. Almandoz, and F. H. Ferretti. Determination of the overlapping  $pK_a$  values of resorcinol using UV-visible spectroscopy and DFT methods. *Spectrochim. Acta, Part A*, 61:93 – 102, 2005.
- [51] Stefan Landgraf. Lecture course - CHE.351: Modern aspects of chemical kinetics, Summer 2009. Graz University of Technology.
- [52] David L. Andrews. *Laser in Chemistry*. Springer, Berlin, 3<sup>th</sup> edition, 1997.
- [53] G. Jackson and G. Porter. Acidity constants in the triplet state. *Proc. R. Soc. London, Ser. A*, 260:13–30, 1961.
- [54] M. V. Encinas, P. J. Wagner, and J. C. Scaiano. Hydrogen abstraction by biradicals. reactions with tri-*n*-butylstannane and octanethiol. *J. Phys. Chem.*, 102:1357–1360, 1980.

- [55] Leonard J. Andrews, Joel M. Levy, and Henry Linschitz. Kinetic analysis of flash photolysis data for sequential first and second order reactions: The photoreduction of triplet fluorenone by dabco. *J. Photochem.*, 6:355 – 364, 1976-1977.
- [56] A. V. Yurkovskaya, O. A. Snytnikova, O. B. Morozova, Y. P. Tsentalovich, and R. Z. Sagdeev. Time-resolved CIDNP and laser flash photolysis study of the photoreaction between triplet 2,2'-dipyridyl and guanosine-5'-monophosphate in water. *Phys. Chem. Chem. Phys.*, 5:3653–3659, 2003.
- [57] C. V. Krishnan, Carol Creutz, Harold A. Schwarz, and Norman Sutin. Reduction potentials for 2,2'-bipyridine and 1,10-phenanthroline couples in aqueous solutions. *J. Am. Chem. Soc.*, 105:5617–5623, 1983.
- [58] Yasuhiko Gondo and Yoshiya Kanda. The phosphorescence spectra of 2,2'- and 4,4'-bipyridyls. *Bull. Chem. Soc. Jpn.*, 38:1187, 1965.
- [59] Shai Inbar, Henry Linschitz, and Saul G. Cohen. Quenching, radical formation, and disproportionation in the photoreduction of 4-carboxybenzophenone by 4-carboxybenzhydrol, hydrazine, and hydrazinium ion. *J. Am. Chem. Soc.*, 103: 7323–7328, 1981.
- [60] J. Sauberlich, O. Brede, and D. Beckert. Investigation of coulomb-coupled radical ion pairs of benzophenonetetracarboxylic acid and triethylamine by laser photolysis fourier transform electro n spin resonance. *Acta Chem. Scand.*, 51: 602–609, 1997.
- [61] Mintu Haldar and Mihir Chowdhury. Magnetic-field effect on the micellar surface-bound benzophenone tetracarboxylic acid-sodium salt in aqueous cetyltrimethylammonium bromide medium. *Chem. Phys. Lett.*, 312:432 – 439, 1999.